

DISSERTATION ZUR ERLANGUNG DES  
DOKTORGRADES  
DER FAKULTÄT FÜR CHEMIE UND PHARMAZIE  
DER LUDWIG-MAXIMILIANS-UNIVERSITÄT  
MÜNCHEN



**Freeze-Drying in Dual Chamber Cartridges**  
**- from Energy Transfer to Process Control -**

Christoph Phillip Korpus

aus

Idar-Oberstein

2017

## ERKLÄRUNG

Diese Dissertation wurde im Sinne von §7 der Promotionsordnung vom 28. November 2011 von Herrn Prof. Dr. Wolfgang Frieß betreut.

## EIDESSTATTLICHE VERSICHERUNG

Diese Dissertation wurde eigenständig und ohne unerlaubte Hilfe erarbeitet.

Frankfurt, den

---

Christoph Korpus

Dissertation eingereicht am: 26.01.2017

1. Gutachter: Prof. Dr. Wolfgang Frieß

2. Gutachter: Prof. Dr. Gerhard Winter

Mündliche Prüfung am: 23.02.2017

Für meine Eltern

# ACKNOWLEDGEMENTS

This thesis was prepared at the Department of Pharmacy, Pharmaceutical Technology and Biopharmaceutics at the Ludwig-Maximilians-Universität München (LMU) under the supervision of Prof. Dr. Wolfgang Frieß.

First and foremost, I would like to express my deepest gratitude to my supervisor, Prof. Dr. Wolfgang Frieß, for giving me the opportunity to join his research group and his continuous encouragement during the past years. I am very grateful for your valuable scientific advice and the possibility to present my work at various conferences. Thank you so much for giving me the freedom to develop own ideas and for organizing my research stay at Dr. Pikal's group at the University of Connecticut. I am also very thankful for your constant support for submitting and publishing most of this work.

Prof. Dr. Gerhard Winter is also highly appreciated for being the co-referee of this work, as well as for establishing excellent working conditions at our institute. Many thanks also for organizing and supporting all these nice social activities for both groups and your valuable advice during the Thursday's seminar.

I also want to express my sincere gratitude to Prof. Dr. Michael Pikal from the School of Pharmacy at the University of Connecticut for his outstanding scientific guidance and for giving me the opportunity to use all these advanced process analytical tools during my research stay. Many thanks also to the whole lab team and Prof. Dr. Bogner for the warm welcome and excellent support during this exciting period.

The German Academic Exchange Service (DAAD) is kindly acknowledged for funding my research stay at the University of Connecticut.

I would also like to thank all the students that supported this thesis with their excellent individual contributions. Special thanks go to Thomas Haase. You did a remarkable job during your Master thesis and really helped to lay the groundwork for this thesis! My thanks are extended to Kornelia Pesl, Rupert Faltlhauser and Jesus Caro. Thank you very much for your ideas and support.

## ACKNOWLEDGEMENTS

---

Coriolis Pharma GmbH is kindly recognized for providing the possibility to use the freeze-drying microscope. Matthias Wurm is kindly thanked for his help.

I want to thank all my former colleagues at the Department of Pharmacy, Pharmaceutical Technology and Biopharmaceutics for the exceptional atmosphere and all the social activities we experienced together. Particularly I want to thank Raimund Geidobler for his support during the installation of the Pressure Rise Test and Tim Menzen for programming the “PRT-Filter” OriginLab macro.

Finally, I would like to thank my parents and family for their continuous support, trust and encouragement.

# TABLE OF CONTENT

<b>1</b>	<b>General Introduction</b> .....	1
1.1	The principle of freeze-drying .....	2
1.2	Market overview and trends for dual chamber cartridges .....	3
1.3	Process challenges for freeze-drying in dual chamber cartridges .....	7
1.4	Design related challenges for DCCs.....	9
1.5	References .....	11
<b>2</b>	<b>Objectives and outline of the thesis</b> .....	15
<b>3</b>	<b>Energy transfer during freeze-drying in dual chamber cartridges</b> .....	17
3.1	Abstract .....	18
3.2	Introduction.....	19
3.3	Materials and Methods .....	21
3.3.1	Materials .....	21
3.3.2	Sublimation experiments.....	22
3.3.3	Ramping phase experiments .....	22
3.3.4	Experiments with suspended aluminum blocks.....	22
3.3.5	Mass and heat transfer theory utilized .....	22
3.3.6	Theoretical calculation of $K_{r/DCC}$ .....	27
3.4	Results and Discussion .....	31
3.4.1	Sublimation rates and product temperatures .....	31
3.4.2	Characterization of the aluminum block heat transfer coefficient $K_{Al}$ ....	33
3.4.3	Different modes of heat transfer for $K_{Al}$ .....	35
3.4.4	Characterization of the DCC heat transfer coefficient $K_{DCC}$ .....	36

3.4.5	Different modes of heat transfer for $K_{DCC}$ .....	38
3.4.6	Overall heat transfer coefficient $K_{tot}$ .....	40
3.5	Summary and Conclusion .....	41
3.6	Acknowledgments .....	42
3.7	References .....	43
<b>4</b>	<b>Heat transfer analysis of an optimized, flexible holder system for freeze-drying in dual chamber cartridges using different state-of-the-art PAT tools .....</b>	<b>45</b>
4.1	Abstract .....	46
4.2	Introduction.....	47
4.3	Materials and Methods .....	49
4.3.1	Materials .....	49
4.3.2	The holder system .....	49
4.3.3	Freeze-dryer configurations and PAT tools used.....	50
4.3.4	Implementation of a self-made pressure rise test system on FD II .....	51
4.3.5	PRT raw data analysis according to the manometric temperature equation.....	52
4.4	Results and Discussion .....	55
4.4.1	Holder system configuration.....	55
4.4.2	Establishment of controlled nucleation for DCCs .....	58
4.4.3	Lyophilization cycle development.....	60
4.4.4	Regular cycle experiment.....	61
4.4.5	Lyo cycle experiment using a preheated plate .....	63
4.4.6	Comparison of TDLAS- and MTM- and gravimetric mass loss data .....	65
4.4.7	Complete heat transfer parameter analysis for the flexible holder device using MTM on FD II .....	68
4.5	Summary and Conclusion .....	71

4.6	Acknowledgments .....	72
4.7	References .....	73
<b>5</b>	<b>Evaluation of different holder devices for freeze-drying in dual chamber cartridges with a focus on energy transfer .....</b>	<b>75</b>
5.1	Abstract .....	76
5.2	Introduction.....	77
5.3	Materials and Methods .....	79
5.3.1	Materials .....	79
5.3.2	Different holder devices .....	79
5.3.3	Shelf mapping experiments – influence of atypical radiation .....	80
5.3.4	Temperature profile determination .....	81
5.3.5	Shell holder heat transfer coefficient experiments .....	82
5.4	Results and Discussion .....	85
5.4.1	Ability of holder devices to minimize the influence of atypical radiation and edge effects .....	85
5.4.2	Temperature profiles analysis during the freezing phase.....	89
5.4.3	Temperature profiles analysis during the drying phase.....	92
5.4.4	Comparison of heat transfer coefficients.....	95
5.5	Summary and Conclusion .....	100
5.6	References .....	103
<b>6</b>	<b>Lyophilization-cycle design for dual chamber cartridges and a method for online process control: The DCC-LyoMate procedure .....</b>	<b>105</b>
6.1	Abstract.....	106
6.2	Introduction.....	107

6.3	Materials and Methods .....	109
6.3.1	Materials .....	109
6.3.2	Freeze-Drying Microscopy .....	109
6.3.3	Lyophilization unit .....	110
6.3.4	DCC holder system.....	110
6.3.5	Sample preparation and freezing protocols .....	110
6.3.6	The DCC LyoMate procedure .....	111
6.4	Results and Discussion .....	115
6.4.1	DCC LyoMate proof of concept study .....	115
6.4.2	Determination of the minimum number of DCCs needed for valid MTM measurements using a 5% sucrose formulation.....	119
6.4.3	High fill volume case study and the influence of the nucleation method on the DCC LyoMate's accuracy .....	121
6.4.4	Collapse temperature determination of different mAb formulations and definition of target product temperatures .....	123
6.4.5	DCC LyoMate results for the 2 mg/ml mAb formulation and the influence of controlled nucleation on product appearance .....	124
6.4.6	DCC LyoMate results for the 2 mg/ml mAb formulation and the influence of shelf-ramped freezing on product appearance .....	126
6.4.7	Applicability of the DCC LyoMate procedure for highly concentrated mAb formulations.....	128
6.5	Summary and Conclusion .....	131
6.6	References .....	133
<b>7</b>	<b>Final Summary .....</b>	<b>137</b>

<b>8 Appendix</b> .....	142
8.1 Publications included in this thesis: .....	142
8.1.1 Research articles .....	142
8.1.2 Book Chapters .....	142
8.1.3 Oral Presentations .....	143
8.1.4 Poster Presentations.....	144
8.2 Curriculum vitae.....	145

# 1 *GENERAL INTRODUCTION*

Parts of the following chapter are intended for publication.

## 1.1 The principle of freeze-drying

To enable long-term storage at room temperature for parenteral drug products that are not adequately stable in liquid, freeze-drying is the method of choice to achieve a stable formulation.<sup>1</sup> Besides their increased stability, freeze-dried products show a decent reconstitution behavior, necessary for fast reconstitution prior to administration, originating from the porous structure of the lyophilized cake.<sup>2,3</sup> This porous structure is the result of the ice crystals which form during the freezing phase and the voids left behind after ice removal via sublimation in the drying.<sup>4,5</sup>

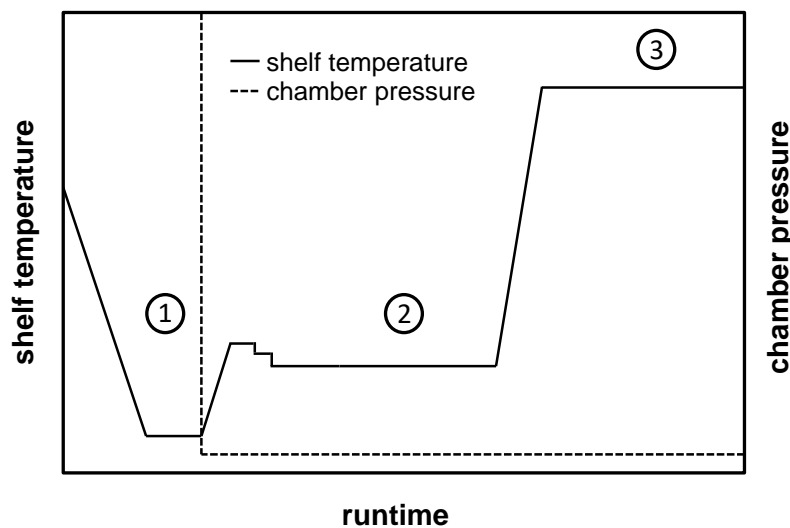


**Figure 1-1 Schematic lyophilization cycle: 1) freezing phase, 2) primary drying phase, 3) secondary drying phase. The solid line represents the shelf temperature and the dotted line the chamber pressure.**

In general, the process of lyophilization can be divided into three stages. During freezing, the shelf temperature is lowered to approx.  $-50^{\circ}\text{C}$  to assure complete solidification of the product solution (Figure 1-1 (1)).<sup>3</sup> As soon as the product temperature falls below the eutectic melting point ( $T_{\text{eu}}$ ) for crystalline components or the glass transition temperature ( $T_{\text{g}}'$ ) for amorphous formulation components, solute solidification occurs.<sup>5</sup>  $T_{\text{g}}'$  and  $T_{\text{eu}}$  are important product characteristics that need to be taken into account as critical process parameters in the subsequent primary drying stage.<sup>6</sup> After complete solidification of the product solution, the pressure in the freeze-drying chamber is lowered below the vapor pressure of ice<sup>5,7</sup>, which initiates water sublimation from the solid state directly to the gassy state (Figure 1-1 (2)).<sup>8</sup> Sublimation consumes substantial amounts of energy (660 calories per 1 gram of

ice)<sup>3</sup> that need to be provided by heating the shelves of the freeze-dryer. A thorough understanding of the relationship between mass and heat transfer is necessary to define the shelf temperature setpoint in a way that results in economic drying rates while maintaining product quality.<sup>9,10</sup> Hereby, the mass transfer resistance rate “ $R_p$ ” is directly correlated with the product temperature ( $T_p$ ).  $R_p$  depends on the morphology of the product (amorphous or crystalline), the solid content within the formulation and the ice nucleation temperature.<sup>3,11</sup> The nucleation temperature defines the number and the volume of the ice crystals and thus the pore size within the dried layer.<sup>5,12</sup> Accordingly, the freezing step is a very important part of the freeze-drying process that can directly influence  $T_p$  during primary drying.<sup>5,13,14</sup> To assure product quality,  $T_p$  needs to stay below a critical value e.g.  $T_g'$  for amorphous components or  $T_{eu}$  for crystalline formulations.<sup>15,16</sup> Otherwise, product damage in form of meltback or cake shrinkage can occur which can be reasons for rejection upon quality control.<sup>17</sup> The shelf temperature is maintained and adjusted to the optimum setpoint until the sublimation process is completed and all frozen bulk water has been removed.<sup>5,6,9</sup> During secondary drying (Figure 1-1 (3)), the unfrozen bound water is removed by elevating the shelf temperature up to 50°C while preserving or further reducing the chamber pressure.<sup>2,5</sup> This stage persists until the residual moisture level is typically < 1% and the freeze-drying process ends.<sup>4</sup> Thus freeze-drying is a costly and time consuming process.

## 1.2 Market overview and trends for dual chamber cartridges

After a period of stagnation between 2010-2013<sup>18,19</sup>, monoclonal antibody products are on the rise again with an increase in approved drug products from 27 in 2013 to 56 in 2016.<sup>20</sup> Based on the current approval rate of 4 drug products per year, around 70 monoclonal antibody drugs will be approved in the year 2020 with a total market volume of more than \$ 125 billion.<sup>21</sup> Around 25% of these drug products are freeze-dried due to insufficient stability in liquid formulations.<sup>20,22</sup> The final product needs to be reconstituted prior to administration with an adequate reconstitution volume.<sup>4,23</sup> Most products are processed in vial container systems. Consequently, this reconstitution step involves basically three steps: 1.) the reconstitution volume needs to be transferred from a diluent vial into the product containing vial with a transfer syringe, 2.) the correct volume of reconstituted drug product needs to be metered into a different syringe and 3.) the needle needs to be changed for injection. Each step

involves a high risk of error and should preferably be performed by trained care personnel.<sup>24 16</sup> With a clear trend towards self-injection and home-care use, more innovative, easy-to-use container formats like dual chamber cartridges (“DCCs”, Figure 1-2 (a)) in combination with pen injectors (Figure 1-2 (b)) gained importance for freeze-dried formulations over the last years.<sup>25-28</sup> Table 1-1 provides an overview of currently marketed drug products manufactured in dual chamber systems.<sup>28</sup>

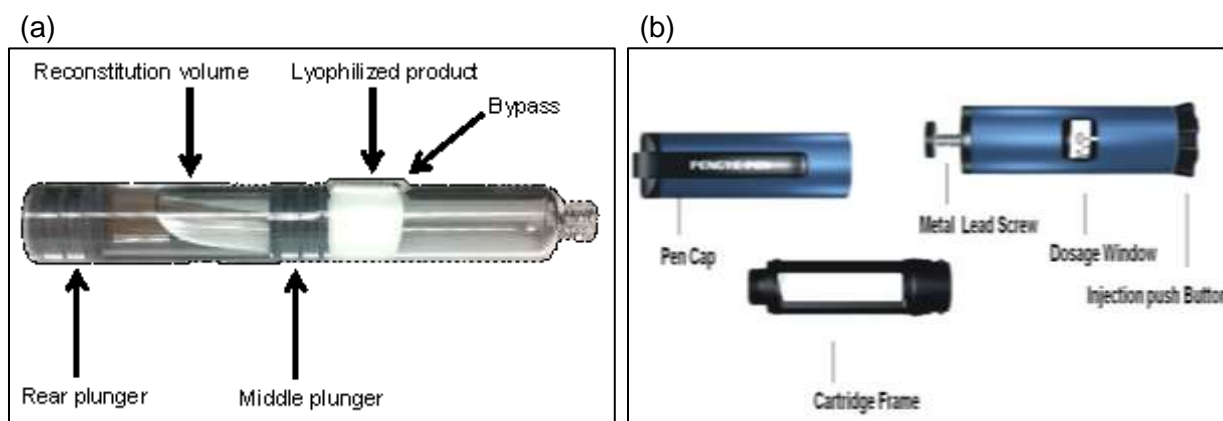


**Figure 1-2 The Dual Chamber Cartridge (a) and the structure of a DCC pen injector ([http://www.delfu-medical.com/photo/delfu-medical/editor/20140915145540\\_39244.jpg](http://www.delfu-medical.com/photo/delfu-medical/editor/20140915145540_39244.jpg), accessed October, 28<sup>th</sup> 2016) (b)**

Compared to vials these dual chamber systems provide numerous advantages.<sup>16</sup>

- 1.) DCCs reduce the risk of microbial contamination due to the closed system,<sup>24</sup>
- 2.) the overfill volume is significantly decreased to around 2-3%<sup>27</sup> compared to vials which are normally overfilled to around 20-35%.<sup>27,29</sup> Since DCCs are commonly used in combination with high-value products, this reduction in overfill volume represents a chance to reduce manufacturing costs.<sup>27,28</sup>
- 3.) the major benefit of these systems is the straight forward reconstitution procedure.<sup>24</sup> Since the front part contains the lyophilized drug product and the rear part the reconstitution volume, the patient can easily reconstitute the product by pushing the rear plunger via the pen device, which then triggers the flow of reconstitution volume through the bypass to the front chamber.<sup>12,16,24,29</sup> Afterwards, the system is ready to use and the patient can administer the dose. Hence, the number of products manufactured in DCCs is expected to rise within the next years.<sup>28,30</sup>

**Table 1-1 Overview of marketed drug products manufactured in dual chamber container formats – modified after <sup>24</sup> and <sup>28</sup>**

<i>Name / API</i>	<i>Formulation</i>	<i>Indication</i>	<i>Company</i>	<i>Device</i>	<i>Volume</i>	<i>Route of Application</i>
<b>Caverject/ Alprostadil</b>	10 µg Alprostadil 324.7 mg Cyclodextrin 45.4 mg Lactose 23.5 mg Sodium Citrate 4.45 mg Benzyl Alcohol	Erectile dysfunction	Pfizer	Disposable, variable dose pen injector	0.6 ml	Intracavernous (ic)
<b>Edex/ Alprostadil</b>	10.8 µg Alprostadil 347.6 mg Cyclodextrin 51.1 mg Lactose	Erectile dysfunction	Schwarz Pharma	Reusable, variable dose pen injector	0.6 ml	ic
<b>Genotropin/ rhGH</b>	1.5 mg rhGH 27.6 mg Glycine 0.6 mg Disodium/ Sodium Phosphate	Growth hormone deficiency, Prader-Willi syndrome, Turner syndrome	Pfizer	Reusable, variable dose pen injector	1 ml	Subcutaneous (sc)
<b>Humatrope/ rhGH</b>	6 mg rhGH 18 mg Mannitol 6 mg Glycine 1.4 mg Disodium/Sodium Phosphate	Growth hormone deficiency, Turner syndrome, idiopathic short stature	Eli Lilly	Reusable, variable dose pen injector	3 ml	sc
<b>Lupron depot/ Leuprolide acetat</b>	3.75 mg Leuprolide Acetate 0.65 mg Purified Gelatin 33.1 DL-lactic/Glycolic Acids Copolymer 6.6 mg Mannitol	Prostate cancer	TAP Pharmaceuticals	No device, Atrix technology for controlled release	1 ml	Intramuscular (im)
<b>NeoRecormon/ Epoetin Beta</b>	6667 I.U./ml micrograms Epoetin Beta 10.06 mg/m Disodium phosphate 15 mg/ml Glycine 2 mg/ml L-Isoleucine 0.5 mg/ml Phenylalanin 0.5mg/ml L-Threonine 0.6 mg/ml Sodium Chloride Polysorbate 20	Anemia	Roche	Reusable, variable dose pen injector	0.3 ml	sc

<b>Name / API</b>	<b>Formulation</b>	<b>Indication</b>	<b>Company</b>	<b>Device</b>	<b>Volume</b>	<b>Route of Application</b>
<b>PEG-Intron/ pegylated Interferon α-2b</b>	67.5 µg PEG-Intron 2.02 mg Disodium/Sodium Phosphate 54 mg Sucrose 0.068 mg Polysorbate 80	Hepatitis C	Schering	Disposable, single use pen injector (Redipen <sup>®</sup> )	0.5 ml	im
<b>Preatact/ Parathyroid hormone</b>	100 µg Parathyroid hormone Citric Acid Sodium Chloride Mannitol	Osteoporosis	Nycomed, NPS Pharmaceutical	Reusable, fixed dose pen injector	1 ml	sc
<b>Saizen/ rhGH</b>	8.8 mg Somatropin 60.2 mg Sucrose 2.05 mg Phosphoric acid	Growth hormone deficiency	Merck Serono	Reusable, variable dose pen	1 ml	sc/im
<b>ViVAXIM/ Salmonella typhi Vi polysaccharide + hepatitis A virus antigen</b>	25 µg Salmonella Typhi VI Polysaccharide 0.088 mg Dibasic/Monobasic Sodium Phosphate 160 ELISA units Hepatitis A Virus Antigen 0.3 mg Aluminium Hydroxide 2.5 µg Phenoxyethanol 12.5 µg Formaldehyde	Salmonella Typhi + Hepatitis A vaccination	Sanofi Pasteur	Syringe	1 ml	im
<b>Xyntha Solofuse/ Antihemophilic factor</b>	250 IU Antihemophilic factor 0.4 mg Polysorbate 80 12 mg Sucrose 6 mg Histidine 1 mg Calcium Chloride 72 mg Sodium Chloride	Factor VIII deficiency or Hemophilia	Pfizer	Lyo-Ject (Vetter)	4 ml	Intravenous iv

### 1.3 Process challenges for freeze-drying in dual chamber cartridges

Despite their clear advantages for the end-user, DCCs represent a challenge for freeze-drying cycle development compared to the traditional vial.<sup>12,16,27</sup> Figure 1-3 summarizes the most important process-related differences between both container formats. For DCCs, the distance between the heated shelf and the product containing front chamber is significantly increased compared to vials.<sup>16</sup> This leads to a decrease in energy transfer efficiency which is further deteriorated by the limited contact area of the hollow glass bottom of the DCC with the shelf.<sup>16,24</sup> Moreover, slow responses to shelf temperature changes<sup>16</sup> demand longer holding times and process control becomes more complicated.<sup>24,31</sup> An integral, if not the most important part of the lyophilization process control is product temperature monitoring, which is normally performed using standard type-T thermocouples (TCs) with a diameter of 0.51 mm.<sup>3,4,32</sup> In the case of the traditional vial, the TCs are inserted from the top through the cavity left by the partially closed vial stopper. Due to the small neck size of the DCCs, these standard TCs cannot be utilized for this novel container format. Special thin-wire TCs<sup>16</sup> need to be used that can be either inserted from the top via special stoppers<sup>16</sup> or through the bottom of the DCC via the middle plunger.<sup>12</sup> The latter option requires special DCC holder system.<sup>12,31</sup>

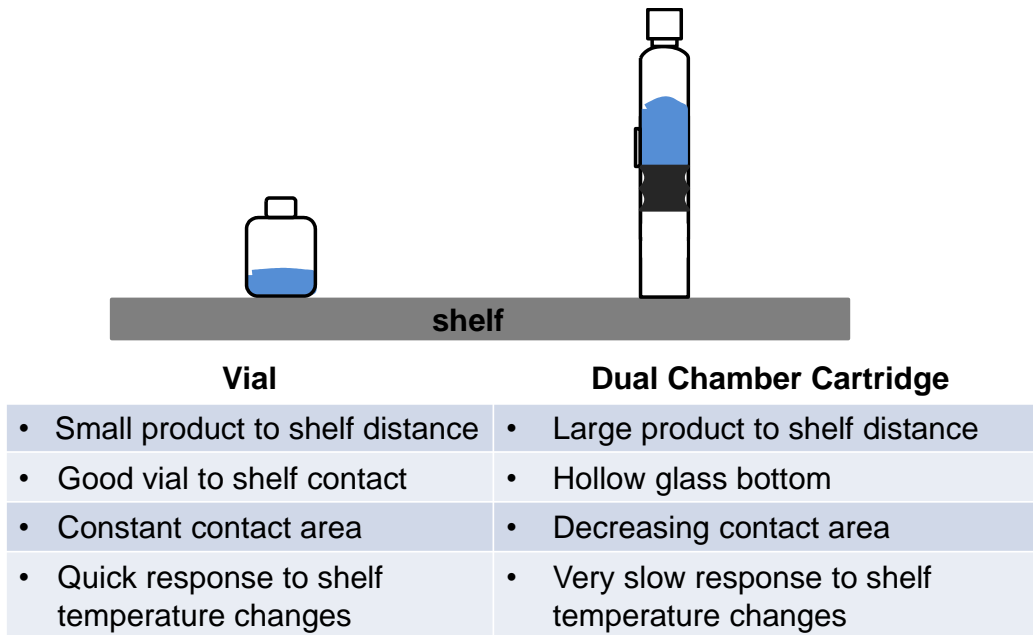


**Figure 1-3 Vial container vs. Dual Chamber Cartridge – modified after Teagarden et al. 2010<sup>24</sup>**

Since DCCs have a smaller diameter than vials, the fill height is larger for the same product volume compared to vials e.g. 19 mm for a fill volume of 1 ml compared to 9.5 mm in a DIN-2R vial container.<sup>12</sup> The result is a larger shell surface area of the frozen product solution with a higher susceptibility to atypical radiation.<sup>16,33</sup> Atypical radiation is an additional amount of energy that is emitted from surfaces within the freeze-dryer that are warmer than the product during the process.<sup>33</sup> DCCs standing at the outer rows of the array, “edge DCCs”, receive this atypical radiation in addition to the heat coming from the shelf which results in faster drying rates and higher temperatures with a potential risk for meltback and collapse.<sup>16,22,31,33</sup> From an end user perspective, another drawback originating from the combined large fill height with a small inner diameter of the DCC, is the decreased wettability of the lyophilized cake due to the small initial contact area of the lyophilisate with the reconstitution volume.<sup>28</sup> This can, especially in the case of highly concentrated protein formulations, lead to prolonged reconstitution times and can complicate the application procedure for the patient.<sup>14</sup> Due to their high center of gravity, DCCs tend to fall over and thus cannot be arranged in the same manner as vials within the freeze-dryer unit but need to be placed in special holder devices.<sup>12,16,31</sup> These holder devices represent barriers against energy transfer and can act as an energy reservoir which is why they need to be thoroughly considered for the lyophilization cycle development.<sup>27,31</sup>

## 1.4 Design related challenges for DCCs

Since DCCs are designed for ready-to-use (after combination with a pen injector), they need to combine the function of a syringe as an applicator, and a traditional vial container as the drug reservoir. Similar to a syringe, DCCs need to provide adequately low gliding forces of the plungers within the DCC barrel (Figure 1-2 (a)) in order to assure an easy and smooth injection.<sup>34</sup> For this reason, the glass barrels of the DCCs are commonly siliconized. For DCCs, spray-baking is the method of choice for the siliconization process since it yields the lowest overall silicone level within the DCC in combination with the most homogeneous silicon oil layer.<sup>24,35</sup> Other rubber components, assembled within the DCC e.g. plungers or stoppers, are siliconized as well to allow better processing due to less sticking to manufacturing equipment.<sup>36</sup> However, silicone oil can disassociate from the inner wall of DCC or rubber components and interact with the product formulation.<sup>24</sup> After reconstitution, this fraction of disassociated silicone oil can lead to foaming and cloudiness of the product solution<sup>24</sup> or impair protein stability and lead to aggregation.<sup>37</sup> This might especially be a problem during the drying stage of the lyophilization process where particularly low molecular weight silicones might leach into the formulation after evaporation due to their low vapor pressure.<sup>24,38</sup> Recent investigations focus on the optimization of the siliconization process step for cartridges in order to circumvent these challenges and to improve long-term product storage.<sup>35,39,40</sup>

Another important design-related challenge is moisture uptake. The unfavorable large ratio of plunger size to lyophilized product cake area and a rear chamber that is completely filled with diluent necessitates strong and impermeable plungers as well as reliable and reproducible drying procedures of all involved rubber components.<sup>24</sup> Additional moisture coming from insufficiently dried rubber components would be easily absorbed by the amorphous lyophilized cake and could impact the physical and chemical stability of the drug product.<sup>41</sup> The residual moisture level within the final product cake is mainly determined by the secondary drying protocol. The shelf temperature setpoint and the runtime of secondary drying strongly impact the amount of bound water remaining in the lyophilisate.<sup>3,8,42</sup>

After this last process step, the DCCs must be sealed quickly in order to maintain the desired level of residual moisture. This sealing or capping step can either be performed inside or outside the freeze-dryer. In contrast to vials where regular

stoppers can be employed, sealing of DCCs inside the lyophilizer entails special lyocaps that can be closed by moving the upper and the lower shelf towards each other.<sup>28,30</sup> If these special caps are not available the DCCs need to be sealed outside the freeze-dryer, exposing the dried product cake to the external environment and atmospheric humidity. Hence, the DCCs should be sealed in a humidity-controlled environment to assure limited moisture uptake. Teagarden et al.<sup>24</sup> showed exemplarily for Caverject<sup>®</sup> that the level of residual moisture is only marginally increased if the unsealed, final product is stored for 24 hours in a transfer cabinet with a relative humidity of 10%. Upon storage in a common clean room environment with a relative humidity of 15% the level of residual moisture increased significantly by a factor of around 2.5 over 24 hours. This indicates that short storage times at low levels of relative humidity, preferably less than 10%, are required for the capping step outside the freeze-dryer unit in order to maintain the intended level of residual moisture.

Furthermore, all other possible sources for moisture uptake to the final formulation must be carefully assessed. Teagarden et al.<sup>24</sup> demonstrated that the residual moisture increased from initially around 1% to almost 3% in the case of Caverject<sup>®</sup> over 35 months storage at 25°C. Around 40% of the additional moisture originated from the diluent chamber and 60% from the plungers<sup>24</sup>. This emphasizes the importance of the aforementioned use of impermeable plungers and reliable drying procedures for all rubber components assembled within the DCC. Similarly, sufficient container closure integrity data must be generated within the development process of a DCC product in order to minimize the risk of leakage upon storage.<sup>24,43</sup>

## 1.5 References

1. Rey LR 1992. Basic aspects and future trends in the freeze-drying of pharmaceuticals. *Developments in biological standardization* 74:3-8.
2. Franks F 1998. Freeze-drying of bioproducts: putting principles into practice. *European Journal of Pharmaceutics and Biopharmaceutics* 45(3):221-229.
3. Pikal MJ, Roy ML, Shah S 1984. Mass and heat transfer in vial freeze-drying of pharmaceuticals: Role of the vial. *Journal of Pharmaceutical Sciences* 73(9):1224-1237.
4. Carpenter J, Pikal M, Chang B, Randolph T 1997. Rational Design of Stable Lyophilized Protein Formulations: Some Practical Advice. *Pharm Res* 14(8):969-975.
5. Kasper JC, Friess W 2011. The freezing step in lyophilization: Physico-chemical fundamentals, freezing methods and consequences on process performance and quality attributes of biopharmaceuticals. *European Journal of Pharmaceutics and Biopharmaceutics* 78(2):248-263.
6. Tang XC, Nail SL, Pikal MJ 2005. Freeze-drying process design by manometric temperature measurement: design of a smart freeze-dryer. *Pharm Res* 22(4):685-700.
7. Konstantinidis AK, Kuu W, Otten L, Nail SL, Sever RR 2011. Controlled nucleation in freeze-drying: effects on pore size in the dried product layer, mass transfer resistance, and primary drying rate. *Journal of Pharmaceutical Sciences* 100(8):3453-3470.
8. Pikal MJ, Shah S, Senior D, Lang JE 1983. Physical chemistry of freeze-drying: Measurement of sublimation rates for frozen aqueous solutions by a microbalance technique. *Journal of Pharmaceutical Sciences* 72(6):635-650.
9. Patel SM, Pikal MJ 2011. Emerging freeze-drying process development and scale-up issues. *AAPS PharmSciTech* 12(1):372-378.
10. Pikal MJ 1985. Use of laboratory data in freeze drying process design: heat and mass transfer coefficients and the computer simulation of freeze drying. *Journal of parenteral science and technology : a publication of the Parenteral Drug Association* 39(3):115-139.
11. Xiang J, Hey JM, Liedtke V, Wang DQ 2004. Investigation of freeze-drying sublimation rates using a freeze-drying microbalance technique. *International Journal of Pharmaceutics* 279(1-2):95-105.
12. Korpus C, Pikal M, Friess W 2016. Heat Transfer Analysis of an Optimized, Flexible Holder System for Freeze-Drying in Dual Chamber Cartridges Using Different State-of-the-Art PAT Tools. *Journal of Pharmaceutical Sciences* 105(11):3304-3313.

13. Geidobler R, Winter G 2013. Controlled ice nucleation in the field of freeze-drying: Fundamentals and technology review. *European Journal of Pharmaceutics and Biopharmaceutics* 85(2):214-222.
14. Geidobler R, Konrad I, Winter G 2013. Can Controlled Ice Nucleation Improve Freeze-Drying of Highly-Concentrated Protein Formulations? *Journal of Pharmaceutical Sciences*: 102(11):3915-3919.
15. Jennings TA. 1999. *Lyophilization : introduction and basic principles*. ed., Denver, Colo. [u.a.]: Interpharm Press. p XVII, 646 S.
16. Korpus C, Haase T, Sönnichsen C, Friess W 2015. Energy Transfer During Freeze-Drying in Dual-Chamber Cartridges. *Journal of Pharmaceutical Sciences* 104(5):1750-1758.
17. Association USFaD. U.S. Food and Drug Administration. *Guide to inspections of lyophilization of parenterals*. ed.
18. Walsh G 2010. Biopharmaceutical benchmarks 2010. *Nature biotechnology* 28(9):917-924.
19. Walsh G 2014. Biopharmaceutical benchmarks 2014. *Nature biotechnology* 32(10):992-1000.
20. Dingjiang Liu DD. 2016. *Antibody Drug Product Formulation: Current Status and Future Directions*. ed., Eighth Annual Bioprocessing Summit, Boston, MA.
21. Ecker DM, Jones SD, Levine HL 2015. The therapeutic monoclonal antibody market. *mAbs* 7(1):9-14.
22. Tang X, Pikal M 2004. Design of Freeze-Drying Processes for Pharmaceuticals: Practical Advice. *Pharm Res* 21(2):191-200.
23. Schwegman JJ, Hardwick LM, Akers MJ 2005. Practical Formulation and Process Development of Freeze-Dried Products. *Pharmaceutical Development and Technology* 10(2):151-173.
24. Teagarden DL, Speaker SM, Martin SWH, Österberg T. 2010. Practical Considerations for Freeze-Drying in Dual Chamber Package Systems. *Freeze Drying/Lyophilization of Pharmaceutical and Biological Products*, ed. p 494-526.
25. Reynolds G 2006. The market need for reconstitution systems. *BioProcess Int* 4(10).
26. Mathaes R, Koulov A, Joerg S, Mahler HC 2016. Subcutaneous Injection Volume of Biopharmaceuticals-Pushing the Boundaries. *Journal of Pharmaceutical Sciences* 105(8):2255-2259.
27. Patel SM, Pikal MJ 2010. Freeze-drying in novel container system: Characterization of heat and mass transfer in glass syringes. *Journal of Pharmaceutical Sciences* 99(7):3188-3204.

28. Werk T, Ludwig IS, Luemkemann J, Mahler HC, Huwyler J, Hafner M 2016. Technology, Applications, and Process Challenges of Dual Chamber Systems. *Journal of Pharmaceutical Sciences* 105(1):4-9.
29. Polin JB 2003. The ins and outs of prefilled syringes. *Pharm Med Packag News* 11(5):40-43.
30. Werk T, Ludwig IS, Luemkemann J, Huwyler J, Mahler H-C, Haeuser CR, Hafner M 2016. New Processes for Freeze-Drying in Dual Chamber Systems. *PDA Journal of Pharmaceutical Science and Technology*:pdajpst. 2015.006155.
31. Korpus C, Friess W 2017. Evaluation of different holder devices for freeze-drying in dual chamber cartridges with a focus on energy transfer. *Journal of Pharmaceutical Sciences* 106(4):1092-1101
32. Kasper JC, Wiggendorf M, Resch M, Friess W 2013. Implementation and evaluation of an optical fiber system as novel process monitoring tool during lyophilization. *European journal of pharmaceuticals and biopharmaceutics* 83(3):449-459.
33. Rambhatla S, Pikal M 2003. Heat and mass transfer scale-up issues during freeze-drying, I: Atypical radiation and the edge vial effect. *AAPS PharmSciTech* 4(2):22-31.
34. Sacha GA, Saffell-Clemmer W, Abram K, Akers MJ 2010. Practical fundamentals of glass, rubber, and plastic sterile packaging systems. *Pharm Dev Technol* 15(1):6-34.
35. Funke S, Matilainen J, Nalenz H, Bechtold-Peters K, Mahler HC, Friess W 2016. Optimization of the bake-on siliconization of cartridges. Part I: Optimization of the spray-on parameters. *European journal of pharmaceuticals and biopharmaceutics* 104:200-215.
36. Sacha G, Rogers JA, Miller RL 2015. Pre-filled syringes: a review of the history, manufacturing and challenges. *Pharm Dev Technol* 20(1):1-11.
37. Gerhardt A, McGraw NR, Schwartz DK, Bee JS, Carpenter JF, Randolph TW 2014. Protein Aggregation and Particle Formation in Prefilled Glass Syringes. *Journal of Pharmaceutical Sciences* 103(6):1601-1612.
38. Mundry T, Schurreit T, Surmann P 2000. The fate of silicone oil during heat-curing glass siliconization--changes in molecular parameters analyzed by size exclusion and high temperature gas chromatography. *PDA journal of pharmaceutical science and technology / PDA* 54(5):383-397.
39. Funke S, Matilainen J, Nalenz H, Bechtold-Peters K, Mahler HC, Friess W 2015. Analysis of thin baked-on silicone layers by FTIR and 3D-Laser Scanning Microscopy. *European journal of pharmaceuticals and biopharmaceutics*: 96:304-313
40. Funke S, Matilainen J, Nalenz H, Bechtold-Peters K, Mahler HC, Vetter F, Muller C, Bracher F, Friess W 2016. Optimization of the bake-on siliconization of

cartridges. Part II: Investigations into burn-in time and temperature. *European journal of pharmaceutics and biopharmaceutics* : 105:209-222.

41. Shalaev EY, Zografi G 1996. How Does Residual Water Affect the Solid-state Degradation of Drugs in the Amorphous State? *Journal of Pharmaceutical Sciences* 85(11):1137-1141.

42. Sheehan P, Liapis AI 1998. Modeling of the primary and secondary drying stages of the freeze drying of pharmaceutical products in vials: numerical results obtained from the solution of a dynamic and spatially multi-dimensional lyophilization model for different operational policies. *Biotechnology and bioengineering* 60(6):712-728.

43. Brown H, Mahler HC, Mellman J, Nieto A, Wagner D, Schaar M, Mathaes R, Kossinna J, Schmitting F, Dreher S, Roehl H, Hemminger M, Wuchner K 2016. Container Closure Integrity Testing - Practical Aspects and Approaches in the Pharmaceutical Industry. *PDA journal of pharmaceutical science and technology / PDA*.

## 2 OBJECTIVES AND OUTLINE OF THE THESIS

The aim of this thesis was to enable an optimal lyophilization process design for freeze-drying of biopharmaceuticals e.g. monoclonal antibody (mAb) formulations in dual chamber cartridges (DCCs) based on a profound process understanding instead of a trial and error approach. Since process development using this modern container device with various advantages compared to the traditional vial had been hardly studied before, fundamental knowledge had to be generated within this thesis.

At the start of the project it was unclear how energy is transferred to the product solution in the DCC during lyophilization in detail. Hence, as a first step, the groundwork of energy transfer during lyophilization in DCCs was elaborated (**Chapter 3**). Sublimation experiments were carried out using pure water and drying rates were determined gravimetrically. Simple aluminum blocks were used as holder devices and heat transfer coefficients were calculated and subdivided into the different modes of energy transfer. The substantial influence of the holder device on the freeze-drying process became obvious and apparently the basic aluminum block device posed a significant need for optimization leading to the design of better holders.

The expertise obtained from studying the aluminum blocks was subsequently used to build and analyze a novel and innovative holder system, the “flexible holder” (**Chapter 4**). The flexible holder should possess a higher heat transfer efficiency, provide an improved shielding against atypical radiation and thus enable the development of optimized freeze-drying cycles. Consequently, the product was embedded into an aluminum plate that completely surrounded the product containing part of the DCC. Aluminum pins that were in direct contact with the shelf should contribute to an efficient energy transfer from shelf to product. To monitor the drying kinetics during the lyophilization process, different state-of-the-art process analytical tools (PAT) e.g. tunable diode laser adsorption spectroscopy (TDLAS) and the pressure rise test (PRT) were applied in addition to the gravimetric procedure. The establishment of a self-made PRT system was delineated that can be easily installed without the need for cost-intensive equipment or software modifications. Another focus was set on the freezing step of the lyophilization process that influences the porosity of the lyophilisate and hence the mass transfer resistance rate ( $R_p$ ). Since  $R_p$  has a

significant impact on the product temperature ( $T_p$ ) and thus product quality, different methods for the controlled nucleation of ice were studied for their applicability for DCCs. Controlled nucleation is a new technology that has not been tested with DCC before. It became evident that due to the small opening of the DCC and with it the slower gas exchange, not every controlled nucleation method is applicable for DCCs.

Since there was no comprehensive data published concerning the advantages and disadvantages of the different types of holder devices commonly used for freeze-drying in DCCs, one example out of each group (block- , flexible- , shell- and a guardrail holder) was analyzed in **Chapter 5**. The main criteria were energy transfer efficiency, drying homogeneity and the ability to shield the product against atypical radiation. Holder devices in which the product containing part of the DCC was completely surrounded by the holder material (flexible- and shell holder) generated more homogeneous drying rates and enhanced process control since they reacted faster to shelf temperature changes. The individual shell holder had the best overall performance with freezing rates that were even faster than for the traditional vial.

That gained knowledge about energy transfer (**Chapter 3**), the purposeful applicability of different PAT tools and controlled nucleation techniques (**Chapter 4**) and the differences between holder systems (**Chapter 5**) was combined in **Chapter 6**. The objective of this chapter was to develop an automated manometric temperature measurement (MTM)-based process control strategy. The “DCC LyoMate” procedure in combination with a self-made PRT system (**Chapter 4**) was successfully applied to conveniently plan and optimize lyophilization processes for DCCs online for different mAb formulations, including highly concentrated mAb formulations. This interesting tool helps to reduce development cost and can be used to build up in-depth process knowledge for this rather new container format. This system helps to shift the process development for DCCs from a trial and error approach towards a science-based, quality-by-design approach which was not possible before.

Finally the main conclusions were summarized in **Chapter 7**.

### 3 *ENERGY TRANSFER DURING FREEZE- DRYING IN DUAL CHAMBER CARTRIDGES*

The following chapter has been published in the Journal of Pharmaceutical Sciences and appears in this thesis with the journal's permission:

**Christoph Korpus**, Thomas Haase , Caren Sönnichsen, Wolfgang Friess 2015

Energy Transfer During Freeze-Drying in Dual-Chamber Cartridges.

Journal of Pharmaceutical Sciences 104(5):1750-1758

### 3.1 Abstract

Freeze-drying essentially requires knowledge about the heat and mass transfer characteristics to assure product quality. Whereas this understanding has been created for freeze-drying in vials, only limited information is available for state-of-the-art multiple compartment container systems such as dual-chamber cartridges (DCCs). Therefore, the aim of this study was to investigate the heat transfer characteristics of this novel container format. Sublimation tests were carried out using pure water at 60, 100, 150, and 200 mTorr chamber pressure at a shelf temperature of 0°C. Custom-made aluminum blocks were used as holder systems. Two heat transfer coefficients could be identified: the coefficient characterizing heat transfer between shelf and block,  $K_{Al}$ , and between block and cartridge,  $K_{DCC}$ .  $K_{Al}$  was dependent on all three modes of heat transfer: contact conduction, gas conduction, and radiation. For  $K_{DCC}$ , contact conduction was negligible. Radiation strongly influenced the overall energy transfer as it is the major mode of heat transfer for  $K_{DCC}$  and contributes up to 44% to  $K_{Al}$ . A third coefficient,  $K_{tot}$ , was defined as an overall heat transfer coefficient. This knowledge about heat transfer enables a purposeful development and control of optimized lyophilization processes for this novel container system.

### 3.2 Introduction

Many biopharmaceuticals, specifically proteins, do not show adequate stability in aqueous solution. Freeze-drying is an effective and gentle approach typically used to enhance chemical stability of these drugs.<sup>1,2</sup> The most common container used for lyophilization is the single dose vial.<sup>3</sup> Prior to administration, reconstitution of the freeze-dried cake with an additional syringe transfer is required. This procedure implies a risk of wrong dosage and needle stick injuries for patients or care personnel. Dual chamber cartridges (DCCs) for lyophilisates are a promising and rather new approach to overcome this critical issue and to enhance patient safety and compliance.<sup>4</sup> The DCC (Figure 3-1) consist of a hollow glass cylinder that is departed into two chambers by an elastomeric middle plunger.

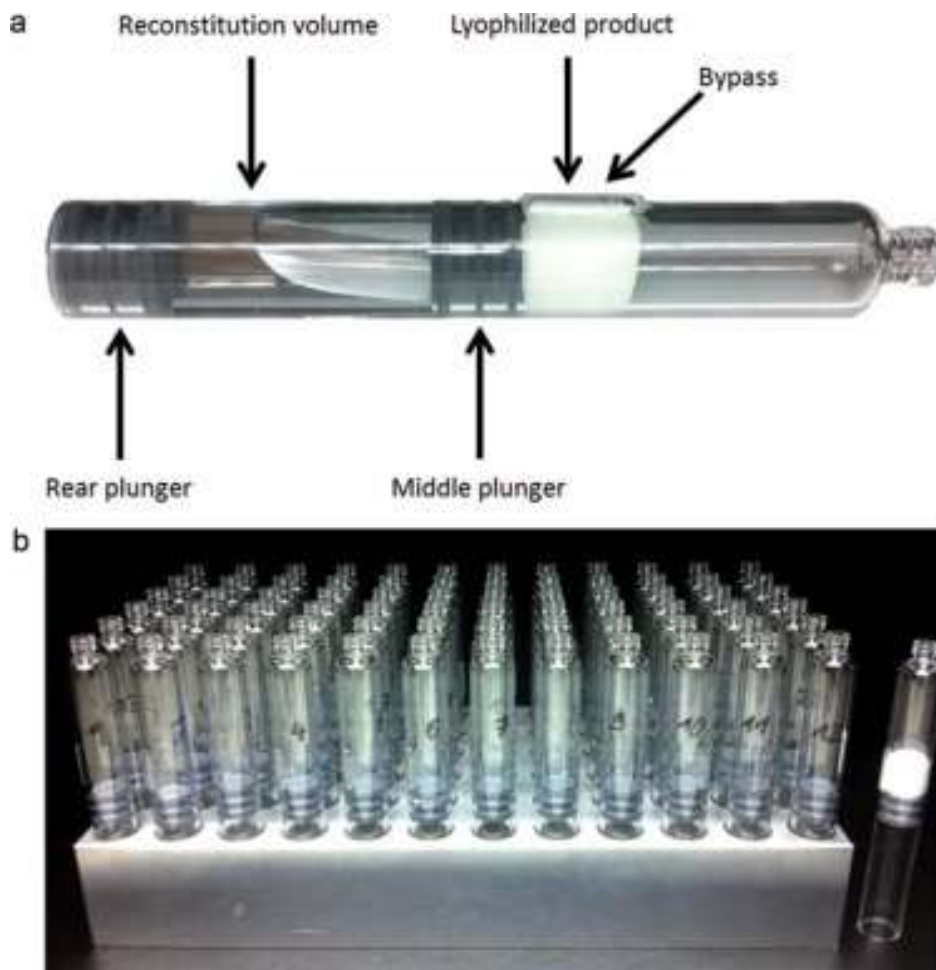


Figure 3-1 (a) The DCC. (b) DCCs standing in the aluminum block holder

The front chamber contains the freeze-dried drug product and the rear chamber contains the reconstitution volume. The external bypass allows the liquid to flow from the rear to the front chamber while reconstituting the drug product.<sup>5</sup> This reconstitution step is performed in combination with a pen injector that has a needle attached to its top. After reconstitution, the drug can be directly administered and no additional transfer step is necessary.

Compared with a traditional vial, the DCC has several advantages: easy reconstitution, increased dose accuracy, lower risk of microbial contamination as well as minimal overfill.<sup>6</sup> Yet the lyophilization process development is more complex than compared with a traditional vial. The increased distance between the shelf and the product solution in the DCC and the small contact area between the bottom of the DCC and the shelf result in a poor heat transfer, slow responses to shelf temperature changes, and therefore longer processing times.<sup>5,7</sup> In order to overcome these process challenges, a suitable DCC holder device is necessary. There are basically three categories of holder devices commonly used in industry. Systems where each DCC is standing in an individual holder are called “sleeve-systems.” If a whole array of DCCs is stabilized via drillings in a block, this version is called “cassette- or block-system,” respectively. The third type is named “test tube rack.” Here, the DCCs are suspended above the shelf hanging in a plastic rack.<sup>5</sup> In the present study, a “block-system” was used. Each type of holder system has a different influence on the freezing and drying behavior of the product in the DCC.

During lyophilization the product temperature ( $T_p$ ) of the formulation is the most important process parameter.<sup>8</sup> If it exceeds a critical temperature like the glass transition temperature ( $T_g'$ ) for an amorphous formulation, product damage can occur.<sup>9</sup> To achieve a  $T_p < T_g$ , a sound process understanding is necessary.<sup>10,11</sup> This essentially requires the knowledge about the heat transfer coefficient of the DCC and its holder device. On the basis of these parameters and in combination with the formulation-specific mass transfer resistance rate ( $R_p$ ), one can design an optimized lyophilization cycle within a limited number of developments runs instead of a larger number of experience based, iterative trial, and error runs. This can help to reduce development costs and to assure product quality. Therefore, the aim of this study was to delineate how energy is transferred from the shelves to the product in the DCCs and which parameters influence this process.

### 3.3 Materials and Methods

#### 3.3.1 Materials

An array of 215 DCCs containing 56 edge and 159 center DCCs (outer diameter 10.75 mm, inner diameter 8.65 mm, 1 ml fill volume) standing in three custom-made aluminum blocks (Figure 3-1b) ( $19.3 \times 9.6 \times 3.0 \text{ cm}^3$ , 958 g, and 72 drillings each) was used to determine the heat transfer coefficient of the aluminum block ( $K_{Al}$ ) and for all DCCs ( $K_{DCC}$ ). The diameter of each drilling in the aluminum block was  $10.8 \pm 0.1 \text{ mm}$ . Aluminum was chosen as the holder material because of its high-thermal conductivity [ $\lambda_{Al} = 237 \text{ W/(m} \cdot \text{K)}$ ]. DCCs used for the sublimation experiments were kindly provided by Nipro Glass Germany AG (Münnerstadt, Germany) and made of clear neutral glass, USP type I. Plungers were made of bromobutyl rubber (FM457-0; Helvoet Pharma, Lommel, Belgium). The lower end of middle plunger was placed  $32 \pm 0.2 \text{ mm}$  away from the bottom of the DCC (Figure 3-1 (a)).

Freeze-drying was performed in a laboratory freeze-dryer Lyostar III (SP Scientific, Stone Ridge, New York) where only the middle shelf was used for all runs. This corresponds to a shelf area of  $0.14 \text{ m}^2$ . The pressure in the freeze-dryer chamber was monitored via a Pirani gauge and a capacitive manometer (MKS Instruments, Andover, Massachusetts). The capacitive manometer was used to determine chamber pressure. Fifteen superthin thermocouples (TC, accuracy  $\pm 0.5^\circ\text{C}$ ; Newport Electronics, Deckenpfronn, Germany) were used to measure temperatures within the cartridges as well as surface temperatures of shelves, walls, and the door of the freeze dryer. TCs were calibrated at  $0^\circ\text{C}$  using an ice water bath and a reference thermometer (Orion™-Star, accuracy  $\pm 0.1^\circ\text{C}$ ; Thermo Scientific, Waltham, Massachusetts). Sublimation experiments were conducted with highly purified water (Purelab Plus; USF Elga, Celle, Germany), which was additionally filtered through a  $0.2\text{-}\mu\text{m}$  membrane filter (VWR, Radnor, Pennsylvania).

### 3.3.2 Sublimation experiments

All DCCs were filled with 1.00 ml highly purified water corresponding to a fill height of 17 mm. Drying was performed at 60, 100, 150, and 200 mTorr chamber pressure. All changes in shelf temperature ( $T_s$ ) were performed at 1°C/min. Holding times for freezing were 15 min at 5°C and -5°C and finally 720 min at -40°C. Drying was performed at 0°C for 260 min. During this time period, a maximum of 35% of the ice was removed via sublimation.<sup>7</sup> In order to determine the sublimation rate  $dm/dt$ , all DCCs were weighed before and after the run on a precision scale ( $\pm 0.01$  mg; Mettler Toledo, Columbus, Ohio).

### 3.3.3 Ramping phase experiments

As the calculations of the heat transfer coefficients refer to a steady-state model, the initial ramping phase of the primary drying step needs to be excluded.<sup>9,12</sup> Therefore, additional runs were already aborted after 70 min (40 min ramping phase and 30 min holding time until steady-state was reached).<sup>9</sup> The amount of ice removed prior to reaching steady-state conditions in primary drying was determined gravimetrically.

### 3.3.4 Experiments with suspended aluminum blocks

In experiments without direct contact conduction and gas conduction between the shelf and the aluminum block, the whole array of aluminum blocks and DCCs was lifted to 72 mm above the shelf using a plastic frame with a low thermal conductivity:  $\lambda = 0.14\text{--}0.21$  W/(mK).<sup>13</sup>

### 3.3.5 Mass and heat transfer theory utilized

The sublimation rate  $dm/dt$  (g/s) describes the amount of ice ( $dm$ ) removed during the time period ( $dt$ ). This mass transfer requires a certain amount of energy, which is represented by the heat flow  $dQ/dt$  (cal/s) in Equation (3-1):

$$\frac{dQ}{dt} = \Delta H_s^* \frac{dm}{dt} \quad (3-1)$$

The heat flow needed to sublime a particular amount of water depends on the sublimation rate  $dm/dt$  and the heat of sublimation of ice that is 660 calories/g.<sup>11</sup> During primary drying, the energy for the sublimation of ice is provided by the heated shelf and can be described by the following relationship<sup>14</sup>:

$$\frac{dQ}{dt} = A_x * K_x * (T_{source} - T_{sink}) \quad (3-2)$$

$T_{source}$  and  $T_{sink}$  are the temperatures (K) of the heat source and the heat sink.  $A_x$  ( $cm^2$ ) represents the area of heat input that is container and holder specific. In the case of the aluminum, block  $A_{Al}$  is the surface area of the block ( $cm^2$ ) divided by the number of DCCs in the block. For the DCCs,  $A_{DCC}$  has to be calculated based on geometrical properties and theoretical considerations. In this study,  $A_{DCC}$  was determined by averaging the shell surface area of the ice in the DCC at the beginning and the end of primary drying Equation (3-3):

$$A_{DCC} = 2 * \pi * r * \frac{(h_0 - h_{end PD})}{2} \quad (3-3)$$

$h_0$  and  $h_{end PD}$  represent the height of the frozen solution at the beginning and the end of primary drying and  $r$  is the inner radius of a DCC (Figure 3-2).

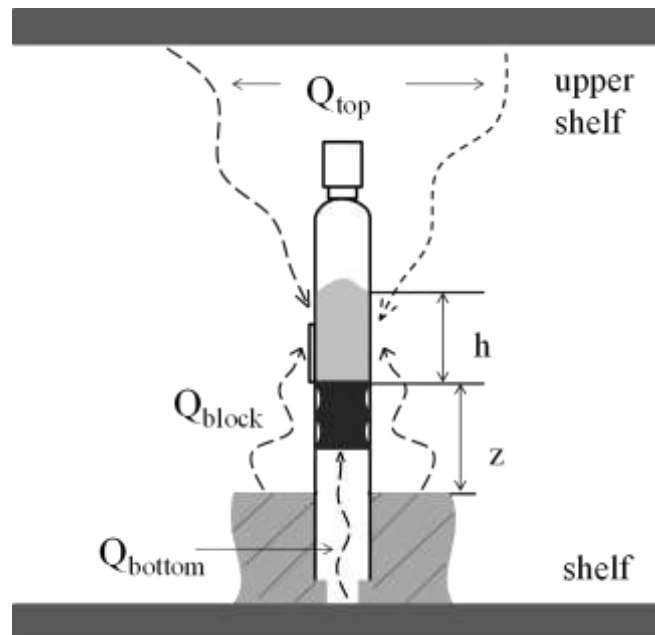


**Figure 3-2 Radiative heat flow to a center DCC.  $Q_{top}$ : heat flow from the upper shelf to the side of the DCC.  $Q_{block}$ : radiation from the aluminum block to the side of the DCC.  $Q_{bottom}$ : radiation from the shelf to the bottom of the middle plunger.**

$K_x$  is the heat transfer coefficient of the corresponding container or holder system [cal/(s cm<sup>2</sup> K)]. It is defined as the “area-normalized heat flow to the temperature difference between heat source and heat sink.”<sup>9</sup> In other words it expresses how effective energy transfer between heat source and heat sink takes place.  $K_x$  represents either  $K_{Al}$  or  $K_{DCC}$ .  $K_{Al}$  describes the heat flow between shelf and aluminum block.  $K_{DCC}$  depicts the heat flow from the aluminum block and the upper shelf to one DCC standing in the block. The combination of Equations(3-1) and (3-2) yields Equation (3-4), which describes the combined heat and mass flow on the example of an aluminum block holder<sup>7</sup>:

$$A_{Al} * K_{Al} * (T_s - T_{Al}) = \Delta H_s * \frac{dm}{dt} \quad (3-4)$$

$T_s$  and  $T_{Al}$  are the temperatures (K) of the shelf and the aluminum block. The left side of the equation shows the energy brought into the system coming from the heated shelf and the right side represents the heat removed via sublimation. Equation (3-4) is valid when all heat provided by the shelf is solely used to sustain ice sublimation. This condition is called steady-state.<sup>9</sup>

The DCC heat transfer coefficient,  $K_{DCC}$ , was determined individually for every DCC in the experimental setup. Here, the product temperature,  $T_p$ , acts as heat sink and  $T_{Al}$  as heat source.  $T_p$  represents the average product temperature during steady-state. In order to distinguish between DCCs standing in the center and the edge positions of the array, different average thermocouple readouts, corresponding to edge or center positions, were used to determine  $T_p$ . Both heat transfer coefficients can be divided into three parts (Figure 3-3)<sup>9</sup>:

$$K_x = K_{c/x} + K_{r/x} + K_{g/x} \quad (3-5)$$

Correspondingly,  $K_{Al}$  is the sum of radiation coming from the shelves hitting the block ( $K_{r/Al}$ ), direct contact conduction ( $K_{c/Al}$ ) between the shelf and the block, and gas conduction ( $K_{g/Al}$ ) from the gas entrapped between the lower shelf and the aluminum block.  $K_{DCC}$  is the sum of radiation from the aluminum block and the upper shelf ( $K_{r/DCC}$ ), direct contact ( $K_{c/DCC}$ ), and gas conduction ( $K_{g/DCC}$ ) between the block and the cartridge. During primary drying, the walls and the door of the freeze-dryer run at a higher temperature than the product in the DCCs and the aluminum block, and therefore emit an additional amount of radiation that is called “atypical radiation.”<sup>15</sup>

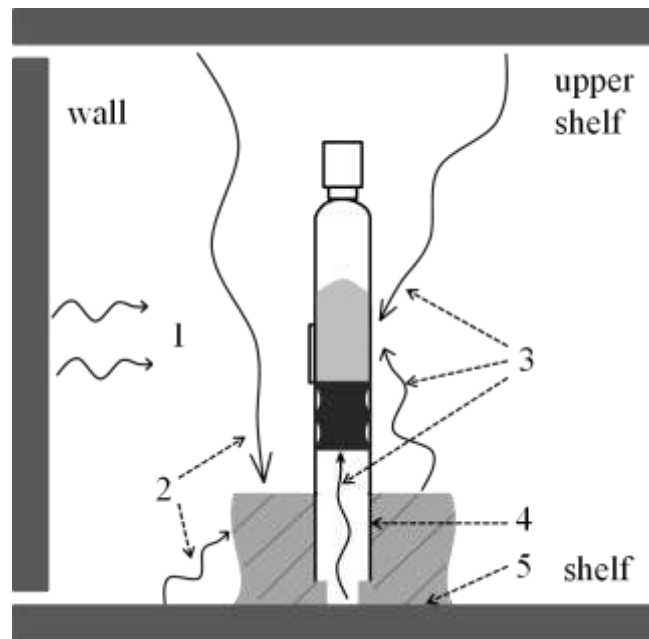


**Figure 3-3 Different modes of heat transfer into the DCC standing in an aluminum block. 1: Atypical radiation coming from the side, hitting the aluminum block and the DCC; 2: Radiation from the shelves hitting the aluminum block; 3: Radiation from the aluminum block and the upper shelf, hitting the DCC; 4: Direct contact conduction and gas conduction between the aluminum block and the DCC; 5: Direct contact conduction and gas conduction between the shelf and the aluminum block.**

Although  $K_c$  and  $K_r$  are independent of the gas pressure in the freeze-drying chamber, the contribution of  $K_g$  increases with a rise in chamber pressure according to Equation (3-6):

$$K_g = \frac{\alpha \Lambda_0 P}{1 + l_x \left( \frac{\alpha \Lambda_0}{\lambda_0} \right) P} \quad (3-6)$$

where  $\lambda_0$  is the heat conductivity of the gas at ambient pressure [4.29E-5 cal/(cm s K)],  $\Lambda_0$  is the free molecular heat conductivity of the gas at 0°C [6.34E-3 cal/(cm<sup>2</sup> s Torr)],  $P$  is the chamber pressure (Torr),  $l_x$  is the mean separation distance between the heat source and the heat sink (cm) and  $\alpha$  is a function of the heat accommodation coefficient,  $\alpha_c$ , and the absolute temperature of the of the gas,  $T_{\text{gas}}$ .<sup>9</sup>

$$\alpha = \frac{\alpha_c}{2-\alpha_c} * \sqrt{\frac{273,15}{T_{gas}}} \quad (3-7)$$

By combination of Equations. (3-5) and (3-6), one can describe  $K_x$  based on Equation (3-8)<sup>9</sup>:

$$K_{Al} = K_{r/Al} + K_{c/Al} + \frac{\alpha * \lambda_0 * P}{1 + l_x * \left(\frac{\alpha * \lambda_0}{\lambda_0}\right) * P} \quad (3-8)$$

When investigating  $K_{Al}$  at different pressure settings, Equation (3-8) was used for a nonlinear regression analysis with Origin 8 (OriginLab Corporation, Northampton, Massachusetts). The y-intercept of the fitted curve ( $P = 0$  Torr) was equal to  $K_{r/Al} + K_{c/Al}$ . Furthermore,  $l_x$  was obtained as an output parameter of the fit. Radiative heat input  $(dQ/dt)_r$  can be described by the Stefan— Boltzmann law<sup>7</sup>:

$$\frac{dQ}{dt}_r = A_x * \epsilon * \sigma * (T_1^4 - T_2^4) \quad (3-9)$$

$T_1$  (K) is the temperature of a body running at higher temperature than the body receiving the radiation with its temperature  $T_2$  (K).  $\sigma$  is the Stefan—Boltzmann constant ( $1.35E-12$  cal/(s\*cm<sup>2</sup>\*K<sup>4</sup>) and  $\epsilon$  is the effective emissivity for heat exchange. The effective emissivity depends on the emissivities of the emitting and receiving surfaces and the geometric view factor. The geometric view factor represents the distances and areas of heat source and heat sink as well as the “view” in terms of emission angles. For the aluminum blocks,  $K_{r/Al}$  could be determined via suspending the array of holder and DCCs above the shelf as described earlier. For the DCCs, the influence of radiation,  $K_{r/DCC}$ , could be specified by a rather complex calculation that will be outlined in the following.

### 3.3.6 Theoretical calculation of $K_{r/DCC}$

Radiation hitting a DCC standing in the center of the array can be departed into three contributions coming from the upper shelf, the aluminum block, and the lower shelf (Figure 3-2). The combination of the Stefan–Boltzmann law and Equation (3-2) was used to calculate the heat transfer coefficients corresponding to the three different sources of radiation. To quantify the radiative heat transfer from the bottom of the upper shelf to the side of one DCC (“ $Q_{top}$ ”; Figure 3-2), the mean shell surface area of the DCC,  $A_{DCC}$  Equation (3-3), and the effective emissivity of the shelf  $e_s$  (0.84) were used as parameters for the calculations.<sup>9</sup> Moreover, the mean temperature of the upper shelf,  $T_{us}$ , and mean values of TCs monitoring center DCCs,  $T_p$ , were used.<sup>9</sup> The heat transfer coefficient for top radiation hitting a center DCC,  $K_{r/DCCtop}$ , was calculated using Equation (3-10):

$$K_{r/DCC\ top} = \frac{Q_{top}}{A_{DCC} * (T_{us} - T_p)} \quad (3-10)$$

Radiation from the lower shelf (“ $Q_{bottom}$ ”; Figure 3-2) could be neglected for these calculations as it only hits the middle plunger made of bromobutyl rubber with a very low-thermal conductivity of 0.09 W/(m\*K).<sup>13</sup> To quantify the heat flow from the aluminum block hitting the side of the DCC,  $Q_{block}$ , the effective emissivity ( $\epsilon_{12}$ ) of the aluminum block had to be determined to be able to use the Stefan-Boltzmann law. As the radiation emitted by the aluminum block is hitting an elevated product, the geometric dimensions had to be taken into account by using a geometric view factor. The calculation of this geometric view factor  $F_{21}$  of a cylindrical surface, like the DCC, to a circular area was described by Shukla and Ghosh<sup>16</sup> and is summarized in Equation (3-11):

$$\begin{aligned}
2\pi F_{21} = & \cos^{-1} \left\{ \frac{(z+h)^2 - r_1^2 + r_2^2}{(z+h)^2 + r_1^2 - r_2^2} \right\} - \cos^{-1} \left\{ \frac{z^2 - r_1^2 + r_2^2}{z^2 + r_1^2 - r_2^2} \right\} \\
& - \frac{[\{(z+h)^2 + r_1^2 + r_2^2\}^2 - 4 * r_1^2 * r_2^2]^{\frac{1}{2}}}{2 * r_2 * (z+h)} * \cos^{-1} \left[ \frac{r_2}{r_1} * \left\{ \frac{(z+h)^2 - r_1^2 + r_2^2}{z^2 + r_1^2 - r_2^2} \right\} \right] \\
& + \frac{[\{z^2 + r_1^2 + r_2^2\}^2 - 4 * r_1^2 * r_2^2]^{\frac{1}{2}}}{2 * r_2 * z} * \cos^{-1} \left\{ \frac{r_2}{r_1} * \left( \frac{z^2 - r_1^2 + r_2^2}{z^2 + r_1^2 - r_2^2} \right) \right\} \\
& + \frac{h}{2 * r_2} * \cos^{-1} \left( \frac{r_2}{r_1} \right) + \left( \frac{r_1^2 - r_2^2}{2 * r_2} \right) * \left( \frac{1}{z+h} - \frac{1}{z} \right) * \left( \frac{\pi}{2} + \sin^{-1} \frac{r_2}{r_1} \right)
\end{aligned} \tag{3-11}$$

The parameters included in Equation (3-11) are the distance between the aluminum block and the bottom of the frozen product,  $z$ , the height of the frozen solution,  $h$ , the inside radius of a DCC,  $r^2$  (Figure 3-2), and the radius of an imaginary disk on the shelf,  $r_1$ . As mentioned above, this equation was defined for a circular area, which was not given with the aluminum block. Hence, a simplified imaginary disk with its radius  $r_1$  was defined, containing the same area as the surface of the block having a view to the DCC (Figure 3-4).

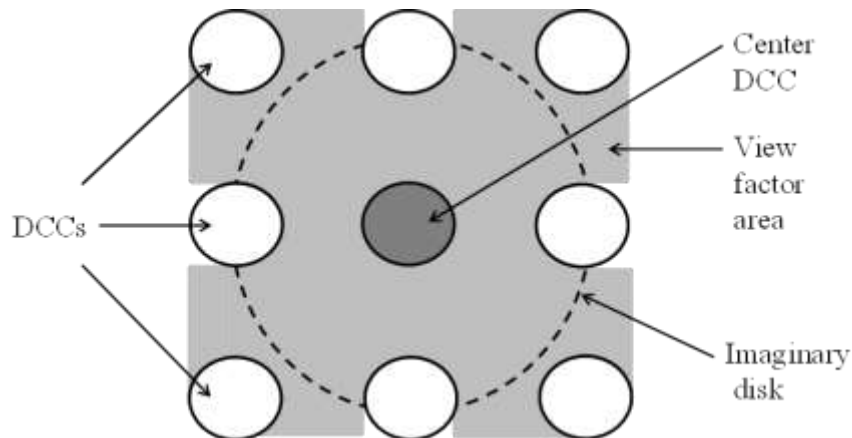


**Figure 3-4** Illustration of the imaginary disk on the aluminum block having a view on a characteristic center DCC. The circular area of the imaginary disk was calculated to be equal to the grey surface area of the aluminum block having a view on the sides of the center DCC (“view factor area”)

The view factor area (gray area in Figure 3-4) was calculated based on geometrical dimensions and was determined to be  $6.93 \text{ cm}^2$ . The radius of the imaginary disk,  $r_1$ , was then calculated using Equation (3-12) and Equation (3-13).

$$A_{grey} = A_{disk} = r_1^2 * \pi \quad (3-12)$$

$$r_1 = \sqrt{\frac{A_{grey}}{\pi}} = \sqrt{\frac{6.93 \text{ cm}^2}{\pi}} = 1.485 \text{ cm} \quad (3-13)$$

To evaluate the view factor from the imaginary disk to the side of the cartridge, the view factor  $F_{21}$  was transformed to the view factor  $F_{12}$ . This was achieved by using the reciprocal relationship of the view factors and the corresponding areas given in Equation (3-14).  $A_{DCC}$  is the mean shell surface area of the cartridge, correlating to the height of the frozen solution as described in Equation (3-3).

$$F_{12} = F_{21} * \frac{A_{DCC}}{A_{disk}} = F_{21} \frac{2 * r_2 * h * \pi}{r_1^2 * \pi} \quad (3-14)$$

The view factor  $F_{12}$ , the surfaces  $A_{DCC}$  and  $A_{disk}$ , as well as the emissivities of the Al-block  $e_{Al}$  (0.33) and the glass cartridge  $e_g$  (0.95) were then used to calculate the effective emissivity  $\epsilon_{12}$  according to Equation (3-15):<sup>7</sup>

$$\epsilon_{12} = \frac{1}{\frac{1}{F_{12}} + \frac{1}{e_{Al} - 1} + \frac{A_{disk}}{A_{DCC}} * \left(\frac{1}{e_g} - 1\right)} \quad (3-15)$$

Now the radiative heat flow from the aluminum block to the side of a typical center DCC could be determined using the Stefan-Boltzmann law:

$$Q_{block} = \sigma * A_{disk} * \epsilon_{12} * (T_{Al}^4 - T_p^4) \quad (3-16)$$

where  $T_{Al}$  is the mean temperature of the aluminum block measured with a thermocouple and  $T_p$  is the mean value of thermocouples monitoring center DCCs. The heat transfer coefficient of radiation to a center DCC coming from the aluminum block,  $K_{r/DCC/block}$ , was calculated analogue to Equation (3-10) but with  $T_{Al}$  as heat source and  $T_p$  as heat sink.

## 3.4 Results and Discussion

### 3.4.1 Sublimation rates and product temperatures

According to the steady-state theory of heat and mass transfer, the heat input during primary drying is proportional to the amount of ice removed via sublimation.<sup>9,12</sup> Hence, the sublimation rate is an important parameter for process analysis and can be used to characterize the energy transfer efficiency during primary drying (Equation (3-4)). Figure 3-5 illustrates the sublimation rates and product temperatures of DCCs, standing in the center of the array, at different chamber pressures.

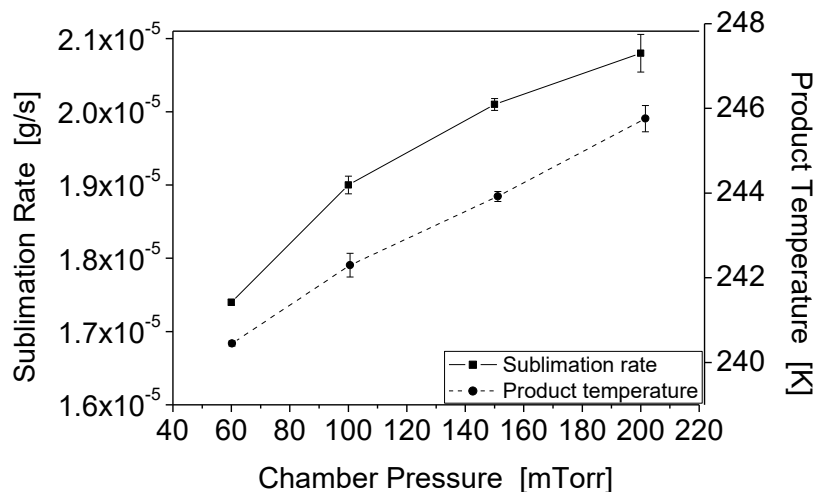


**Figure 3-5 Sublimation rates and product temperatures of center DCCs at different chamber pressures. Error bars represent standard deviations from triplicates**

The average sublimation rate increased by approximately 20% with an increase in chamber pressure from 60 to 200 mTorr. This is in good accordance to literature: Patel and Pikal<sup>7</sup> observed an increase of the sublimation rate by approximately 31%, for glass syringes that were completely immersed into an aluminum block, with an increase in chamber pressure from 60 to 250 mTorr. In a different study, Hottot et al.<sup>17</sup> investigated the drying kinetics of an array of plastic syringes hanging in a plastic-rack holder. They showed that the sublimation rates decreased with an increase in chamber pressure as no gas layer was formed between the shelf and the holder system. In the present study, not only the sublimation rate increased with pressure but also the product temperature went up by approximately 5 K (Figure 3-5).

Normally, one would expect a decreasing product temperature with an increase in sublimation rate because of a higher degree of self-cooling.<sup>8,11</sup> However, as will be outlined in the course of this study, this effect was being diminished by a pressure-dependent increase in heat transfer. Moreover, a clear edge effect as it is known from vials could be seen. The outermost row of DCCs showed a significantly higher sublimation rate than center DCCs (Figure 3-6).<sup>15</sup>

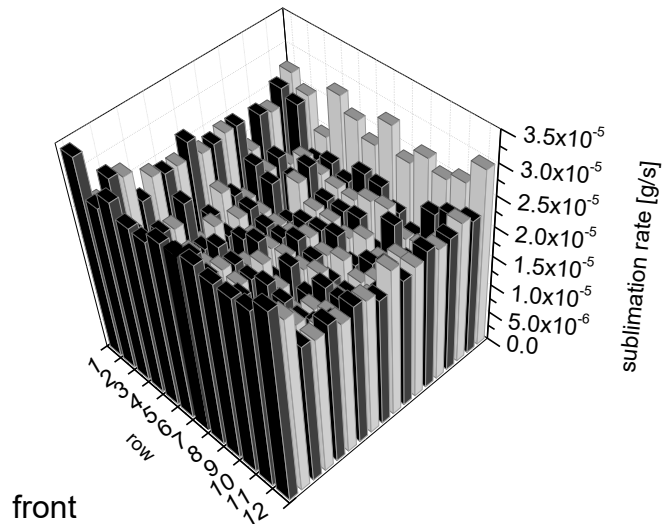


**Figure 3-6 Shelf mapping of sublimation rates at 150 mTorr. Each column represents the sublimation rate of a DCC at the respective position. The mean sublimation rate for center DCCs was  $1.88\text{E-}5$  g/s and  $2.82\text{E-}5$  g/s for edge DCCs. This corresponds to a difference of 33% for this experiment.**

On average, the sublimation rates were around 30% higher for edge DCCs compared with center DCCs. In exceptional cases, sublimation rates were elevated by up to 50% for edge cartridges. Although significantly higher sublimation rates for edge vials are common, Pikal and coworkers<sup>7,11</sup> observed only an approximate 4% higher sublimation rate for edge syringes with the drying product completely embedded in an aluminum block. The present setup with the product above the aluminum block is hence more exposed to atypical radiation and does not provide an adequate radiation shielding for the DCCs standing in the edge positions.

### 3.4.2 Characterization of the aluminum block heat transfer coefficient

$$K_{Al}$$

Values for  $K_{Al}$  were calculated according to Equation (3-4) and corrected for the nonsteady-state conditions during the ramping phase, as well as for the heating up of the aluminum block during primary drying:

$$\frac{dQ}{dt_{Al}} = \frac{c_{p/Al} * m_{Al} * \Delta T_{Al}}{t} \quad (3-17)$$

where  $c_{p/Al}$  is the specific heat capacity of aluminum [897 J/(kg K)],  $m_{Al}$  is the mass of the aluminum blocks,  $\Delta T_{Al}$  is the temperature difference between the beginning and the end of the steady-state, and  $t$  is the time of the steady-state.<sup>18</sup> Table 3-1 provides an overview of the heat flows due to the sublimation of ice ( $Q_{sub}$ ) and to heat up the aluminum block ( $Q_{Al}$ ).

**Table 3-1 Comparison of heat flows because of sublimation of ice ( $Q_{sub}$ ) and heating up of the aluminum block during pseudo steady-state conditions ( $Q_{Al}$ ) at different pressure settings**

Pressure [mTorr]	60	100	150	200
$Q_{sub}$ [cal/s]	1.15E-02	1.25E-02	1.33E-02	1.37E-02
$Q_{Al}$ [cal/s]	1.76E-03	1.58E-03	1.29E-03	1.04E-03
$Q_{total}$ [cal/s]	1.33E-02	1.41E-02	1.46E-02	1.48E-02
$Q_{Al}$ - portion of $Q_{total}$	13.30 %	11.19 %	8.83 %	7.02 %

The overall heat flow " $Q_{total}$ ", in combination with Equation (3-4), was then used to calculate  $K_{Al}$ . Hereby, the right side of Equation (3-4), which is equal to  $Q_{sub}$ , was replaced by  $Q_{tot}$ . Furthermore, the heat flow was corrected for the ramping phase prior to steady-state conditions as mentioned earlier. The amount of ice removed during this nonsteady-state ramp period was rather small with portions of 3.5%, 3.0%, 2.6%, and 2.3% of the fill volume at chamber pressures of 60, 100, 150 and 200 mTorr. The corrected values for  $K_{Al}$  at different pressure settings are summarized in Table 3-2.

**Table 3-2 Heat transfer coefficient between the shelf and the Al block,  $K_{Al}$ , for different pressure settings**

Pressure [mTorr]	60	100	150	200
$K_{Al}$ [cal/(s*cm <sup>2</sup> *K)]	3.51E-04	4.54E-04	5.80E-04	6.21E-04
	± 9.65E-06	± 1.21E-05	± 1.90E-05	± 1.79E-05

In two similar studies, a value of  $5.8E-4$  cal/(s\*cm<sup>2</sup>\*K) for an aluminum tray and approximately  $2.2E-4$  cal/(s\*cm<sup>2</sup>\*K) for aluminum blocks resting on a shelf at 100 mTorr has been reported.<sup>7,9</sup> The discrepancies between these values may arise from different emissivities of the shelf surfaces and the aluminum and differences in the mean separation distance between the shelf and the aluminum holder.<sup>7</sup> Overall, heat transfer from the shelf to the aluminum block can be regarded as efficient in the present setup. The plot of  $K_{Al}$  versus chamber pressure shows the typical nonlinear dependence well known from vials (Figure 3-7).

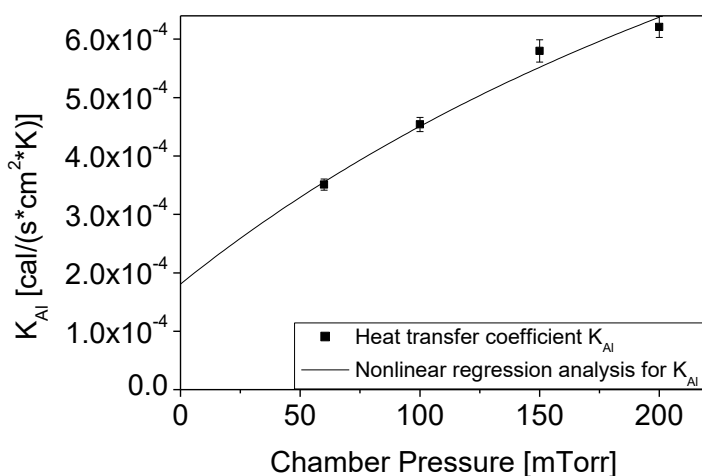


**Figure 3-7 Nonlinear regression analysis of  $K_{Al}$  versus chamber pressure.  $K_{Al}$  values represent mean values of triplicates; error bars represent standard deviations. The coefficient of determination,  $R^2$ , is 0.979; the y-intercept is at  $1.8E-4$  cal/(s\*cm<sup>2</sup>\*K).**

The y-intercept, corresponding to the sum of the pressure-independent terms  $K_{c/Al}$  and  $K_{r/Al}$  was  $1.8E-4 \text{ cal}/(\text{s}\cdot\text{cm}^2\cdot\text{K})$ . The mean separation distance between the shelf and the aluminum block obtained by regression analysis was 0.03 cm. This value is in good accordance to reported literature values of 0.02 cm for an aluminum tray and 0.09 cm for an aluminum block resting on a shelf.<sup>7,9</sup>

### 3.4.3 Different modes of heat transfer for $K_{Al}$

Figure 3-8 summarizes the heat flow via all three modes of heat transfer, namely, gas conduction, radiation, and direct contact conduction from the shelf to the aluminum block.

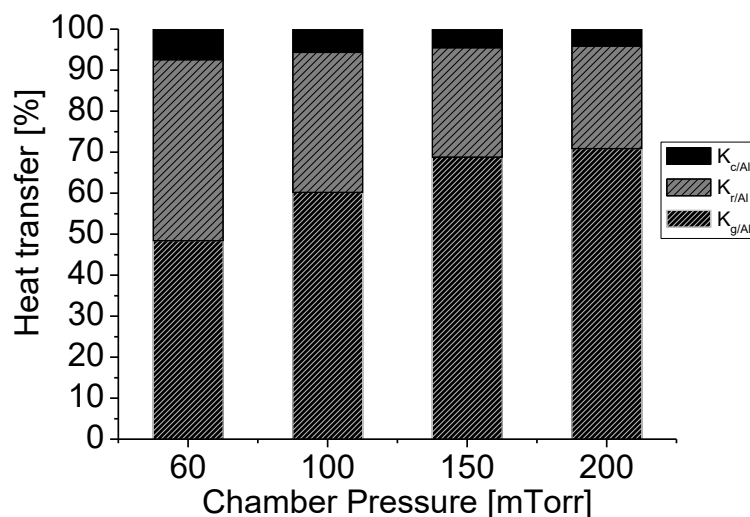


**Figure 3-8 Contribution of  $K_g$ ,  $K_r$ , and  $K_c$  to  $K_{Al}$  at different chamber pressures.**

$K_{g/Al}$  increased by a factor of 2.6, both theoretically calculated and experimentally determined over the pressure range investigated. Generally, the results obtained experimentally and theoretically were in very good agreement (Table 3-3). Compared with literature, the influence of gas conduction in our holder system was rather low: for an aluminum block resting on a shelf, a  $K_g$ - share of  $K_{Al}$  of approximately 78% at 60 mTorr and approximately 87% at 200 mTorr was reported.<sup>7</sup>

**Table 3-3 Absolute values of  $K_{g/Al}$  and portions of  $K_{Al}$ , determined both by theoretical calculations and experimentally.**

Pressure [mTorr]		60	100	150	200
Calculated	$K_{g/Al}$ [cal/(s*cm <sup>2</sup> *K)]	1.75E-04	2.69E-04	3.69E-04	4.53E-04
	Portion of $K_{Al}$ [%]	49.9%	59.2%	63.6%	73.0%
Experimentally determined	$K_{g/Al}$ [cal/(s*cm <sup>2</sup> *K)]	1.70E-04	2.74E-04	3.99E-04	4.40E-04
	Portion of $K_{Al}$ [%]	48.4%	60.2%	68.8%	70.9%

In contrast, the influence of heat transfer via radiation,  $K_{r/Al}$ , determined via suspending the aluminum blocks, was increased with 44.2% at 60 mTorr in the present study versus approximately 10% reported by literature.<sup>7</sup> The results of  $K_{r/Al}$  were 1.54E-4 cal/(s\*cm<sup>2</sup>\*K) for 30 mTorr and 1.56E-4 cal/(s\*cm<sup>2</sup>\*K) for 200 mTorr, indicating that suspending the blocks successfully eliminated gas conduction and its pressure dependence. The relative contribution of  $K_{r/Al}$  to  $K_{Al}$  at 100 mTorr of 34% corresponded well to the contribution of radiation during lyophilization in vials.<sup>9</sup> The influence of direct contact conduction,  $K_c$ , to the heat transfer coefficient  $K_{Al}$  was calculated according to Equation (3-8). As  $K_{c/Al}$  was pressure-independent and  $K_{Al}$  increased with pressure, the relative influence of  $K_{c/Al}$  decreased with increasing pressure from 7.4% at 60 mTorr to 4.1% at 200 mTorr (Figure 3-8).

### 3.4.4 Characterization of the DCC heat transfer coefficient $K_{DCC}$

Subsequently, the heat transfer coefficient between the aluminum block and the DCC was studied. As a first approximation,  $K_{DCC}$  was calculated using Equation (3-4) with the temperature of the aluminum block as the only heat source. However, preliminary calculations for  $K_{r/DCC}$  based on Equation (3-9) revealed the upper shelf to be the most important heat source for the energy transfer to one typical center DCC. Thus, a “weighted temperature” had to be used for the calculation of  $K_{DCC}$ . The weighting was pressure-dependent and in the range of 4:1 – 4.5:1 based on the calculated heat transfer coefficients between the upper shelf and the DCC ( $K_{r/DCC/top}$ ) and between the aluminum block and the DCC ( $K_{r/DCC/block}$ ). The ratio between  $K_{r/DCC/top}$ – $K_{r/DCC/block}$  varies from 4.5:1 at 60 mTorr to 4.24:1 at 200 mTorr (Table 3-4).

**Table 3-4 Radiative heat transfer coefficients and  $K_{r/DCC}$  portions of  $K_{DCC}$  at different chamber pressures.**

Pressure [mTorr]	60	100	150	200
$K_{r/DCC/block}$ [cal/(s*cm <sup>2</sup> *K)]	1.68E-05	1.75E-05	1.80E-05	1.85E-05
$K_{r/DCC/top}$ [cal/(s*cm <sup>2</sup> *K)]	7.56E-05	7.66E-05	7.72E-05	7.84E-05
$K_{r/DCC}$ [cal/(s*cm <sup>2</sup> *K)]	9.23E-05	9.41E-05	9.53E-05	9.69E-05
Portion of $K_{DCC}$	91.0 %	81.4 %	75.0 %	69.3 %

The reason for this difference in heat flows will be explained in the next section. As for  $K_{AI}$  values, the heating of the block during steady-state was taken into account.  $K_{DCC}$  values ranged from 1.01E-7 cal/(s\*cm<sup>2</sup>\*K) at 60 mTorr to 1.4E-4 cal/(s\*cm<sup>2</sup>\*K) at 200 mTorr for center DCCs and from 1.78E-4 to 2.21E-4 cal/(s\*cm<sup>2</sup>\*K) for edge DCCs. The energy difference between edge and center DCCs was pressure-independent, and the result of atypical radiation as outlined by Rambhatla and Pikal.<sup>15</sup> Theoretical calculation of this additional amount of radiation based on Equation (3-9) yielded a value of 7.81E-5 cal/(s\*cm<sup>2</sup>\*K), which was in excellent agreement with the experimental value of approximately 7.8E-5 cal/(s\*cm<sup>2</sup>\*K). Generally,  $K_{DCC}$  values were smaller as compared with values for vials [3E-4 to 6E-4 cal/(s\*cm<sup>2</sup>\*K) for the investigated pressure range] or compared with syringes completely immersed into an aluminum block [ $\sim$  3E-4 cal/(s\*cm<sup>2</sup>\*K) at a chamber pressure of 60 mTorr].<sup>7,9</sup> In the current setup, one would expect  $K_{DCC}$  to be pressure independent, as gas conduction does not play a significant role if the separation distance is in the order of millimeter or greater.<sup>7</sup> Still,  $K_{DCC}$  increased slightly with pressure (Figure 3-9). The linear increase was rather unexpected, as gas conduction followed a nonlinear trend (Figure 3-7). Possibly, the gas layer formed between aluminum block and DCC only heated up the glass of the DCC. As the product was not embedded in the block, the heat had to be transported upwards along the glass and then into the product, minimizing the overall influence of chamber pressure.

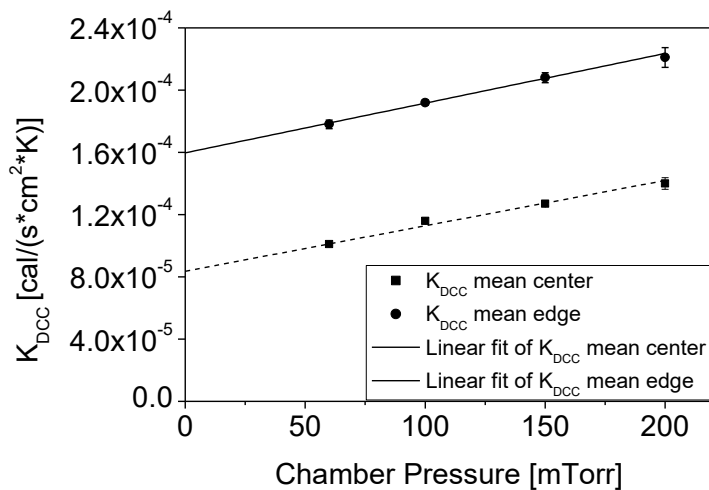


**Figure 3-9 Linear regression analysis of  $K_{DCC}$  values versus pressure for both edge and center DCCs. Error bars represent standard deviations from triplicates.**

### 3.4.5 Different modes of heat transfer for $K_{DCC}$

Radiative heat flows from the aluminum block and the upper shelf to the DCC were calculated as delineated earlier. For the amount of radiation emitted by the aluminum block hitting the DCCs, a view factor of 0.18 was determined. The effective emissivity was calculated to be 0.13 and met the expectations that it had to be lower than the emissivity of the aluminum block, which was determined to be 0.33. The limited area on the block surface having a view to the elevated product restrained the emissivity. The results obtained for  $K_{r/DCC}$  are summarized in Table 3-4.  $K_{r/DCC}$  was the sum of the radiative heat flow from the upper shelf,  $K_{r/DCC/top}$ , and from the aluminum block,  $K_{r/DCC/block}$  (Figure 3-4). Radiation coming from the upper shelf was fourfold to 4.5-fold higher than the radiation from the aluminum block. This was for two reasons, the higher effective emissivity of the stainless steel shelf of 0.84 compared with the aluminum block (0.13) and the higher temperature of the emitting surface  $T_s$  (269.3 K) versus  $T_{Al}$  (255.2 K) at 60 mTorr. Interestingly,  $K_{r/DCC}$  increased by about 5% within the investigated pressure range. This would implicate a pressure dependence of radiation, which contradicts its definition. However, radiation is dependent on the temperatures of heat source and heat sink. With higher pressure, the product temperature increased by approximately 5 K, whereas the upper shelf temperature increased only by approximately 1 K leading to a smaller temperature

difference and higher  $K_{r/DCC}$  values with increasing pressure. This heat transfer to a product elevated above the heat source may be compared with experiments using suspended syringes. In a setup like this, no direct contact between heat source and heat sink exists and thus direct contact conduction is considered to be minimal.<sup>7</sup> In the present study,  $K_{DCC}$  increased slightly with pressure suggesting that the heat transfer is not solely derived from radiation. Hence, gas conduction was assumed to be the second source of energy contributing to  $K_{DCC}$ . The heat flow derived from gas conduction was determined by subtracting the radiative component from the total amount of heat flow to the DCC. Afterwards,  $K_{g/DCC}$  ranged from  $9.1E-6$  cal/(s\*cm<sup>2</sup>\*K) at 60 mTorr to  $4.3E-5$  cal/(s\*cm<sup>2</sup>\*K) at 200 mTorr. Figure 3-10 provides an overview of the different contributions to the heat transfer coefficient between the aluminum block and a typical center DCC. The relative influence of the pressure- dependent gas conduction increased with an increase in pressure, whereas the relative contribution deriving from radiation decreased. In conclusion, radiation was the dominant mode of heat transfer from the aluminum block and upper shelf to the DCC throughout the pressure range investigated, ranging from 91% at 60 mTorr to 69% at 200 mTorr.

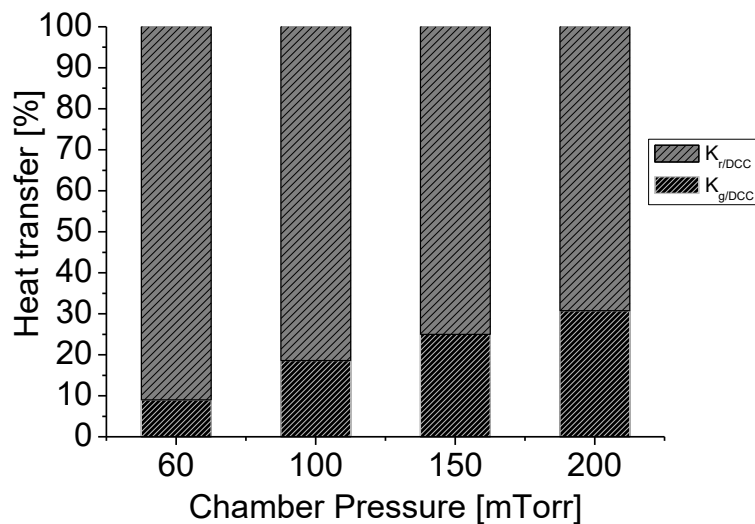


**Figure 3-10 Contribution of  $K_r$  and  $K_g$  to  $K_{DCC}$  at different chamber pressures. The values shown in Figure 3-10 refer to center DCCs.**

### 3.4.6 Overall heat transfer coefficient $K_{tot}$

An overall heat transfer coefficient,  $K_{tot}$ , covering heat transfer from the shelf to the block and from the block to the DCC was defined according to Equation (3-18), where  $A_{tot}$  represents the mean of  $A_{Al}$  and  $A_{DCC}$ .

$$K_{tot} = \frac{1}{\left(\frac{1}{K_{Al} * A_{Al}} + \frac{1}{K_{DCC} * A_{DCC}}\right) * A_{tot}} \quad (3-18)$$

$K_{tot}$  can be used to compare different holder and container systems. Values for  $K_{tot}$  vary from  $8.47E-5$  cal/(s\*cm<sup>2</sup>\*K) at 60 mTorr to  $1.27E-4$  cal/(s\*cm<sup>2</sup>\*K) at 200 mTorr.  $K_{tot}$  shows the same trend as  $K_{DCC}$  as a function of pressure since the values of  $K_{Al}$  and  $K_{DCC}$  are added up reciprocally and hence the influence of  $K_{DCC}$  is bigger (Figure 3-11). It becomes apparent that the heat transfer coefficient between the aluminum block and the DCC,  $K_{DCC}$ , is the most limiting factor for an efficient overall heat transfer. Compared with the heat transfer coefficients for a traditional vial directly resting on the shelf of  $3-6E-4$  cal/(s\*cm<sup>2</sup>\*K), the heat transfer for the DCC in this aluminum block holder can be regarded as poor.<sup>9</sup>

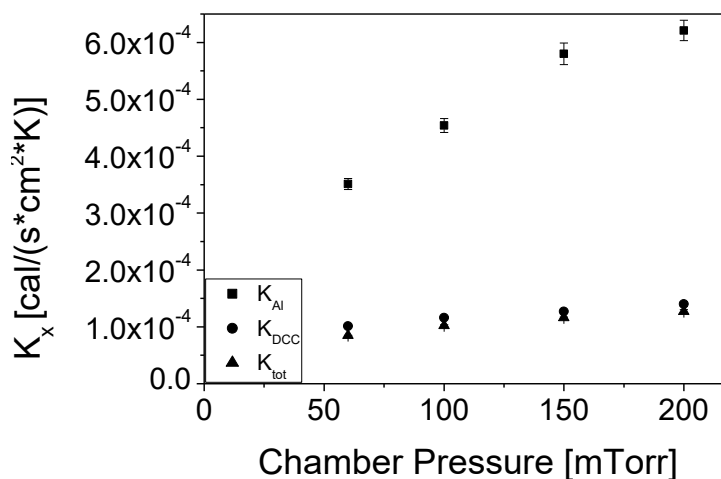


**Figure 3-11 Heat transfer coefficients at different chamber pressures. Values are mean values of triplicates; error bars represent standard deviations. Values for  $K_{DCC}$  refer to center DCCs.**

### 3.5 Summary and Conclusion

This study was aimed to characterize heat and mass flow in DCCs. An aluminum block was used as a holder system and two heat transfer coefficients were defined: the heat transfer coefficient characterizing heat transfer between the shelf and the block,  $K_{AI}$ , and between the block and the cartridge,  $K_{DCC}$ . Sublimation tests were carried out using pure water.

The sublimation rate increased by approximately 20% from approximately  $1.7E-5$  g/s at 60 mTorr to approximately  $2.1E-5$  g/s at 200 mTorr. Accordingly, the product temperature rose in the same pressure range by approximately 5 K. A clear edge effect as it is known from vials was observed in the outermost row of DCCs, showing elevated temperatures by 1–2 K and up to 50% higher sublimation rates.

To calculate heat transfer coefficients, the steady-state model was modified, taking into account the heat flow needed to heat up the aluminum block during steady-state and the decreasing shell surface area available for heat transfer. In the aluminum block, heat transfer occurred via all three modes: gas conduction, radiation, and direct contact conduction. Gas conduction was shown to be the dominant mode of heat transfer, contributing 48%–71% to  $K_{AI}$  at 60 and 200 mTorr, respectively. The contribution deriving from radiation decreased in the same pressure range from 44% to 25%. Direct contact conduction was found to be the least important contribution to  $K_{AI}$ . Generally, heat transfer from the shelf to the aluminum block appeared to be efficient with  $K_{AI}$  values ranging from  $3.5E-4$  cal/(s\*cm<sup>2</sup>\*K) at 60 mTorr to  $6.2E-4$  cal/(s\*cm<sup>2</sup>\*K) at 200 mTorr, showing a nonlinear pressure dependence.

$K_{DCC}$  values were calculated using weighted parameters, as the upper shelf was found to be more important for radiative heat flow than the aluminum block. Generally,  $K_{DCC}$  in the present holder system can be regarded as poor, yielding values between  $1.0E-4$  cal/(s\*cm<sup>2</sup>\*K) at 60 mTorr to  $1.4E-4$  cal/(s\*cm<sup>2</sup>\*K) at 200 mTorr. A slight pressure-dependence could be observed for  $K_{DCC}$  following a linear trend. As the product was elevated above the aluminum block, gas conduction only heated up the glass of the cartridge, minimizing its influence to portions between 9% at 60 mTorr to 31% at 200 mTorr. As expected, radiation was the dominant mode of heat transfer for  $K_{DCC}$ , contributing 91% at 60 mTorr and 69% at 200 mTorr.

Direct contact conduction between the aluminum block and the DCC was neglected, as the contact area of the ring bottom and the shell surface with the block was small and the product was elevated above the block. The poor heat transfer from the aluminum block to the DCC was most limiting to an overall heat transfer, indicating considerable optimization potential for this holder system.

This fundamental knowledge about the heat transfer characteristics of this novel container system can be transferred to different holder and dual-chamber system configurations and enables the development of optimized lyophilization cycles.

### 3.6 Acknowledgments

We gratefully thank Prof. Dr. Michael Pikal from the University of Connecticut for supporting this study with his knowledge and expertise.

### 3.7 References

1. Wang W 1999. Instability, stabilization, and formulation of liquid protein pharmaceuticals. *International journal of pharmaceutics* 185(2):129-188.
2. Wang W 2000. Lyophilization and development of solid protein pharmaceuticals. *International Journal of Pharmaceutics* 203(1–2):1-60.
3. Hibler S, Gieseler H 2012. Heat transfer characteristics of current primary packaging systems for pharmaceutical freeze-drying. *Journal of Pharmaceutical Sciences* 101(11):4025-4031.
4. Patel SM, Pikal MJ 2011. Emerging freeze-drying process development and scale-up issues. *AAPS PharmSciTech* 12(1):372-378.
5. Teagarden DL, Speaker SM, Martin SWH, Österberg T. 2010. Practical Considerations for Freeze-Drying in Dual Chamber Package Systems. *Freeze Drying/Lyophilization of Pharmaceutical and Biological Products*, ed. p 494-526.
6. Sacha GA, Saffell-Clemmer W, Abram K, Akers MJ 2010. Practical fundamentals of glass, rubber, and plastic sterile packaging systems. *Pharmaceutical Development and Technology* 15(1):6-34.
7. Patel SM, Pikal MJ 2010. Freeze-drying in novel container system: Characterization of heat and mass transfer in glass syringes. *Journal of Pharmaceutical Sciences* 99(7):3188-3204.
8. Franks F 1998. Freeze-drying of bioproducts: putting principles into practice. *European Journal of Pharmaceutics and Biopharmaceutics* 45(3):221-229.
9. Pikal MJ, Roy ML, Shah S 1984. Mass and heat transfer in vial freeze-drying of pharmaceuticals: Role of the vial. *Journal of Pharmaceutical Sciences* 73(9):1224-1237.
10. Tang X, Pikal M 2004. Design of Freeze-Drying Processes for Pharmaceuticals: Practical Advice. *Pharm Res* 21(2):191-200.
11. Pikal MJ 1985. Use of laboratory data in freeze drying process design: heat and mass transfer coefficients and the computer simulation of freeze drying. *Journal of parenteral science and technology : a publication of the Parenteral Drug Association* 39(3):115-139.
12. Hibler S, Wagner C, Gieseler H 2012. Vial freeze-drying, part 1: New insights into heat transfer characteristics of tubing and molded vials. *Journal of Pharmaceutical Sciences* 101(3):1189-1201.
13. Lasance CJM 2001. Thermal conductivity of unfilled plastics. *Electronics Cooling* 11.

14. Hottot A, Vessot S, Andrieu J 2005. Determination of mass and heat transfer parameters during freeze-drying cycles of pharmaceutical products. *PDA journal of pharmaceutical science and technology / PDA* 59(2):138-153.
15. Rambhatla S, Pikal M 2003. Heat and mass transfer scale-up issues during freeze-drying, I: Atypical radiation and the edge vial effect. *AAPS PharmSciTech* 4(2):22-31.
16. Shukla K, Ghosh D 1985. Radiation configuration factors for concentric cylinder bodies in enclosure. *Indian J Technology* 23:244-246.
17. Hottot A, Andrieu J, Hoang V, Shalaev EY, Gatlin LA, Ricketts S 2009. Experimental Study and Modeling of Freeze-Drying in Syringe Configuration. Part II: Mass and Heat Transfer Parameters and Sublimation End-Points. *Drying Technology* 27(1):49-58.
18. Jaworske DA 1993. Thermal modeling of a calorimetric technique for measuring the emittance of surfaces and coatings. *Thin Solid Films* 236(1–2):146-152.

#### 4 *HEAT TRANSFER ANALYSIS OF AN OPTIMIZED, FLEXIBLE HOLDER SYSTEM FOR FREEZE-DRYING IN DUAL CHAMBER CARTRIDGES USING DIFFERENT STATE-OF-THE-ART PAT TOOLS*

The following chapter has been published in the Journal of Pharmaceutical Sciences and appears in this thesis with the journal's permission:

**Christoph Korpus**, Michael Pikal, Wolfgang Friess 2016

Heat Transfer Analysis of an Optimized, Flexible Holder System for Freeze-Drying in Dual Chamber Cartridges Using Different State-of-the-Art PAT Tools.

Journal of Pharmaceutical Sciences 105(11):3304-3313

## 4.1 Abstract

The aim of this study was to determine the heat transfer characteristics of an optimized flexible holder device, using Tunable Diode Laser Absorption Spectroscopy, the Pressure Rise Test and the gravimetric procedure. Two different controlled nucleation methods were tested, and an improved sublimation process, “preheated plate”, was developed. Tunable Diode Laser Absorption Spectroscopy identified an initial sublimation burst phase. Accordingly, steady-state equations were adapted for the gravimetric procedure, to account for this initial nonsteady-state period. The heat transfer coefficient,  $K_{DCC}$ , describing the transfer from the holder to the DCC, was the only heat transfer coefficient showing a clear pressure dependence with values ranging from  $3.81E-04 \text{ cal}/(\text{s}\cdot\text{cm}^2\cdot\text{K})$  at 40 mTorr to  $7.38E-04 \text{ cal}/(\text{s}\cdot\text{cm}^2\cdot\text{K})$  at 200 mTorr. The heat transfer coefficient,  $K_{tot}$ , reflecting the overall energy transfer via the holder, increased by around 24 % from 40 to 200 mTorr. This resulted in a pressure-independent sublimation rate of around  $42 \text{ mg/h} \pm 1.06 \text{ mg/h}$  over the whole pressure range. Hence, this pressure dependent increase in energy transfer completely compensated the decrease in driving force of sublimation. The “flexible holder” shows a substantially reduced impact of atypical radiation, improved drying homogeneity, and ultimately a better transferability of the freeze-drying cycle for process optimization.

## 4.2 Introduction

For biopharmaceutical drugs which are unstable in liquid formulation, freeze-drying is an effective and gentle approach to enhance chemical and physical stability of these drugs during storage and shipping.<sup>1,2</sup> However, this process consumes large amounts of energy, is rather costly and requires a substantial effort in process and formulation optimization.<sup>3</sup> If a Dual Chamber Cartridge (DCC) is used as a cutting-edge container system, with various benefits over the traditional vial container, the manufacturing process becomes even more challenging.<sup>4,5</sup> Firstly, freeze-drying in DCCs requires an adequate holder system to prevent the DCCs from falling over and to avoid drying heterogeneities. The holder device both takes up energy from the shelf and releases energy to the product, depending on the process design. This strongly influences the lyophilization process and has to be taken into account for lyophilization cycle development and scale-up. Secondly, the product in the DCC has no direct contact to the shelf which can lead to longer lyophilization cycle times and slower responses to shelf temperature changes.<sup>6</sup> In order to shorten processing times and to be able to assure product quality, it is of vital importance to quantitatively describe how energy transfer works in DCC/holder combinations and in which ways it can be optimized. Thus, it is crucial to understand the coupling between heat and mass transfer<sup>7</sup>, especially for a system like the DCC, where the small inner diameter leads to a large dry layer thickness ( $L_{dry}$ ) and therefore creates high mass transfer resistance ( $R_p$ ).  $R_p$  has a strong influence on the product temperature ( $T_p$ ), which is the most important process parameter and should not exceed a critical value to sustain product quality during manufacturing.<sup>8,9</sup>

In a previous study, we used an aluminum block as a holder device and delineated the fundamentals of the combined energy- and mass transfer during lyophilization in DCCs using pure water and the gravimetric procedure.<sup>4</sup> We could show that radiation was the dominant mode of heat transfer, leading to significant drying heterogeneities for DCCs standing in the first row of an array. Furthermore, it became obvious that the heat transfer between the aluminum block and the DCC was rather inefficient. Based on the previously gained knowledge we designed and built an optimized three-piece holder device, a “flexible holder” (Figure 4-1), that should provide an adequate radiation shielding and improved energy transfer.

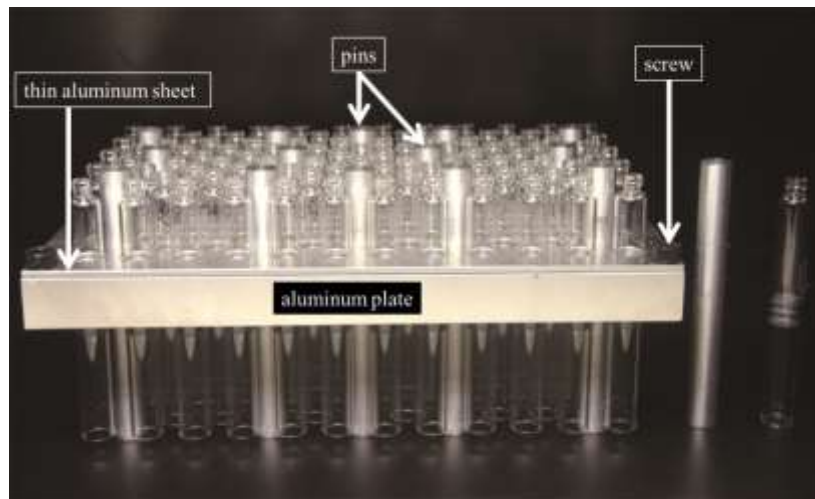


**Figure 4-1 Three-piece holder device with aluminum pin and DCC standing next to it.**

The objective of this present study was to test this new holder device and analyze the mass and heat transfer effects during lyophilization of DCCs. In order to reduce the initial nonsteady-state period caused by the heating of the holder system<sup>4</sup>, we defined a lyophilization cycle, which can be used to obtain valid sublimation rate data, in order to completely characterize the heat transfer characteristics of the flexible holder system. The Tunable Diode Laser Absorption Spectroscopy (TDLAS) method and the Pressure Rise Test (PRT) / Manometric Temperature Measurement (MTM) were utilized to generate sublimation rate data directly in the steady-state (plateau phase) and then compared with the mean gravimetric sublimation rates. TDLAS revealed several interesting facts about the flexible holder device and also helped to understand the relationship between the different methods used for sublimation rate determination (gravimetric vs. MTM vs. TDLAS). Since MTM cannot be used if there is no product resistance (which is the case with pure water) we decided to use Mannitol. Mannitol shows a typical linear increase in  $R_p$  with  $L_{dry}$  and enables an accurate  $dm/dt$  determination with MTM. Furthermore, drying water gives a cone structure and therefore a decreasing area of contact between ice and the container wall.<sup>4</sup> This loss in contact between the wall of the DCCs and the ice leads to errors in calculation of area of sublimation and hence heat transfer coefficients. Furthermore, two different controlled ice nucleation methods currently used for vials were tested for their suitability for DCCs: the ControlLy<sup>®</sup> depressurization technique and the method described by Geidobler et al.<sup>10</sup>

## 4.3 Materials and Methods

### 4.3.1 Materials

A 5% Mannitol (Sigma-Aldrich, Seelze, Germany) solution was used as a model formulation and filtered through a 0.2  $\mu\text{m}$  membrane filter (VWR, Radnor, USA) prior to filling into the DCCs. The DCCs (outer diameter 10.75 mm, inner diameter 8.65 mm, 1 ml max. fill volume) were purchased from Nuova Ompi (Piombino Dese, Italy), with plungers made of bromobutyl rubber (FM457-0; Helvoet Pharma, Lommel, Belgium). Three customized holder devices, made of aluminum, were used. Surface temperatures were measured using eight adhesive type-T thermocouples (Omega Engineering, CT, USA). Product temperatures were measured with eight 36-gauge type-T thermocouples (Omega Engineering, CT, USA). A capacitive manometer (MKS Baratron) was used to monitor the pressure in the freeze-dryer chamber.

### 4.3.2 The holder system

A three-piece holder device ("flexible holder") was custom made and used for the energy transfer studies (Figure 4-1). The first part of the holder consisted of solid aluminum pins with exactly the same outer diameter as the DCCs (10.75 mm) and a height of 85 mm. These aluminum pins were the only parts of the holder device that were in direct contact with the shelf. The second part, the basis of the holder system, was a massive aluminum plate (210\*115\*15 mm<sup>3</sup>) with 104 drillings in which the DCCs and pins were inserted. The diameter of each drilling was slightly larger than the outer diameter of the DCCs. 104 smaller drillings, right next to the first one, with a diameter of 4 mm each and a depth of only 14 mm served as an interlock system for the bypass of the DCCs and kept the DCCs in the right position. A thin aluminum sheet (210\*115\*2 mm<sup>3</sup>), including 104 cutouts for the DCCs, was placed on top of the plate loaded with DCCs and fixed with 4 screws at the edges of the plate. Thus the bypasses of the DCCs were trapped between the lower end of the smaller drilling in the plate and the thin aluminum sheet at the top of the plate. Consequently the whole holder device could be turned without DCCs falling out. An array of 3 flexible holders was used during each sublimation experiment. During these experiments only the middle shelf of the freeze-dryer was used.

### 4.3.3 Freeze-dryer configurations and PAT tools used

Two Lyostar III freeze-dryers (SP Scientific, Stone Ridge, USA) were used in this study. Freeze Dryer One (FD I) was equipped with SMART<sup>®</sup> (SP Scientific, Stone Ridge, USA), ControLyo<sup>®</sup> (Praxair Inc., Danbury, USA) and LyoFlux<sup>®</sup> technology (Physical Sciences Inc., Andover, USA).<sup>11</sup> The SMART<sup>®</sup> system is a commercially available technology that uses information, gained by the Pressure Rise Test (PRT) in combination with the steady-state theory of heat and mass transfer, to automatically control and optimize a lyophilization cycle.<sup>12</sup> The LyoFlux<sup>®</sup> system is a Tunable Diode Laser Absorption Spectroscopy (TDLAS) method to determine the sublimation rate online during primary drying every minute. Freeze Dryer Two (FD II) had the same technical specifications as FD I but only a customized/self-made PRT system as Process Analytical Tool (PAT). Furthermore, FD I had a stainless steel door instead of a plexiglass door like FD II. Since plexiglass has a higher emissivity than stainless steel, this can lead to a higher portion of radiation received by the DCCs standing in the front of FD II.<sup>13</sup> Throughout this study, FD I was used to compare the different PAT tools with each other concerning their ability to determine sublimation rates. As heat transfer coefficients may be somewhat freeze-dryer specific, the overall heat transfer parameter analysis for the flexible holder device was done on FD II using the MTM system. A 5% Mannitol solution was used for all sublimation experiments. Thus the only product specific variable was the nucleation temperature which was to be controlled by the ControLyo<sup>®</sup> technology available on FD I or with an ice fog technique, as described by Geidobler et al., which could be used for both freeze-dryers.<sup>10</sup>

During the ControLyo<sup>®</sup> method, the freeze-drying chamber was purged with argon gas to around 2 bar (28 psig) after a holding step of 30 min at a shelf temperature of -5°C. After additional 30 min at a product temperature of -5°C, the chamber was quickly depressurized to approx. 0.13 bar (2 psig) which should result in a controlled nucleation. For the ice fog method, the FD was controlled in the semi automatic mode. The shelf temperature was set to -8°C to cool down the product solution to -4.5°C. Afterwards, the isolation valve was opened and the condenser was preloaded with around 120 ml of highly purified water. Next, the hose connected with the vacuum release valve of the freeze-drying chamber was blocked with a clamp. Hence, the only vacuum release valve that was still operational was the condenser

release valve. To this point, the chamber pressure was still at atmospheric level. Then, the vacuum was pulled and as soon as the chamber pressure reached a value of 3 Torr, the system was vented via the condenser to blow ice in the chamber and seed crystallization of ice in the product.

#### 4.3.4 Implementation of a self-made pressure rise test system on FD II

The PRT is a well-described PAT method commonly used to perform Manometric Temperature Measurement (MTM) and to monitor the freeze-drying process on a laboratory scale.<sup>12</sup> Here, the drying chamber is isolated from the condenser by quickly closing the isolation valve.<sup>14</sup> As a result of the ongoing sublimation, the chamber pressure increases, from which the vapor pressure of ice at the sublimation interface ( $P_{ice}$ ) and the mass transfer resistance rate ( $R_p$ ) of the dried layer that is formed on top of the product are obtained. These two parameters can then be transferred into steady-state model equations used to calculate important process parameters, e.g. the sublimation rate ( $dm/dt$ ) and the product temperature ( $T_p$ ). For the custom made PRT a data logger “MSR-145” (MSR Electronics GmbH, Seuzach, CH) was connected to the capacitance manometer, recording the voltage data at 10 Hz. The first PRT was executed 60 min after the start of primary drying and repeated every 30 min. After the run was finished, the data was exported from the logger to OriginLab. An OriginLab-Macro, written with LabTalk (OriginLab Corporation, Northampton, USA) was used to extract the relevant PRT time points and to identify the end of every PRT, indicated by a sharp voltage decrease. It then automatically extracted the data corresponding to the 25 s before this drop into a single worksheet for every PRT and converted the voltage data into pressure [mTorr] based on a calibration run (Figure 4-2).

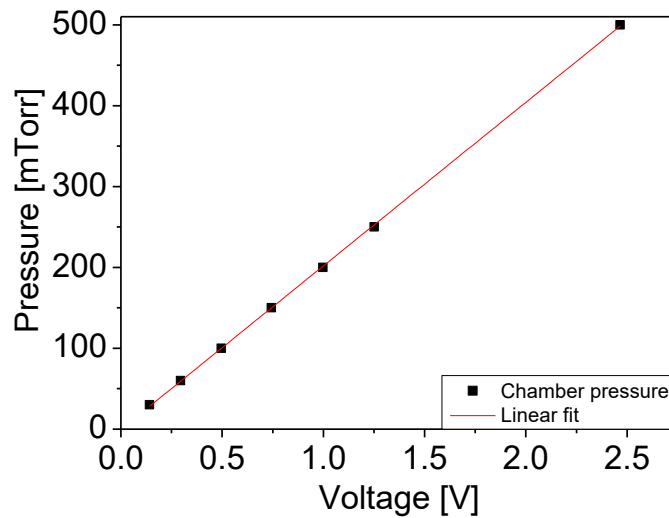


**Figure 4-2 Calibration curve to transform capacitive manometer data [V] into pressure [mTorr].**

#### 4.3.5 PRT raw data analysis according to the manometric temperature equation

Each PRT data set was fitted with a nonlinear regression analysis in Origin using Equation (4-1):<sup>14,15</sup>

$$P(t) = P_{ice} - (P_{ice} - P_0) \exp\left(-\left(\frac{3.41 N A_p T_s}{V R_p}\right) * t\right) + 0.0465 * P_{ice} * \Delta T * \left[1 - 0.811 * \exp\left(\frac{-t * 0.114}{L_{ice}}\right)\right] + x * t \quad (4-1)$$

where  $P(t)$  is the chamber pressure [Torr] at the time point  $t$ ,  $P_{ice}$  is the vapor pressure [Torr] of ice at the sublimation front and  $P_0$  the chamber pressure setpoint [Torr].  $N$  represents the number of DCCs,  $A_p$  is the inner cross sectional area [ $\text{cm}^2$ ] of one DCC and  $T_s$  is the shelf temperature [K].  $V$  is the volume of the freeze drying chamber [l],  $R_p$  the area normalized mass transfer resistance rate [ $\text{cm}^2 * \text{h} * \text{Torr} * \text{g}^{-1}$ ] and  $\Delta T$  the temperature difference [K] between the sublimation interface ( $T_p$ ) and the bottom of the DCC ( $T_b$ ). Large heterogeneities in heat transfer can minimize the accuracy of Equation (4-1). Hence, a procedure was developed where the combination of Controlled Nucleation with an adequate lyophilization cycle should guarantee the accuracy of the method. During freeze-drying in vials this temperature

difference is arbitrarily set to 1 K because the vial cross sectional area is sufficiently large to guarantee small fill heights (<1 cm). However, for lyophilization into DCCs the situation is different. Due to the smaller inner diameter (8.65 mm) the fill heights are increased e.g. 19 mm for 1 ml fill volume compared to 9.5 mm in a standard 2R vial. Consequently the temperature difference,  $\Delta T$ , is increased and has to be calculated according to Equation (4-2):<sup>12</sup>

$$\Delta T = \frac{24.7 * L_{ice} * \frac{(P_{ice} - P_0)}{R_p} - 0.0102 * L_{ice} * (T_s - T_p)}{(1 - 0.0102 * L_{ice})} \quad (4-2)$$

The temperature at the sublimation interface ( $T_p$ ) is related to the vapor pressure of ice ( $P_{ice}$ ) and can be determined using Equation (4-3):<sup>12</sup>

$$T_p = \frac{-6144.96}{(\ln P_{ice} - 24.01849)} \quad (4-3)$$

Both parameters,  $\Delta T$  and  $T_p$ , are directly calculated within the fitting operation using OriginLab. Therefore all 3 equations are combined to one and fitted to the raw data.  $L_{ice}$  is the thickness of the ice layer [cm] in the DCC and has to be calculated separately prior to every nonlinear regression analysis using Microsoft Excel and Equation (4-4)

$$L_{ice} = \frac{m(0) - m(t)}{p_I * A_p * \varepsilon} \quad (4-4)$$

In Equation (4-4),  $m(0)$  is the initial amount of product solution [g] and  $m(t)$  represents the amount of ice removed from time zero to time,  $t$ . To calculate this parameter, the density of ice ( $\rho_i = 0.92 \text{ g/cm}^3$ ), the geometric dimension of the DCC ( $A_p$ ), the porosity of the 5% Mannitol solution ( $\epsilon = 0.97$ )<sup>3</sup> and the rate of ice removal characterized via the sublimation rate [g/s] (Equation (4-5)) are used.

$$\frac{dm}{dt} = A_p * \frac{P_{ice} - P_c}{R_p} \quad (4-5)$$

As the PRT is performed every 30 min, the total amount of ice removed since the start of primary drying,  $m(t)$ , is considered to be the sum of ice removed during each time interval between PRTs. Hence, a mean sublimation rate for the time period of 30 min, based on the last PRT, is used for this iterative procedure.

## 4.4 Results and Discussion

### 4.4.1 Holder system configuration

One of the major benefits of this three-piece holder system is its flexibility concerning the pin placement within the plate of the holder device. These pins are the only parts of the holder that are in direct contact with the shelf. Hence the number of pins per holder and their arrangement influences the drying of the product. Therefore, by constructing this novel holder system, we introduced a third way of process control (besides shelf temperature and chamber pressure setpoint). Two different setups were analyzed during the course of this study: 1.) three straight lines of a total of 15 pins at the edges and the middle of each holder system and 2.) 14 pins scattered equally (Figure 4-3 (a), (b)).

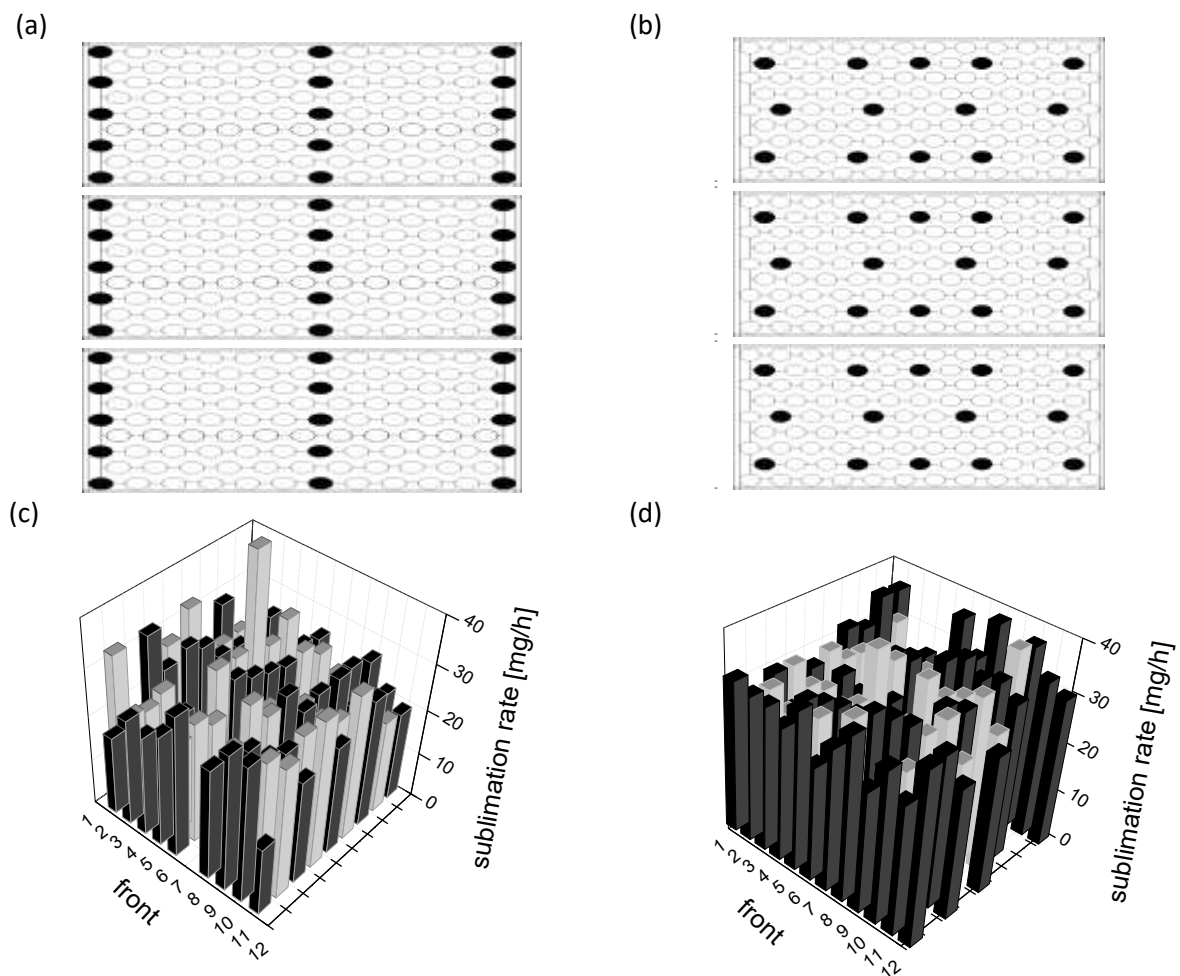


**Figure 4-3** Pin placement within 3 holder devices and the resulting sublimation rates (gravimetric measurement) of individual DCCs at 100 mTorr chamber pressure and a shelf temperature of - 20°C. (a and c) Three straight lines of 15 pins per holder system. (b and d) Scattered array of 14 pins per holder system.

For an experiment carried out at 100 mTorr chamber pressure and a shelf temperature of  $-20^{\circ}\text{C}$ , the linear pin placement led to an average sublimation rate of  $25.2\text{ [mg/h]}$  with a standard deviation of  $4.8\text{ [mg/h]}$  ( $19.3\%$ ) (Figure 4-3 (c)). All sublimation rates shown in Figure 4-3 were determined gravimetrically. If batch methods like the PRT or TDLAS are used for the sublimation rate analysis, a standard deviation of around  $20\%$  is too high for an accurate determination of all heat transfer parameters. With the scatter setup, the sublimation rate increased to  $31.8\text{ [mg/h]}$  and the standard deviation was significantly decreased to  $2.8\text{ [mg/h]}$  or ( $9.0\%$ ) respectively (Figure 4-3 (d)). Consequently the scattered pin array was used in further experiments. To check if this variability in sublimation rates originated from an inhomogeneous temperature distribution between the different parts of the holder device or from atypical radiation<sup>13</sup>, a “worst case” experiment was performed. At a shelf temperature of  $-5^{\circ}\text{C}$  and a chamber pressure of  $60\text{ mTorr}$ , possible radiation effects are enhanced and the influence of gas conduction is decreased.<sup>3</sup> Three pins (two at the edges and one in the center) of the central of the three holder devices and three spots on the plate, directly next to these pins, were monitored with adhesive TCs. Substantial temperature differences of around  $5^{\circ}\text{C}$  and  $2.5^{\circ}\text{C}$  between the pin in the middle of the plate and the one in the front and the back, respectively, were found (Figure 4-4 (a)).

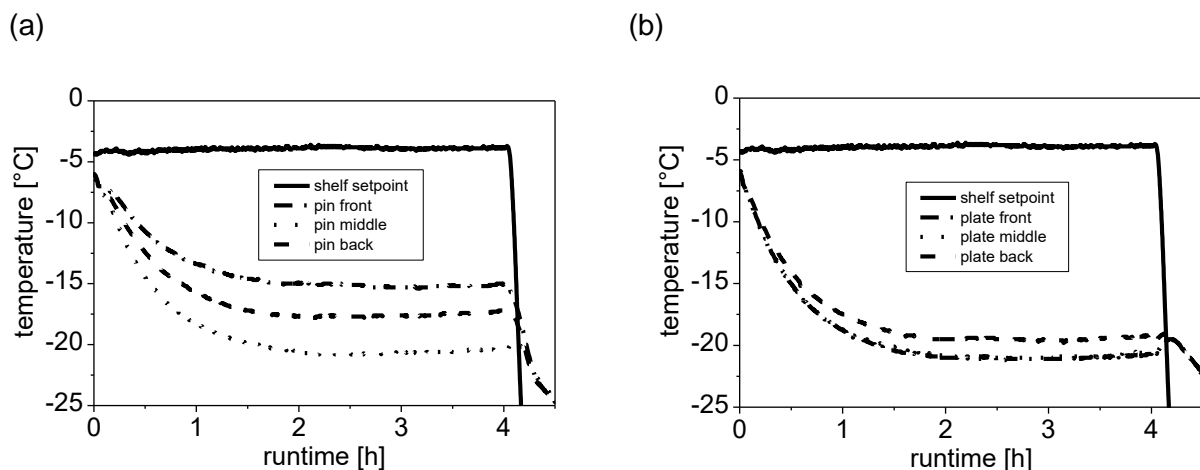


**Figure 4-4 Temperature of 3 pins (a) at different positions within the central holder device and the spots on the plate directly next to the pins (b)**

As the shelves of the freeze-dryer are not completely even and contact area between pin and shelf is rather small ( $0.9\text{ cm}^2/\text{pin}$ ), this temperature heterogeneity was most probably the result of a difference in contact between shelf and pins. However, this

temperature difference did not translate into a comparable temperature difference within the plate (Figure 4-4 (b)): The middle and front part had exactly the same temperature during the whole time of primary drying and the back part of the plate was only about 1.5°C warmer. This did not result in a difference in sublimation rates. The average sublimation rate during the worst case experiment was 1.83E-5 g/s per DCC with a standard deviation of only 7.5%. Obviously, this holder system is able to equalize temperature differences that might potentially arise from variances in shelf or holder construction. The standard deviation for the worst case experiment (7.5%) was even smaller than for the previously described setup at 100 mTorr (9%) (Figure 4-3 (d)). This was most probably due to the use of different freeze-dryers. The worst case experiment was performed on FD I. The stainless steel door of FD I might have reduced the influence of atypical radiation compared to the plexiglass window of FD II, resulting in a lower standard deviation of the sublimation rates.

Moreover, the complete array of three flexible holders diminished the influence of atypical radiation. This was in good agreement with a study of Patel et al.<sup>16</sup> where the authors could show that an increase in dryer load leads to a decreasing influence of atypical radiation on product temperature and drying times. Figure 4-5 (a) shows the temperature readouts for adhesive TCs monitoring different surfaces during the experiment.

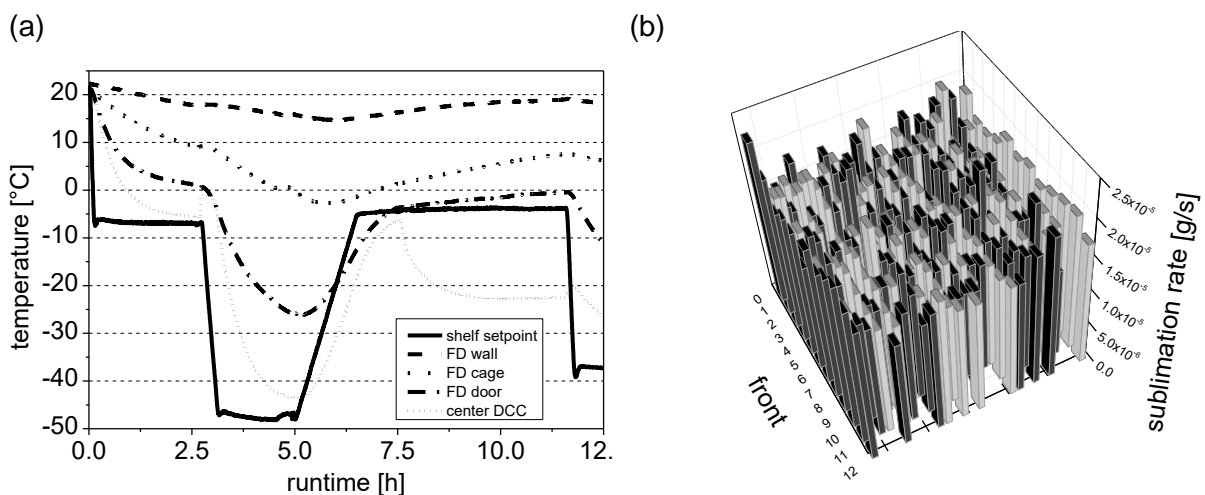


**Figure 4-5 Temperature distribution in FD I (a) during a lyophilization experiment at 60 mTorr chamber pressure and a shelf temperature of - 5°C; (b): corresponding sublimation rate distribution.**

The back wall of the freeze-drying chamber was warmer than the shelf ( $\Delta 25^{\circ}\text{C}$ ) and the product temperature ( $\Delta 40^{\circ}\text{C}$ ). The “cage” within the freeze-dryer, in which the shelves are fixed, and the stainless steel door were in the range of 5 to  $10^{\circ}\text{C}$  and 1 to  $5^{\circ}\text{C}$  respectively, warmer than the shelf. This is a clear indicator for potential radiation effects. Despite this temperature variation in surfaces with a view of the cartridge array, the mean sublimation rate was  $1.62\text{E-}05$  [g/s] with a rather small standard deviation of  $1.94\text{E-}06$  [g/s] (12.0%). For the first row of DCCs, in the front and back of the array, the average sublimation rate was  $1.85\text{E-}05$  [g/s], which is essentially the same as for the DCCs standing in the first side row of the holder devices (Figure 4-5 (b)). This indicates, that the optimized flexible holder system minimizes the effect of atypical radiation and therefore increases the uniformity of sublimation. This is very important for lyophilization cycle development and scale up studies. Still, compared to vials these sublimation rates are small. For an experiment performed with 240 DIN-6-R vials under the same process conditions, an average sublimation rate of 80.2 mg/h was obtained which is around 2.5 times higher than for DCCs freeze-dried with the scattered pin setup.

#### 4.4.2 Establishment of controlled nucleation for DCCs

For the specific approaches used in this study to accurately determine all heat transfer parameters it is important that all DCCs within the batch have a comparable  $R_p$ .  $R_p$  is mainly dependent on three parameters: the morphology of the product (amorphous or crystalline), the solute concentration and the ice nucleation temperature. The nucleation temperature largely determines the size of the ice crystals and therefore the pore size within the dried layer. Accordingly, a difference in the nucleation temperature can lead to a change in the  $R_p$ .<sup>17,18</sup> In order to avoid this variability, a controlled ice nucleation (CN) method was implemented.<sup>19</sup> To compare both CN methods and to identify the best process conditions for the sublimation experiments, three different fill volumes (0.4, 0.6 and 0.75 ml) were tested in combination with different shelf temperature set points ( $T_s$ ). The ControlLy<sup>®</sup> method was first tested with a low fill volume of 0.4 ml to provide enough space in the DCC for gas exchange which is an important consideration for this depressurization-based nucleation technique. Nucleation success was checked via TC readouts and visually. For the ControlLy<sup>®</sup> method two different TC placements were tested: insertion of the TCs from the top of the DCC and from the bottom through the middle plunger. For the

nucleation method described by Geidobler et al.<sup>10</sup>, TCs were inserted via the bottom of the DCC. The favored fill volume for all sublimation experiments was 0.75 ml, reflecting a fill height of 14 mm for the frozen solution in the DCC, which was the maximum to assure that the whole product solution was surrounded by the aluminum plate as a heat transfer surface and a radiation shield. Ice nucleation using ControLyo<sup>®</sup> was not successful at any of the temperatures tested, - 7°C, - 8°C, or - 10°C. (Figure 4-6 (a)).

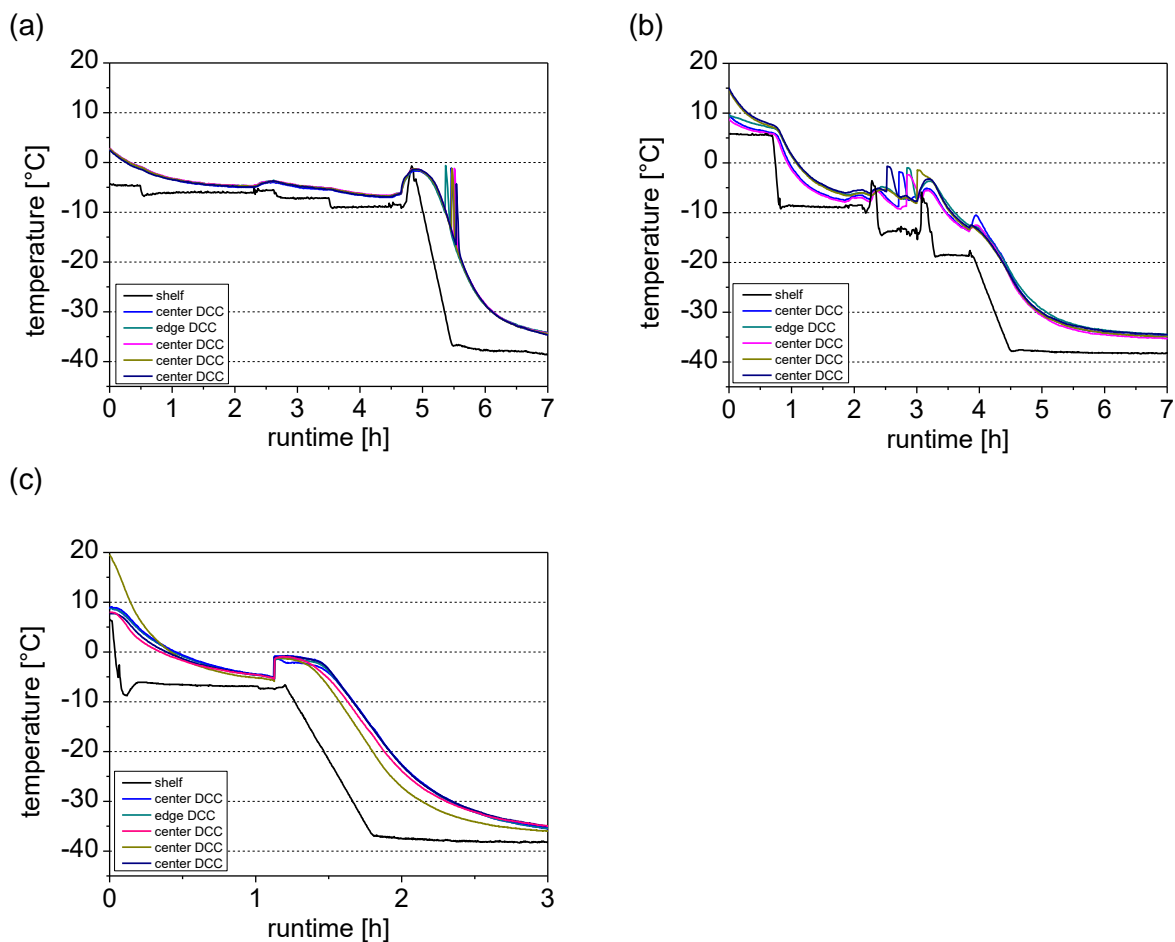


**Figure 4-6 Temperature profile for a CN experiment (a) for the ControLyo<sup>®</sup> method with 0.4 ml fill volume and (b) with 0.6 ml fill volume, at different shelf temperature setpoints and (c) using a ice fog method<sup>10</sup> with a fill volume of 0.75 ml at a shelf temperature of - 8°C.**

Next, the thermocouples were inserted from the bottom of the DCC via the middle plunger. At a higher fill volume of 0.6 ml, a more aggressive freezing protocol was used with  $T_s$  setpoints of - 10°C or - 15°C and hold times of more than 2 hours. Still, the depressurization technique was not able to nucleate the product (Figure 4-6 (b)). Since this method works fine for vials and due to the fact that we varied the fill

volumes, we assume that the reason for this phenomenon was the small neck size of the DCCs, negatively affecting the gas exchange between chamber and DCC.

For the ice fog method described by Geidobler et al.<sup>10</sup> the situation was very different. After equilibrating the DCCs, with a fill volume of 0.75 ml, to a product temperature of -4.5°C ( $T_s$  setpoint of -8°C) with a hold time of 1 hour, the CN procedure was performed (Figure 4-6 (c)). This ice fog method resulted in ice forming in 100% of the cartridges. Hence this procedure was used for all further sublimation experiments during this study.

#### 4.4.3 Lyophilization cycle development

After a suitable CN method was found, it was necessary to create an adequate lyophilization cycle for a successful determination of all heat transfer parameters. Two criteria needed to be met:

- 1.) steady-state conditions must be reached as early as possible during primary drying (temperature of all parts involved within  $\pm 0.2^\circ\text{C}$  over a time period of 10 – 15 min)<sup>3</sup> and
- 2.) temperature differences between all barriers against energy transfer must be sufficiently large (at least 1 - 1.5°C) to minimize errors in the calculation of the particular heat transfer coefficient.

Since for vials, there is only one barrier against energy transfer (from shelf to vial), steady-state is normally reached early during primary drying. For freeze-drying in DCCs, the holder device acts as an additional heat collector that can either absorb or release energy depending on the material of the holder device, the corresponding heat capacity, and its mass. Thus, the heat provided by the shelf during primary drying is not solely used to sublime ice but also to heat up the holder device.

#### 4.4.4 Regular cycle experiment

During a typical lyophilization cycle, the vacuum is applied right after the freezing step, and at the same time or a short time later, the shelf temperature is gradually increased to the final setpoint (Figure 4-7 (a), “regular cycle”).

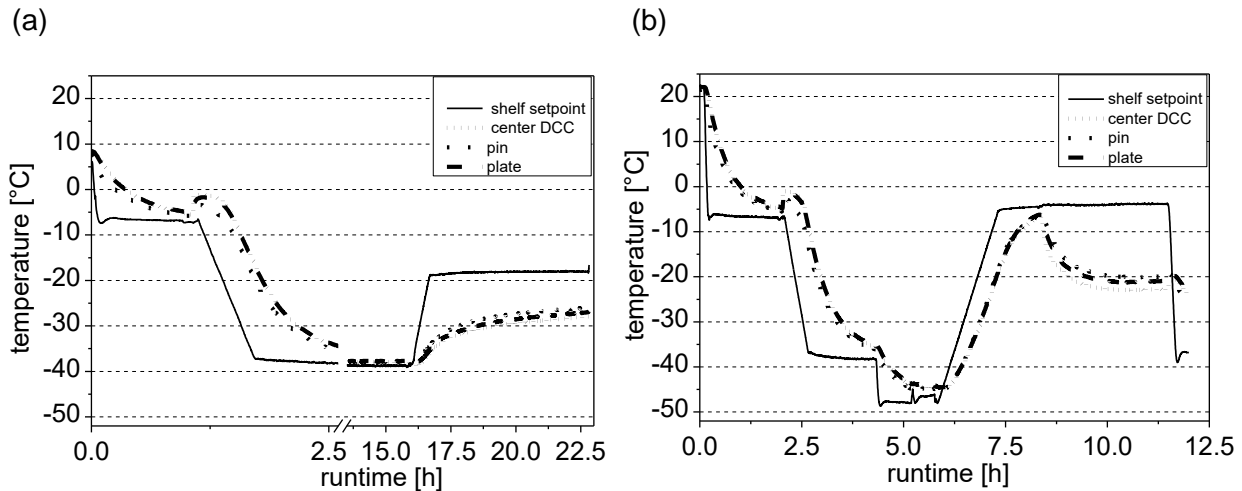


**Figure 4-7 Temperature profile during freeze-drying in DCCs at a chamber pressure of 100 mTorr during primary drying using the “regular ramp” method (a) and the “preheated plate” method (b). Controlled nucleation is indicated via a steep temperature increase at a runtime of around 1.25 h (a) and 2.4 h (b).**

During the primary drying phase of a “regular ramp” experiment, the parts of the holder device continuously warm up creating a prolonged nonsteady-state period of around 4.5 hours. Thus the amount of energy taken up by the holder device had to be quantified by, Equation (4-6):

$$\frac{dQ}{dt}_{plate/pins} = \frac{c_{p/Al} * m_{plate/pins} * \Delta T_{plate/pins}}{t} \quad (4-6)$$

where  $c_{p/Al}$  is the specific heat of aluminum (214.24 cal/(kg\*K)),  $m_{plate/pins}$  is the mass of the aluminum plates and the pins respectively (0.9 kg for all pins and 1.65 kg for the three plates).  $\Delta T_{plate/pins}$  is the temperature difference between the beginning and the end of primary drying [K] for plates and pins and  $t$  is the corresponding time [s].<sup>20</sup> For the flexible holder three heat transfer coefficients were defined: 1.)  $K_{pin}$  describes the energy transfer between the heated shelf and the pin during primary drying, 2.)  $K_{plate}$  characterizes the energy transfer between pin and plate and

3.)  $K_{DCC}$  was used to express the energy transfer efficiency between plate and DCC. Figure 4-8 shows how the corresponding heat transfer coefficients were calculated.

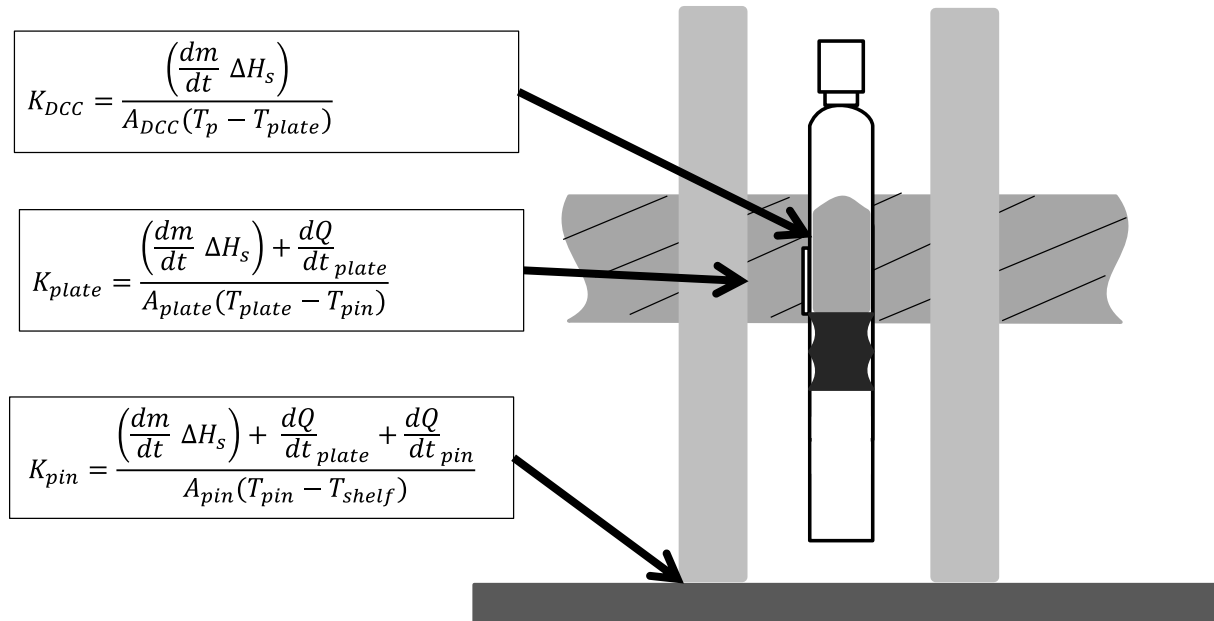


**Figure 4-8 Subtraction of nonsteady-state heat flow from the total heat flow to obtain the steady-state heat flow which is needed for  $K_x$  calculations.  $dQ/dt_{pin}$  = Heat flow used to heat up the pin of the holder [cal/s] ;  $dQ/dt_{plate}$  = Heat flow used to heat up the plate of the holder [cal/s]**

It is important to note that only the heat flow leaving from one heat source to the next heat sink was taken into account for the calculation of that particular heat transfer coefficient. The energy that was transferred between shelf and pin ( $K_{pin}$ ) was used to heat up the pins, the plates, and to sustain the sublimation of ice. The energy transfer at the next barrier, between pin and plate ( $K_{plate}$ ), was used to heat up the plate and to sublime ice. Finally, the energy that was transmitted between plate and the DCC ( $K_{DCC}$ ) was solely used for the sublimation process. By using these corrections, it was possible to adapt the steady-state model of heat and mass transfer to correctly determine all energy transfer coefficients (Table 4-1). Standard deviations for  $K_x$  (MTM) values originate from the last 3 PRTs performed during the sublimation experiment (steady-state conditions). Standard deviations for  $K_x$  (grav.) values are the result of weight differences between the DCCs. By combining Equation (4-6) with the equations illustrated in Figure 4-8, it was possible to correct the gravimetrically determined  $K_x$  values so that they were in good agreement with the coefficients determined via MTM (Table 4-1).

**Table 4-1 Comparison of MTM- heat transfer coefficients with the “regular ramp”- gravimetric procedure (5% Mannitol,  $T_s$ : - 20°C and  $P_c$ : 100 mTorr).  $K_{tot}$  was calculated based on Equation (4-8) on FD I.**

Heat Transfer Coefficient	MTM	Gravimetric
$10^4 K_{pin}$ [cal/(s*cm <sup>2</sup> *K)]	8.18 ± 0.15	7.78 ± 1.33
$10^4 K_{plate}$ [cal/(s*cm <sup>2</sup> *K)]	10.70 ± 0.43	10.30 ± 4.44
$10^4 K_{DCC}$ [cal/(s*cm <sup>2</sup> *K)]	14.40 ± 0.52	15.60 ± 2.14
$10^4 K_{tot}$ [cal/(s*cm <sup>2</sup> *K)]	1.73 ± 0.04	1.74 ± 0.21

#### 4.4.5 Lyo cycle experiment using a preheated plate

In order to reduce the nonsteady-state period to a minimum and to increase the temperature differences between all parts, we developed a lyophilization cycle called “preheated plate” method (Figure 4-7 (b)). This method was used for both freeze-dryers. After freezing via CN, the shelf temperature was increased to - 5°C ( $T_p \sim - 8^\circ\text{C}$ ) with 0.5°C per minute and held for 60 min to heat up all parts of the three piece holder system prior to pulling the vacuum. As soon as the chamber pressure fell below the vapor pressure of ice at the sublimation interface, sublimation started resulting in an immediate temperature drop of the product in the DDCs, as well as of all parts of the holder system. At the same time, the shelf temperature was raised to + 5°C with a ramp rate of 0.5°C/min to minimize this cooling effect that resulted in a nonsteady-state phase. An average temperature difference between all barriers against energy transfer of around 2°C could be observed. This is a significant improvement compared to a regular lyophilization cycle, where steady-state was first reached after 4.5 hours of primary drying and the average temperature difference was 0.5 – 1°C (Figure 4-7 (a)). These steady-state conditions were maintained for 200 min and the sublimation experiment was aborted before approximately 50% of the ice was removed. With this method it is possible to reach steady-state conditions as early as 1 hour after the start of primary drying.

In a system like this, the steady-state theory of heat and mass transfer can then be used to calculate the heat transfer coefficient,  $K_x$  [cal/(s\*cm<sup>2</sup>\*K)], for a barrier against energy transfer (Equation (4-7)) without further adaptations.<sup>3</sup> This means that in

contrast to the gravimetric procedure, neither a cooling nor a heating of the holder device must be taken into account.

$$K_x = \frac{\Delta H_s * \frac{dm}{dt}}{A_x * (T_{source} - T_{sink})} \quad (4-7)$$

$dm/dt$  is the sublimation rate [g/s],  $\Delta H_s$  the heat of sublimation of ice (660 cal/g)<sup>8</sup>,  $T_{source}$  and  $T_{sink}$  are the temperatures [K] of the heat source and the heat sink and  $A_x$  [cm<sup>2</sup>] represents the area of heat input which is container and holder specific.<sup>4</sup> A total heat transfer coefficient was defined, taking into account all individual barriers against energy transfer, which can be used to compare different holder devices with each other (Equation (4-8)).  $A_{tot}$  [cm<sup>2</sup>] represents the mean of  $A_{pin}$ ,  $A_{plate}$  and  $A_{DCC}$ .

$$K_{tot} = \frac{1}{\left( \frac{1}{K_{pin} * A_{pin}} + \frac{1}{K_{plate} * A_{plate}} + \frac{1}{K_{DCC} * A_{DCC}} \right)} * A_{tot} \quad (4-8)$$

However, one drawback of this procedure was that it created an initially 6-fold increased sublimation rate resulting in a nonsteady-state condition of around 0.75 hours (Figure 4-9). This sublimation “burst phase”, at the beginning of primary drying, was the result of the amount of energy stored in the holder system that was instantaneously released as soon as the vacuum was applied. If heat transfer coefficients are calculated based on a gravimetric sublimation rate analysis, this initial burst phase suggests a higher mean sublimation rate during the whole process, although this is just the result of an initial nonsteady-state condition. With MTM or TDLAS as PAT tools, one can avoid these issues by simply using sublimation rate data gained during steady-state conditions.

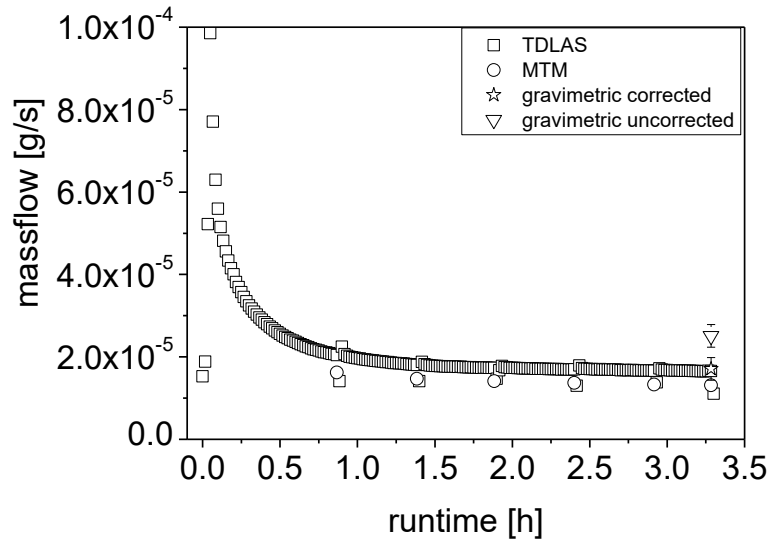


**Figure 4-9 TDLAS- MTM- and gravimetric mass flow data for a “preheated plate” experiment at 150 mTorr chamber pressure and a shelf temperature of + 5°C.**

#### 4.4.6 Comparison of TDLAS- and MTM- and gravimetric mass loss data

For the preheated plate method, the additional amount of ice, sublimed during the burst phase ( $dm_{non-ss}$ ), was quantified using TDLAS and taken into account according to Equation (4-9). In general,  $dm_{non-ss}$  can also be determined gravimetrically by aborting the cycle as soon as the nonsteady-state phase is over.

$$\frac{\Delta m}{\Delta t_{ss}} = \frac{m_{total} - m_{non-ss}}{\Delta t_{ss}} \quad (4-9)$$

This correction led to a much better accordance with TDLAS- and MTM- mass flow data (Table 4-2). The mass loss determined via MTM was lower than the uncorrected TDLAS values. The MTM total mass loss is an average value calculated from the 6 PRTs executed every 30 min, but the first PRT was performed after 1 hour of primary drying and therefore did not take the initial burst phase that ended after around 0.75 hours into account. The non-corrected mass losses detected gravimetrically and with

the TDLAS system were higher because this initial nonsteady-state phase was taken into account. In order to check if this initial burst phase was really caused by the “preheated plate” procedure and not simply by the sublimation of ice coming from atmospheric moisture that was entrapped between the shelves or attached to the freeze-dryer walls, a “blank run” was performed.

**Table 4-2 Comparison of TDLAS- and MTM- total mass loss data per DCC with the gravimetric procedure in combination with the preheated plate method exemplarily for  $T_s$ : + 5°C and  $P_c$ : 150 mTorr.**

Method	Total mass loss / DCC [g]
MTM	0.173 ± 0.012
TDLAS – uncorrected	0.254 ± 0.016
TDLAS – corrected	0.168 ± 0.016
Gravimetric – uncorrected	0.299 ± 0.033
Gravimetric – corrected	0.213 ± 0.033

For this blank run the whole experimental setup was kept the same, except that no product solution was filled into the DCCs. The TDLAS system calculated an average mass flow rate of 7.11E-08 g/s per DCC during the 3.5 hours of primary drying. Only during the first 10 min of primary drying one could see a slightly elevated sublimation rate of around 4.11E-07 g/s per DCC which might originate from the ice that was attached to the shelves. However, these small values are negligible and hence it was assumed that the initial sublimation burst phase had to be the result of the preheated plate method.

After correcting, MTM- and TDLAS- mass loss data were in very good agreement, but the gravimetric value was still somewhat higher. For the gravimetric procedure, Equations (4-7) and (4-9) were combined to calculate the particular heat transfer coefficients that are summarized in Table 4-3 and compared to MTM and TDLAS data. Detailed interpretation of these results will be shown in the next section. The  $K_x$ -values determined with TDLAS and gravimetrically were in rather good agreement and the trend gravimetric > TDLAS > MTM could be confirmed. MTM values were on average around 20% smaller. This may be due to a decrease in sublimation as the

isolation valve is closed. The TDLAS value for the sublimation rate at the timepoint of the PRT (Figure 4-9) was as well decreased by approx. 20%.

**Table 4-3 Comparison of TDLAS-, MTM- and gravimetric heat transfer coefficients obtained with the preheated plate method ( $T_s$ : +5°C and  $P_c$ : 150 mTorr).**

Heat Transfer Coefficient	MTM	TDLAS	Gravimetric
$10^4 K_{pin}$ [cal/(s*cm <sup>2</sup> *K)]	4.95 ± 0.04	6.16 ± 0.08	6.40 ± 0.95
$10^4 K_{plate}$ [cal/(s*cm <sup>2</sup> *K)]	7.22 ± 0.53	8.99 ± 0.58	10.06 ± 1.57
$10^4 K_{DCC}$ [cal/(s*cm <sup>2</sup> *K)]	7.32 ± 0.22	9.08 ± 0.37	8.85 ± 1.53
$10^4 K_{tot}$ [cal/(s*cm <sup>2</sup> *K)]	1.06 ± 0.01	1.32 ± 0.02	1.35 ± 0.21

One has to discuss if this should be considered as a systematic error of the method whereas literature suggests that MTM can be used to correctly determine heat transfer coefficients without further adaption.<sup>21,22</sup>

#### 4.4.7 Complete heat transfer parameter analysis for the flexible holder device using MTM on FD II

The complete heat transfer parameter analysis was performed on FD II with the “preheated plate” method and in combination with the MTM system. Table 4-4 summarizes the pressure dependence of the different heat transfer coefficients of the flexible holder.  $K_{pin}$  was the least efficient heat transfer in the holder system. This rather inefficient heat transfer corresponds to the high temperature difference between shelf and pin and the small contact area between both surfaces of  $0.9 \text{ cm}^2$  per pin.  $K_{plate}$  is approx. 20% higher which goes along with the enhanced contact area of  $5.06 \text{ cm}^2$  between each pin and the plate.  $K_{DCC}$  was the only heat transfer that showed significant pressure dependence. Values for  $K_{DCC}$  ranged from  $3.81\text{E-}04 \text{ cal}/(\text{s}\cdot\text{cm}^2\cdot\text{K})$  at 40 mTorr to  $7.38\text{E-}04 \text{ cal}/(\text{s}\cdot\text{cm}^2\cdot\text{K})$  at 200 mTorr. This suggests that gas conduction plays a major role in the energy transfer between the aluminum plate and the product in the DCC. Furthermore,  $K_{DCC}$  was the most efficient heat transfer in the whole system. This is a significant improvement compared to the previously analyzed aluminum block holder system, where  $K_{DCC}$  values ranged from  $1.01\text{E-}04$  to  $1.40\text{E-}04 \text{ cal}/(\text{s}\cdot\text{cm}^2\cdot\text{K})$  in the same pressure range.<sup>4</sup>

**Table 4-4 Heat transfer coefficients ( $K_{pin}$ ,  $K_{plate}$ ,  $K_{DCC}$  and  $K_{tot}$ ) as a function of the chamber pressure, calculated using MTM in combination with the preheated plate method at a shelf temperature of +5°C on FD II.**

pressure [mTorr]	$10^4 K_{pin}$ [cal/(s*cm <sup>2</sup> *K)]	$10^4 K_{plate}$ [cal/(s*cm <sup>2</sup> *K)]	$10^4 K_{DCC}$ [cal/(s*cm <sup>2</sup> *K)]	$10^4 K_{tot}$ [cal/(s*cm <sup>2</sup> *K)]
40	$3.77 \pm 0.27$	$4.72 \pm 0.35$	$3.81 \pm 0.3$	$0.74 \pm 0.05$
60	$3.85 \pm 0.14$	$6.27 \pm 0.39$	$5.06 \pm 0.10$	$0.81 \pm 0.01$
80	$4.16 \pm 0.14$	$3.49 \pm 0.07$	$6.43 \pm 0.16$	$0.83 \pm 0.01$
100	$3.85 \pm 0.13$	$4.41 \pm 0.16$	$8.32 \pm 0.42$	$0.82 \pm 0.02$
150	$4.21 \pm 0.03$	$5.33 \pm 0.05$	$8.18 \pm 0.35$	$0.92 \pm 0.01$
200	$4.28 \pm 0.01$	$6.41 \pm 0.19$	$7.38 \pm 0.25$	$0.93 \pm 0.01$

This improvement was achieved by completely enclosing the product part of the DCC within the holder device (Figure 4-1). As a result of the ongoing sublimation,  $L_{ice}$  steadily decreased during primary drying and  $L_{dry}$  increased.

As the dried sugar has a very low thermal conductivity compared to the ice layer and does not contribute to heat transfer, the contact area for energy transfer between plate and product in the DCC ( $A_{DCC}$ ) [ $\text{cm}^2$ ] steadily decreased according to Equation (4-10):

$$A_{DCC} = 2 * r * \pi * L_{ice} \quad (4-10)$$

where  $r$  was the radius of the DCC (5.37 mm) and  $L_{ice}$  was calculated after every PRT measurement according to Equation (4-4). For a primary drying at 150 mTorr and +5°C shelf temperature, the incorrect use of a constant contact area led to a decrease of up to 25% for  $K_{DCC}$  (Figure 4-10).

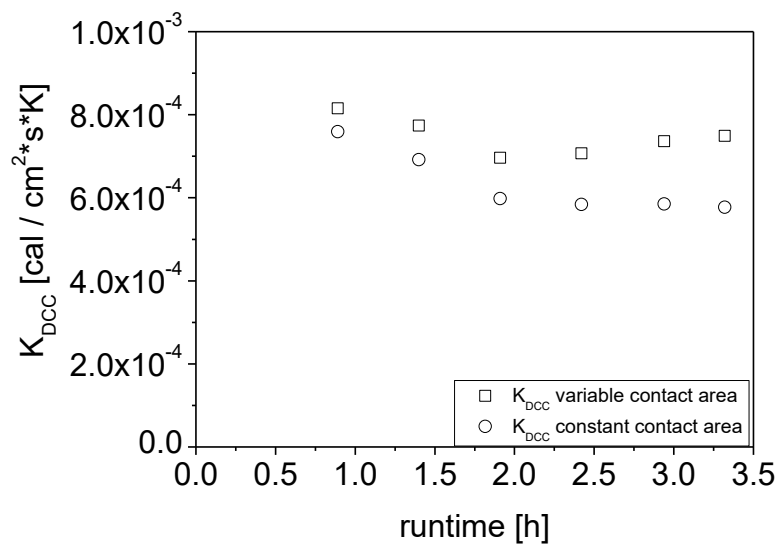


**Figure 4-10 Time dependence of  $K_{DCC}$  due to a change in  $A_{DCC}$  for an experiment carried out at 150 mTorr chamber pressure and a shelf temperature of +5°C.**

Thus, this time dependence has to be taken into account. However, since the sublimation rate constantly decreases with an increase in  $L_{dry}$ , a decrease in  $K_{DCC}$  can be observed for corrected and non-corrected values.  $K_{tot}$ , calculated according to Equation (4-8), showed a slight increase by 24.3% when pressure is increased from 60 to 200 mTorr. This pressure dependent increase of  $K_{tot}$  had an interesting effect on the sublimation rates of the DCCs; sublimation rates were pressure independent (Figure 4-11).

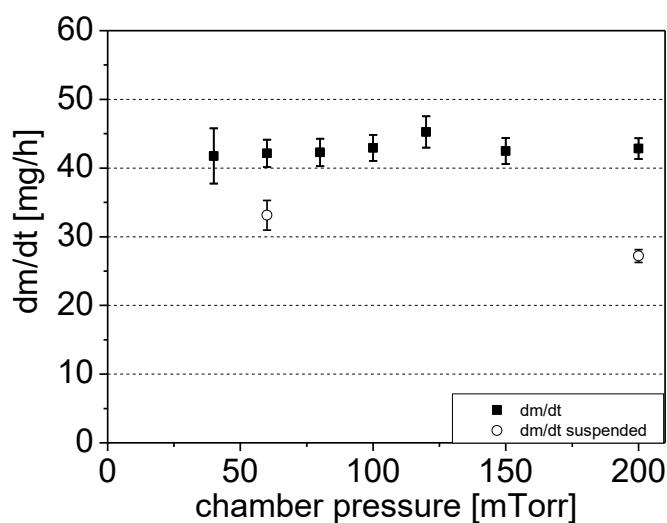


**Figure 4-11 Pressure (in)-dependence of sublimation rates for DCCs. Data was gained via MTM. Squares represent sublimation rates for DCCs standing in the holder system with direct contact to the shelf. Circles represent sublimation rates gained with a setup where the pins were isolated from the shelf.**

To verify this pressure independence, the pins were isolated from the shelf by putting small thermoplastic acrylonitrile butadiene styrene (ABS) blocks, with a very low thermal conductivity of 0.14 – 0.21 W/(m\*K), between both surfaces.<sup>23</sup> This way, the only energy source left to keep up the sublimation process was radiation which is pressure independent.<sup>3</sup> The sublimation rate decreased approx. by one third compared to the regular setup. More importantly, with a pressure increase a mass flow reduction could be observed for the experiments with the isolated pins. Thus, the constant sublimation rate for the regular setup was a result of the pressure dependent heat transfer provided via gas conduction compensating from the decrease in driving force for sublimation rate caused by an increase in pressure. Alternately, since the sublimation rate is directly proportional to the difference between the vapor pressure of ice,  $P_0$ , and the chamber pressure, an increase in pressure without a change in  $P_0$  decreases sublimation rate, but when heat transfer increases with pressure, product temperature and  $P_0$  increase, thereby cancelling the reduction in " $P_0 - P_c$ " caused by the increase in pressure alone. This pressure independence of the sublimation rate is a very unique feature of this novel flexible holder device.

## 4.5 Summary and Conclusion

A 3-piece “flexible holder” was designed and analyzed concerning its heat transfer characteristics, as an optimized holder device for freeze-drying in DCCs. A self-made pressure rise test system (PRT), TDLAS and the gravimetric procedure were used for the determination of sublimation rates. Analysis of different holder system configurations revealed that the scattered pin distribution provided high sublimation rates per DCC and lower variations between the DCCs in the holder.

Furthermore, the flexible holder was able to equalize temperature differences that might potentially arise from variances in shelf or holder construction and minimized the influence of radiation effects from the walls of the dryer on sublimation rates. The ControLyo<sup>®</sup> depressurization technique was not able to successfully nucleate the DCCs. The “ice fog” method described by Geidobler et al.<sup>10</sup> resulted in a nucleation success of 100% of the DCCs and was the method of choice to control the nucleation of ice throughout this study. Moreover, a lyophilization cycle for the correct determination of all heat transfer parameters was defined which employs a preheating of the shelf to -5°C for 1h prior to applying vacuum. This approach ensured that a steady-state was attained within one hour of primary drying and that the temperature difference between all barriers against energy transfer was sufficiently large (1.5 - 2°C) to minimize calculation errors. The TDLAS system identified an initial sublimation burst phase for all experiments carried out with the preheated plate method. This initial 6-fold increased sublimation rate resulted in a nonsteady-state condition of around 0.75 hours and originated from the amount of energy stored in the holder system that was instantaneously released as soon as the vacuum was pulled. If heat transfer coefficients are calculated based on a gravimetric sublimation rate analysis, this initial burst phase gives misleading results. Accordingly, the calculations were modified by subtracting off the burst phase sublimation and analyzing only the steady-state portion of the process. Additionally, for the regular ramp experiments, the continuous warming of all parts of the holder system was determined and appropriately subtracted from the total heat flow to obtain only the steady-state heat flow required to evaluate the corresponding heat transfer coefficient.

Finally, a complete heat transfer parameter analysis, using MTM was performed.  $K_{DCC}$  was the only heat transfer coefficient showing a clear pressure dependence. Compared to a previously studied holder device, values for  $K_{DCC}$  were increased by factors of around 3 to 6. This is a significant improvement as  $K_{DCC}$  represents the most important energy transfer stage. This increased energy transfer efficiency was the result of completely embedding the product part of the DCC in the holder device. Moreover, a time-dependence of  $A_{DCC}$  was observed which could give  $K_{DCC}$  values decreasing by up to 25% during the measurement if the time dependent area for heat transfer is not used in the evaluation of  $K_{DCC}$ . The overall energy transfer coefficient,  $K_{tot}$ , increased by around 24% from 40 to 200 mTorr. This pressure dependent increase in energy transfer compensates the decrease in driving force of sublimation. The result was a pressure independent sublimation rate of around  $42 \text{ mg/h} \pm 1.06 \text{ mg/h}$  over the whole pressure range from 40 to 200 mTorr.

Overall, the combination of increased energy transfer efficiency with an effective shielding against atypical radiation resulting in a comparably high drying homogeneity makes the flexible holder system a promising new system for freeze-drying in DCCs.

## 4.6 Acknowledgments

The authors want to express their gratitude to the German Academic Exchange Service (DAAD) for partly funding this study with a graduate student scholarship to Christoph Korpus. The authors also want to thank Dr. Tim Menzen for programming the “PRT filter” and Dr. Raimund Geidobler for supporting the installation of the self-made PRT system.

## 4.7 References

1. Wang W 1999. Instability, stabilization, and formulation of liquid protein pharmaceuticals. *International journal of pharmaceutics* 185(2):129-188.
2. Wang W 2000. Lyophilization and development of solid protein pharmaceuticals. *International Journal of Pharmaceutics* 203(1–2):1-60.
3. Pikal MJ, Roy ML, Shah S 1984. Mass and heat transfer in vial freeze-drying of pharmaceuticals: Role of the vial. *Journal of Pharmaceutical Sciences* 73(9):1224-1237.
4. Korpus C, Haase T, Sönnichsen C, Friess W 2015. Energy Transfer During Freeze-Drying in Dual-Chamber Cartridges. *Journal of Pharmaceutical Sciences* 104(5):1750-1758.
5. Werk T, Ludwig IS, Luemkemann J, Huwyler J, Mahler H-C, Haeuser CR, Hafner M 2016. New Processes for Freeze-Drying in Dual Chamber Systems. *PDA Journal of Pharmaceutical Science and Technology*:pdajpst. 2015.006155.
6. Teagarden DL, Speaker SM, Martin SWH, Österberg T. 2010. Practical Considerations for Freeze-Drying in Dual Chamber Package Systems. *Freeze Drying/Lyophilization of Pharmaceutical and Biological Products*, ed. p 494-526.
7. Hibler S, Gieseler H 2012. Heat transfer characteristics of current primary packaging systems for pharmaceutical freeze-drying. *Journal of Pharmaceutical Sciences* 101(11):4025-4031.
8. Pikal MJ 1985. Use of laboratory data in freeze drying process design: heat and mass transfer coefficients and the computer simulation of freeze drying. *Journal of parenteral science and technology : a publication of the Parenteral Drug Association* 39(3):115-139.
9. Franks F 1998. Freeze-drying of bioproducts: putting principles into practice. *European Journal of Pharmaceutics and Biopharmaceutics* 45(3):221-229.
10. Geidobler R, Mannschedel S, Winter G 2012. A new approach to achieve controlled ice nucleation of supercooled solutions during the freezing step in freeze-drying. *Journal of Pharmaceutical Sciences* 101(12):4409-4413.
11. Awotwe-Otoo D, Agarabi C, Khan MA 2014. An Integrated Process Analytical Technology (PAT) Approach to Monitoring the Effect of Supercooling on Lyophilization Product and Process Parameters of Model Monoclonal Antibody Formulations. *Journal of Pharmaceutical Sciences* 103(7):2042-2052.
12. Tang XC, Nail SL, Pikal MJ 2005. Freeze-drying process design by manometric temperature measurement: design of a smart freeze-dryer. *Pharm Res* 22(4):685-700.

13. Rambhatla S, Pikal M 2003. Heat and mass transfer scale-up issues during freeze-drying, I: Atypical radiation and the edge vial effect. *AAPS PharmSciTech* 4(2):22-31.
14. Tang X, Nail SL, Pikal MJ. 2006. Evaluation of manometric temperature measurement, a process analytical technology tool for freeze-drying: Part I, product temperature measurement. *AAPS PharmSciTech* 7(4): E95-E103.
15. Milton N, Pikal MJ, Roy ML, Nail SL 1997. Evaluation of manometric temperature measurement as a method of monitoring product temperature during lyophilization. *PDA journal of pharmaceutical science and technology / PDA* 51(1):7-16.
16. Patel SM, Jameel F, Pikal MJ 2010. The effect of dryer load on freeze drying process design. *Journal of Pharmaceutical Sciences* 99(10):4363-4379.
17. Patel SM, Bhugra C, Pikal MJ 2009. Reduced pressure ice fog technique for controlled ice nucleation during freeze-drying. *AAPS PharmSciTech* 10(4):1406-1411.
18. Geidobler R, Winter G 2013. Controlled ice nucleation in the field of freeze-drying: Fundamentals and technology review. *European Journal of Pharmaceutics and Biopharmaceutics* 85(2):214-222.
19. Kasper JC, Friess W 2011. The freezing step in lyophilization: Physico-chemical fundamentals, freezing methods and consequences on process performance and quality attributes of biopharmaceuticals. *European Journal of Pharmaceutics and Biopharmaceutics* 78(2):248-263.
20. Jaworske DA 1993. Thermal modeling of a calorimetric technique for measuring the emittance of surfaces and coatings. *Thin Solid Films* 236(1-2):146-152.
21. Hottot A, Andrieu J, Hoang V, Shalaev EY, Gatlin LA, Ricketts S 2009. Experimental Study and Modeling of Freeze-Drying in Syringe Configuration. Part II: Mass and Heat Transfer Parameters and Sublimation End-Points. *Drying Technology* 27(1):49-58.
22. Tang X, Nail S, Pikal M 2006. Evaluation of manometric temperature measurement (MTM), a process analytical technology tool in freeze drying, part III: Heat and mass transfer measurement. *AAPS PharmSciTech* 7(4):E105-E111.
23. Lasance CJM 2001. Thermal conductivity of unfilled plastics. *Electronics Cooling* 11.

## 5 *EVALUATION OF DIFFERENT HOLDER DEVICES FOR FREEZE-DRYING IN DUAL CHAMBER CARTRIDGES WITH A FOCUS ON ENERGY TRANSFER*

The following chapter has been published in the Journal of Pharmaceutical Sciences and appears in this thesis with the journal's permission:

**Christoph Korpus**, Wolfgang Friess 2017

Evaluation of different Holder Devices for Freeze-Drying in Dual Chamber Cartridges with a Focus on Energy Transfer

Journal of Pharmaceutical Sciences 106(4):1092-1101

## 5.1 Abstract

For freeze-drying in dual chamber cartridges (DCCs) a holder device to enable handling and safe positioning in the freeze-dryer is necessary. The aim of this study was to analyze four different types of holder devices and to define the best system based on energy transfer. The main criteria were drying homogeneity, ability to minimize the influence of atypical radiation on product temperatures and heat transfer effectiveness. The shell holder reduced the influence of atypical radiation by almost 60% compared to a block system and yielded the most homogenous sublimation rates. Besides the most efficient heat transfer with values of  $1.58\text{E-}4 \pm 2.06\text{E-}6 \text{ cal}/(\text{s}\cdot\text{cm}^2\cdot\text{K})$  at 60 mTorr to  $3.63\text{E-}4 \pm 1.85\text{E-}5 \text{ cal}/(\text{s}\cdot\text{cm}^2\cdot\text{K})$  at 200 mTorr for  $K_{\text{tot}}$ , reaction times to shelf temperature changes were up to 4 times shorter compared to the other holder systems and even faster than for vials. The flexible holder provided a comparable shielding against atypical radiation as the shell but introduced a third barrier against energy transfer. Block- and guardrail holder were the least efficient system tested. Hence, the shell holder provided the best radiation shielding, enhanced the transferability of the results to a larger scale and improved the homogeneity between the DCCs.

## 5.2 Introduction

Freeze-Drying is a complex process, commonly used to enhance the stability of protein drugs that are not sufficiently stable in aqueous solutions.<sup>1</sup> During the lyophilization process, the primary packaging system plays an important role. Its heat transfer characteristics determine the actual product temperature and therefore directly impact product quality and stability.<sup>2</sup> Today, most biopharmaceuticals are freeze-dried in the traditional vial container.<sup>3</sup> But whenever a self-administration or home care use is desired, dual chamber cartridges (DCCs) in combination with a pen injector provide numerous advantages compared to the vial system.<sup>4</sup> The major drawback of freeze-drying in DCCs is that they require special holder systems to assure proper placement and protection against tipping and to enhance energy transfer during the manufacturing process.<sup>5</sup> Since the type of holder system strongly influences the freezing- and drying behavior of the product in the DCC, this study aims to provide the reader with a comparison of currently typically used holder devices and how they influence the manufacturing process. As outlined in a previous study, there are basically three categories of holder devices commonly used in industry for freeze-drying in DCCs.<sup>5</sup> In “block systems” a whole array of DCCs is stabilized via drillings in a block (Figure 5-1 (a)). If each DCC stands in an individual holder these systems are called “shell-systems” (Figure 5-1 (b)). In the third type named “flexible holder”, the DCCs are suspended above the shelf hanging in a plate (Figure 5-1 (c)).<sup>6</sup> One representative out of each group and an additional device were tested in this study. Finally, the guardrail holder is a bulk system in which the DCC are tightly packed next to each other (Figure 5-1 (d)). The holder devices were characterized and evaluated after the following criteria: 1.) drying homogeneity with regards to sublimation rates; 2.) ability to minimize the influence of atypical radiation on product temperatures and 3.) heat transfer effectiveness.

The sublimation rate is an important process parameter as it determines the runtime of primary drying which is the most time consuming and hence cost intense part of the lyophilization process.<sup>7</sup> Thus, there exists an economic motivation to optimize this process step. All devices were analyzed concerning their ability to optimize sublimation rates during primary drying. Furthermore, a homogeneous drying rate for all DCCs in the array is very important, especially when batch methods like the pressure rise test (PRT) are used for sublimation rate determination.<sup>8</sup>

On the other side, it is very important to control the product temperature ( $T_p$ ) of the formulation as it is the most important process parameter.<sup>7,9</sup> If it exceeds a critical temperature e.g. the glass transition temperature ( $T_g$ ), product damage can occur.<sup>10</sup> Accordingly, edge effects need to be considered during the manufacturing process to avoid partial collapse and product damage for DCCs standing at the outer positions of the array.<sup>11</sup> For these reasons, a product temperature analysis was performed for each holder system during different stages of the lyophilization process with a special focus on the holders' ability to remove heat during the freezing process and to minimize the influence of atypical radiation during primary drying.

Process development for freeze-drying in DCCs requires knowledge about the heat transfer coefficients of the DCC and the holder device. This study directly compares the heat transfer coefficients of the most common holder devices for DCCs and therefore enables a purposeful lyophilization cycle development.<sup>5</sup> Two different freeze-dryers were used in order to make enough machine time available, but for all calculations only data obtained with the Lyostar-III freeze-dryer were used.

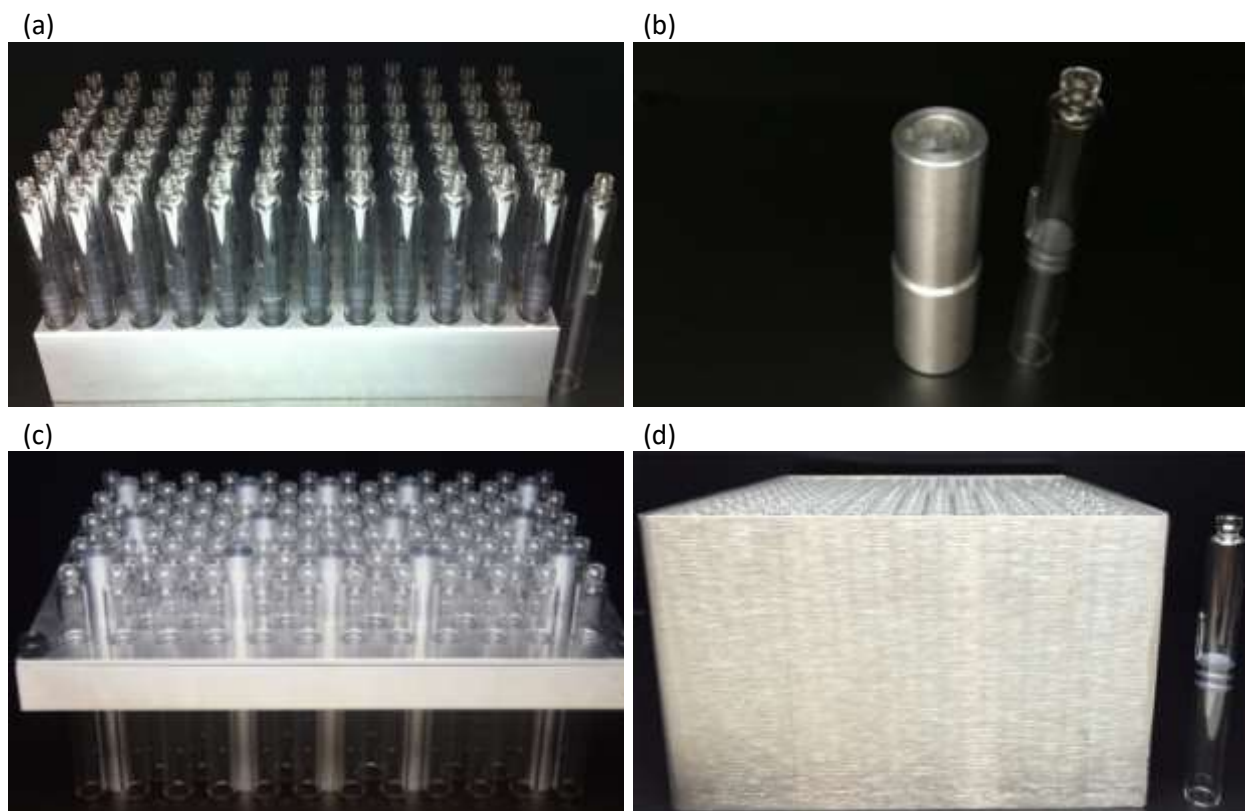


**Figure 5-1** Different DCC holder devices (a) block holder, (b) shell holder, (c) flexible holder and (d) guardrail holder

## 5.3 Materials and Methods

### 5.3.1 Materials

A 5% Mannitol (Sigma Aldrich, Seelze, Germany) solution was used as a model formulation and filtered through a 0.2  $\mu\text{m}$  membrane filter (VWR, Radnor, USA) prior to filling into the DCCs. The DCCs (outer diameter 10.75 mm, inner diameter 8.65 mm, 1 ml fill volume) were purchased by Nuova Ompi (Piombino Dese, Italy). Plungers were made of bromobutyl rubber (FM457-0; Helvoet Pharma, Lommel, Belgium). DIN 6R tubing vials (MGLas AG, Muennerstadt, Germany) with an outer diameter of 22 mm and an inner diameter of 20 mm were semi stoppered with lyophilization stoppers provided by West Pharmaceuticals, Eschweiler, Germany.

### 5.3.2 Different holder devices

Four different holder system were tested: 1.) An aluminum block system ("block holder", Figure 5-1 (a)) with 193x96x30 mm, 72 DCC/holder and a weight of 958 g<sup>5</sup>; 2.) An aluminum shell holder device ("shell holder", Figure 5-1 (b)) with a height of 65 mm, an outer diameter of 21 mm and a weight of 39 g. In order to optimize the center of gravity and to improve the machinability of the shell, the outer diameter was narrowed down to 19 mm starting at a height of 31 mm up to the top. A major drilling with a diameter of 10.9 mm and a smaller drilling, with a diameter of 4 mm for the bypass, guaranteed that each DCC was fixed in the holder system. The major drilling stopped at a depth of 63 mm, making sure that the bottom of the DCC rested on a 2 mm thick base. For the sake of weight reduction and heat sterilizability, a second hole with a diameter of 8 mm was drilled through the bottom of the shell holder; 3.) A three-piece flexible holder device ("flexible holder", Figure 5-1 (c)) with an aluminum plate (210x115x15 mm) as the basis of the holder, 85 DCC/holder and a total weight of 948 g<sup>6</sup>; 4.) An aluminum "guardrail holder" system (Figure 5-1 (d); 146x156x80 mm) where 203 DCCs were tightly packed within a guardrail and in direct contact with the shelf.

### 5.3.3 Shelf mapping experiments – influence of atypical radiation

An Epsilon 2-6D laboratory-scale freeze-dryer (Martin Christ, Osterode am Harz, Germany) with a shelf area of 0.067 m<sup>2</sup> was used for the shelf mapping experiments. This freeze dryer is defined as “Epsilon-Freeze-Dryer” (Epsilon-FD) throughout this study. Due to the height of the DCCs, only the lower shelf of the Epsilon-FD was used. According to the different geometries of the holder systems, a different number of DCCs per run was analyzed: 216 DCCs for the block holder; 152 for the shell holder; 169 for the flexible holder and 203 for the guardrail holder. All DCCs were filled with 0.75 ml of a 5% mannitol solution corresponding to a fill height of 14.38 mm. As mannitol crystallizes, the model formulation enables sublimation experiments with high mass flow rates. Table 5-1 summarizes the lyophilization cycle protocol used for each sublimation experiment. All DCCs were weighed before and after the run on a precision scale ( $\pm 0.01$  mg; Mettler Toledo, Columbus, Ohio). Sublimation rates were calculated according to Equation (5-1).  $m(0)$  represents the weight of the solution [g] before the start of primary drying and  $m(t)$  the weight at the end of the process, after 150 min runtime and  $dt$  is the runtime [s].

$$\frac{dm}{dt} = \frac{m(0) - m(t)}{dt} \quad (5-1)$$

**Table 5-1 Lyophilization protocol for the shelf mapping experiments performed with the Epsilon FD at a chamber pressure of 100 mTorr.**

Step	Start temp. [°C]	End temp. [°C]	Step duration [min]
Freezing	≈ 19	5	≈ 15
	5	5	15
	5	-5	10
	-5	-5	15
	-5	-40	35
	-40	-40	120
Drying	-40	0	40
	0	0	150

### 5.3.4 Temperature profile determination

Experiments were performed on a Lyostar III freeze-dryer (SP Scientific, Stone Ridge, USA) that was equipped with a customized Pressure Rise Test (PRT) system. The specifics and the theoretical background of this process analytical tool were described in detail in a previous study.<sup>6</sup> This freeze dryer is defined as “Lyostar-Freeze-Dryer (Lyostar-FD) throughout this analysis. DCCs were filled with 0.75 ml of 5% mannitol formulation. The freezing protocol included a holding step of around 1 hour at a shelf temperature of - 8°C, followed by a controlled nucleation procedure as described by Geidobler et al.<sup>12</sup> Subsequently, the shelf temperature was lowered to - 40°C with ramp rate of 1°C/min and kept there over night. In order to simulate process conditions commonly used for freeze-drying of biopharmaceuticals, a shelf temperature setpoint of - 20°C with a ramp rate of 0.5°C/min was used during primary drying at a chamber pressure of 200 mTorr. The cycle was aborted after a runtime of 360 min to assure that primary drying progress did not exceed 50%. Product temperatures were monitored with at least four 36-gauge type-t thermocouples (Omega Engineering, Stamford, USA). Surface temperatures were measured using four adhesive type-t thermocouples (Omega Engineering, Stamford, USA). DCCs standing in the first row of the corresponding holder were referred to as “edge DCCs”. DCCs standing in the center of the array that were surrounded by other DCCs were defined as “center DCCs”. For the temperature profile determination, the same number of DCCs per holder was used as for the shelf mapping experiments. To compare the freezing and drying behavior of the product in the DCCs to the traditional vial container system, 240 DIN 6R vials filled with 1.5 ml mannitol solution were analyzed. The vials were arranged on the shelf in the closest hexagonal packing. The lyophilization cycle protocol was the same as for the DCCs, only the first holding step was performed at a shelf temperature of - 5°C instead of - 8°C to prevent the vials from nucleating randomly.

### 5.3.5 Shell holder heat transfer coefficient experiments

Since the shell holder is a novel holder device, its heat transfer characteristics were assessed on the Lyostar-FD in order to compare it to the other holder devices that have been completely characterized in previous studies.<sup>5,6</sup> Product temperatures were measured with four 36-gauge type-t thermocouples. Surface temperatures were measured using four adhesive type-t thermocouples. A capacitive manometer (MKS Baratron) was used to monitor the pressure in the freeze-dryer chamber. 583 custom made aluminum sleeves (Figure 5-1 (b)) were utilized for each sublimation experiment and placed on the middle and lower shelf of the freeze dryer. Table 5-2 summarizes the used freeze-drying protocol. The nonsteady-state period at the beginning of primary drying was minimized and the temperature differences between all barriers against energy transfer were increased by incorporating a 60 min holding step at - 8°C prior to pulling the vacuum and a shelf temperature setpoint of 5°C during primary drying.<sup>6</sup> Both measures enhance the applicability of the steady-state equations and thus the validity of the gained heat transfer coefficients. This is especially important if a PRT-based method is used to determine sublimation rates, since this is an iterative approach.<sup>6</sup> The cycle was performed at chamber pressures of 60, 100, 150 and 200 mTorr.

**Table 5-2 Shelf temperature setpoints for the determination of the shell heat transfer coefficients on the Epsilon FD. The cycle was repeated at chamber pressures of 60, 100, 150 and 200 mTorr.**

Step	Start temp. [°C]	End temp. [°C]	Step duration [min]
Freezing	≈ 19	-6	≈ 26
	-6	-6	60
	Controlled Nucleation of Ice		
	-6	-50	44
	-50	-50	>720
	-50	-8	84
Drying	-8	-8	60
	-8	5	26
	5	5	206

Heat transfer coefficients were calculated based on the steady-state theory of heat and mass transfer.<sup>6</sup> The self-made pressure rise test system yielded the raw data parameters  $P_{ice}$  [Torr], which is the water vapor pressure at the sublimation front and  $R_p$  [ $cm^2 \cdot h \cdot Torr \cdot g^{-1}$ ], the mass transfer resistance rate of the dried layer that is formed during primary drying.<sup>8</sup> These parameters, in combination with thermocouple readout data, were then used in Equation (5-2) to calculate the according heat transfer coefficients. The use of this PRT-based method instead of the gravimetric procedure allowed the direct calculation of the corresponding heat transfer coefficients. As outlined in detail in a previous study<sup>6</sup>, the use of the gravimetric procedure necessitates correction for the energy uptake of the holder device that acts as an additional heat sink during the process.

$$K_x = \frac{\Delta H_s * A_p * \frac{P_{ice} - P_c}{R_p}}{A_x * (T_{source} - T_{sink})} \quad (5-2)$$

$\Delta H_s$  represents the heat of sublimation of ice ( $660 \text{ cal/g}$ )<sup>13</sup>,  $A_p$  the inner area of the DCC [ $cm^2$ ] and  $P_c$  is the chamber pressure [Torr].  $T_{source}$  and  $T_{sink}$  are the temperatures [K] of the heat source and the heat sink.  $A_x$  [ $cm^2$ ] is the area of heat

input which is container and holder specific.<sup>5</sup> Each heat transfer coefficient describes how effective energy is being transferred from one surface to another, overcoming a single barrier.<sup>13</sup>

Depending on the type of holder system there are different barriers against energy transfer and therefore a varying number of heat transfer coefficients per holder system needed to be defined. Table 5-3 summarizes all heat transfer coefficients that were gained in the course of this study (shell holder) and in previous studies (block holder; flexible holder). The calculation of these coefficients exemplarily for the most complex system, the flexible holder, are given in <sup>6</sup>.

**Table 5-3 Overview of heat transfer coefficients between the shelf, different parts of the holder devices and the DCC.**

Barrier	Block holder	Shell holder	Flexible holder
shelf – 1 <sup>st</sup> part	$K_{Al}$	$K_{shell}$	$K_{pin}$
1 <sup>st</sup> part – 2 <sup>nd</sup> part	$K_{DCC}$	$K_{DCC}$	$K_{plate}$
2 <sup>nd</sup> part – 3 <sup>rd</sup> part	-	-	$K_{DCC}$
overall	$K_{tot}$	$K_{tot}$	$K_{tot}$

## 5.4 Results and Discussion

### 5.4.1 Ability of holder devices to minimize the influence of atypical radiation and edge effects

At first, shelf-mapping experiments were performed in order to evaluate the ability of each holder device to reduce the impact of atypical radiation. Atypical radiation is caused by additional radiation coming from surfaces running at higher temperatures than the product in the DCCs e.g. freeze-dryer door and walls. This additional source of energy leads to higher sublimation rates, shorter primary drying times and ultimately higher product temperatures for DCCs that are standing at the edges of the array.<sup>5,11</sup> In our experiments we defined the difference between the mean sublimation rate of the first two front rows and the whole array as the influence of atypical radiation (Table 5-4). The optimum holder device should minimize this effect, increase drying homogeneity and thus enhance the transferability of the laboratory results to larger scale. Figure 5-2 provides an overview of the sublimation rates for DCCs on a shelf, fixed with different holder devices. Each bar represents one DCC.

The shelf mapping of DCCs in the block revealed the most distinct influence of atypical radiation for this holder. The mean sublimation rate for the whole array was  $121.9 \pm 32.1$  mg/h. Compared to this, sublimation rates of the DCCs standing in the first two front rows of the array were elevated by 54.8% (Table 5-4). Additionally, the sublimation rates decreased continuously from the front to the back of the freeze-dryer (Figure 5-2 (a)). This was the result of the DCCs being elevated above the holder system, receiving atypical radiation from the plastic front-door. Accordingly, minimum and maximum sublimation rates differ by a factor of around 3.4 with values of 73.7 mg/h and 252.2 mg/h, respectively. Furthermore, the 10% quantile, with 94.9 mg/h and the 90% quantile with 161.5 mg/h substantiate the pronounced heterogeneity in sublimation rates. The results demonstrate the inability of the block holder to efficiently shield the DCCs from the impact of atypical radiation.

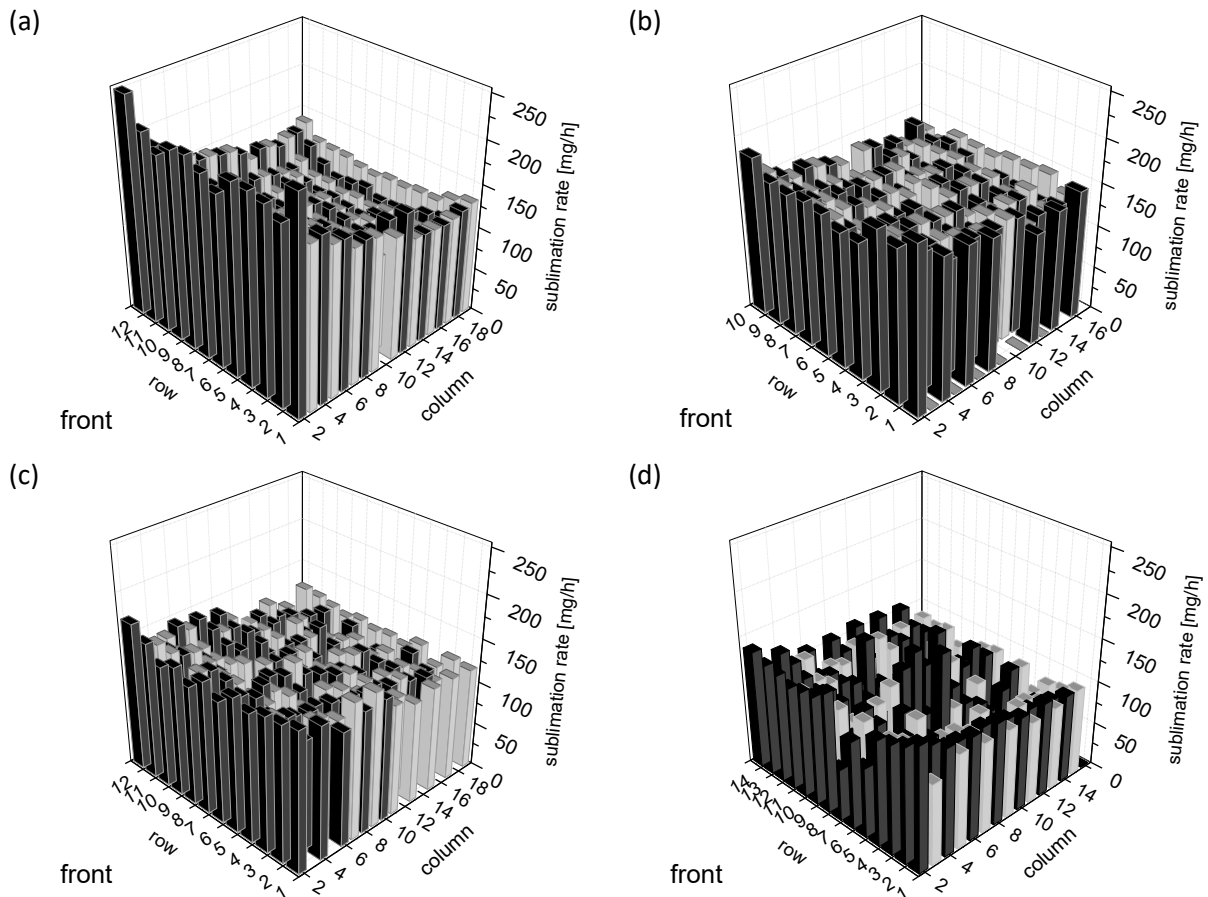


**Figure 5-2 Position-dependent sublimation rate for DCCs in different holder devices: (a) block holder (b) shell holder (c) flexible holder (d) guardrail holder. Each bar represents one DCC.**

The situation is different for the shell holder device: As a result of the complete embedding of the product in the holder system (Figure 5-1 (b)), the influence of atypical radiation was substantially reduced to around 22% (Table 5-4). Embedding of the product in combination with the direct contact between shell and shelf led to homogenous sublimation rates for the whole DCC batch with a standard deviation of only 7% and values for the 10% and 90% quantile of 121.1 mg/h and 154.9 mg/h respectively. Furthermore, the shell holder device transferred the heat from the shelf to the product efficiently and without any position dependence (Figure 5-2 (b)). Thus, the shell device led to the highest average sublimation rate of all holder systems with  $133.2 \pm 9.4$  mg/h.

The flexible holder showed a comparable ability to shield the DCCs from atypical radiation as the shell device with a relative influence of atypical radiation of 24.2% (Table 5-4). This resulted from the complete surrounding of the product by aluminum preventing direct views from warmer surfaces to the product.

However, the sublimation rate standard deviation was almost twice as high (around 14%) compared to the shell system but less pronounced than for the aluminum block holder. The use of a controlled nucleation technique could reduce this value.<sup>6</sup> Similarly, minimum and maximum sublimation rates differ more than in the shell holder but less than in the case of the block device (Table 5-4). Despite this rather narrow distribution with values for the 10% and 90% quantile of 101.5 mg/h and 141.8 mg/h respectively, the average sublimation rate with a value of 121.7 mg/h was basically the same as for the aluminum block. Most probably this effect originated from the rather small contact area of the pins to the heated shelf. Additionally, with the flexible device a third barrier against energy transfer is introduced, as it consists of three individual parts.

**Table 5-4 Comparison of sublimation rates and the influence of atypical radiation for all holder devices (5% Mannitol, T<sub>s</sub>: + 0°C and P<sub>c</sub>: 100 mTorr).**

Sublimation rate [mg/h]	Block holder	Shell holder	Flexible holder	Guardrail holder
<b>First two front rows</b>				
Mean	188.7	162.0	151.2	117.1
SD	± 32.8	± 14.4	± 8.9	± 38.8
Influence of atypical radiation	66.7 = 54.8%	28.8 = 21.6%	29.5 = 24.2%	32.4 = 38.3
<b>Whole array</b>				
Mean	121.9	133.2	121.7	84.7
SD	± 32.1	± 9.4	± 17.0	± 37.8
SD [%]	= 26,3 %	= 7,0 %	= 13,9 %	= 44,7 %
Median	111.4	134.2	119.3	95.2
Minimum	73.7	112.9	78.8	9.1
Maximum	252.2	191.4	202.1	284.3
10% quantile	94.9	121.1	101.5	14.6
90% quantile	161.5	154.9	141.8	119.6

The guardrail holder was the least efficient device tested. The low sublimation rate of only 84.7 mg/h was the result of the hollow ring bottom of the glass DCCs being the only area of contact to the heated shelf in this setup. In contrast to a study performed by Teagarden et al. we could not observe an elevated sublimation rate for DCCs standing in the outermost row of the array.<sup>14</sup> In the present setup only the first 2 rows at the front, close to the plastic door showed a sublimation rate increase by 38.3%, which was the result of the aforementioned atypical radiation. More importantly, the sublimation rate was overall highly variable with minimum and maximum values of 9.1 mg/h and 284.3 mg/h respectively, and a standard deviation of around 45% (Table 5-4). Therefore, the use of the simple guardrail device, as a holder for freeze-drying in DCCs, should be restrained. With the guardrail holder it is not possible to perform a thorough heat transfer analysis using a batch method like the pressure rise test system. Furthermore, a scientific lyophilization process design, based on a mathematical model approach for the whole batch, is not possible. Similarly, it is difficult to scale-up a process from lab- to manufacturing scale without valid heat transfer coefficient data.<sup>15</sup> Thus, the guardrail holder device was not further analyzed concerning its heat transfer parameters within this study.

### 5.4.2 Temperature profiles analysis during the freezing phase

Holder devices can exhibit a different quality of temperature control and reaction to shelf temperature changes. For a good process control, short reaction times to shelf temperature changes are necessary to assure that the product temperature stays within the desired corridor and subsequently to guarantee product quality.<sup>5,16</sup> Therefore, temperature profiles were assessed during the freezing and drying stage of the lyophilization process for each holder device. Figure 5-3 illustrates the freezing behavior of the product solution filled into the DCCs, standing in the different holder devices compared to a traditional vial. Each graph clearly shows the exothermic nucleation after a runtime of approx. 0.5 hours.

In the traditional vial container, the product temperature followed the shelf temperature very closely with a “lag time” of only 20 min. Furthermore, the temperature difference between both edge and center vials and the shelf after the end of the ramp was only 10°C. The vial behavior was not surprising, as there was only one barrier against energy transfer in this setup, namely the gas entrapped between the shelf and the molded glass bottom of the vial.<sup>13</sup>

The block holder showed a different response to shelf temperature changes. The holder system itself represented an additional barrier against heat transfer as well as a heat sink. The energy created via the exothermic nucleation process was removed very slowly and lag time of around 45 min between product- and shelf temperature was observed. One could discuss how far this could affect the ice crystal growth and therefore the pore sizes but this would be beyond the scope of this study. In addition, the temperature difference between shelf and product at the end of the ramp of 38°C was rather high. Both phenomena resulted from the suboptimal holder design without direct contact between the product solution in the DCC and the holder device itself.<sup>5</sup> Furthermore, the weight of one block with around 960 g represented a large heat sink which resulted in a rather warm block temperature of - 15.6°C in the middle of the ramping phase at - 25°C. As a consequence, holding times need to be significantly prolonged if the block holder should be used in manufacturing.

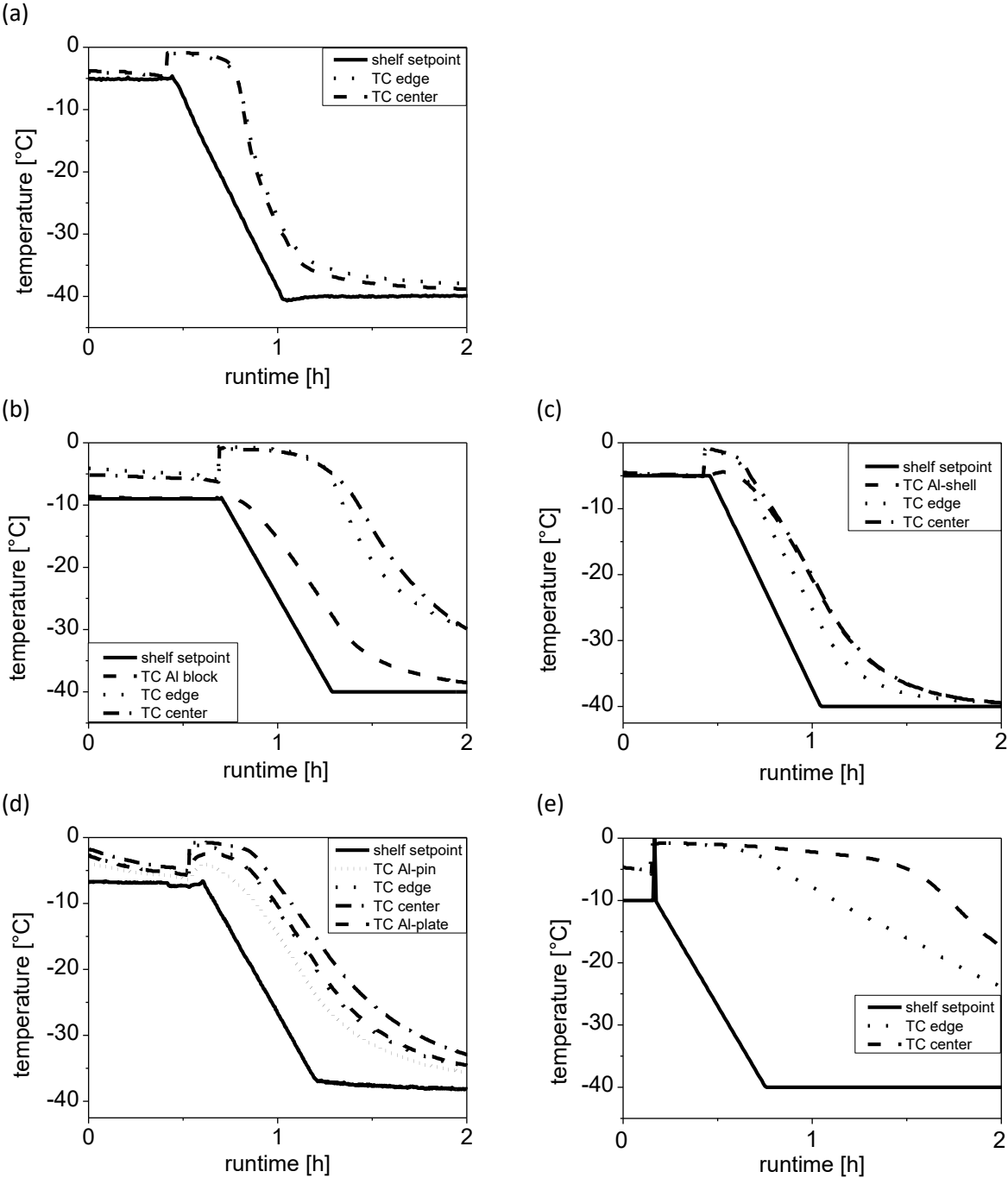


**Figure 5-3 Typical temperature profiles during the freezing step of a 5% mannitol solution filled into vials (a) and DCCs standing in the block holder (b), shell holder (c), flexible holder (d) and the guardrail holder (e).**

The shell holder provides a much better freezing behavior of the product solution: The lag time between shelf and product temperature of only 10 min was only half compared to vials. The steep decrease in the product temperature profile after nucleation was the result of the product solution being completely surrounded by the holder system (Figure 5-1 (b)). The initial cooling rate of the solution was even higher than in the vial container. The shell temperature in the middle of the ramp was  $-13.8^{\circ}\text{C}$  and hence warmer than for the block device. This could be the result of the smaller contact area between holder device and shelf compared to the block. The temperature difference between shelf and product at the end of the ramp was only  $15^{\circ}\text{C}$ .

The flexible holder device was the most complex holder system analyzed as it was made out of 3 different parts and therefore introduces a third barrier against energy transfer (Table 5-3). This resulted in a high aluminum plate temperature of around  $-4.4^{\circ}\text{C}$  in the middle of the ramp. The lag time between shelf- and product temperature was around 30 min and the ramp ended with a difference of  $24^{\circ}\text{C}$  between both.

For the guardrail holder, the lag time between shelf and product temperature was around 100 min and hence significantly longer compared to the other devices. The temperature difference at the end of the ramp was  $38.7^{\circ}\text{C}$ . Most probably this was due the fact that the only contact between shelf and product was the hollow glass bottom of the DCC leading to a decrease in energy transfer. Furthermore, the temperature difference between edge and center DCCs of around  $10^{\circ}\text{C}$  was twice as high than for the other devices where it did not exceed  $5^{\circ}\text{C}$ . In all cases, the edge DCCs were cooler than the center DCCs which was surprising since they receive more atypical radiation even at atmospheric pressure. For vials no significant difference between edge and center vials was visible.

Thus, concerning the freezing behavior clear differences were visible. The shell holder could most efficiently remove the heat caused by the controlled nucleation even faster than the traditional vial. This should enable an economic freezing phase in a larger scale freeze-dryer. The flexible holder showed a quite reasonable behavior as well but the shelf-product temperature lag time was almost three times as high as for the shell device. Both block and guardrail holder resulted in inefficient product freezing behaviors with large temperature differences between shelf and product at

the end of the ramp. Hence, the shell device would be preferred for process development.

### 5.4.3 Temperature profiles analysis during the drying phase

The temperature profiles of container, holder and product during primary drying are summarized in Figure 5-4. The goal was to study the influence of atypical radiation on the product temperature. As delineated above, it is of vital importance that the product temperature does not exceed a critical value to avoid collapse and product damage. Therefore it is necessary that the holder device equally distributes heat over the whole batch of DCCs and minimizes radiation effects.

The results for the traditional vial container are given in Figure 5-4 (a). The average temperature difference between edge and center vials was around 2°C, indicating a distinct impact of atypical radiation. This effect and ways to overcome it are well described in literature for the vial container.<sup>11,13,17,18</sup> The temperature difference between the shelf and center vials was around 13°C.

The block holder (Figure 5-4 (b)) did not sufficiently shield the DCCs standing in the first row of the array. This resulted in a temperature difference of around 3°C between edge and center DCCs. The higher product temperature of DCCs standing in the outermost row of the aluminum holder was in good accordance with the elevated sublimation rates outlined in the previous section due to atypical radiation. Consequently, edge DCCs finished primary drying earlier than the center DCCs. This was the case after a runtime of approx. 6 hours, as soon as the TC readouts of the edge DCCs reached the aluminum block temperature. This very much reduced the transferability of temperature- and sublimation rate data for scale-up, where homogenous sublimations rates and thus drying times are highly beneficial. The block temperature followed the shelf closely. After around 3 hours of primary drying, the temperature difference between block and shelf was less than 2.5°C.

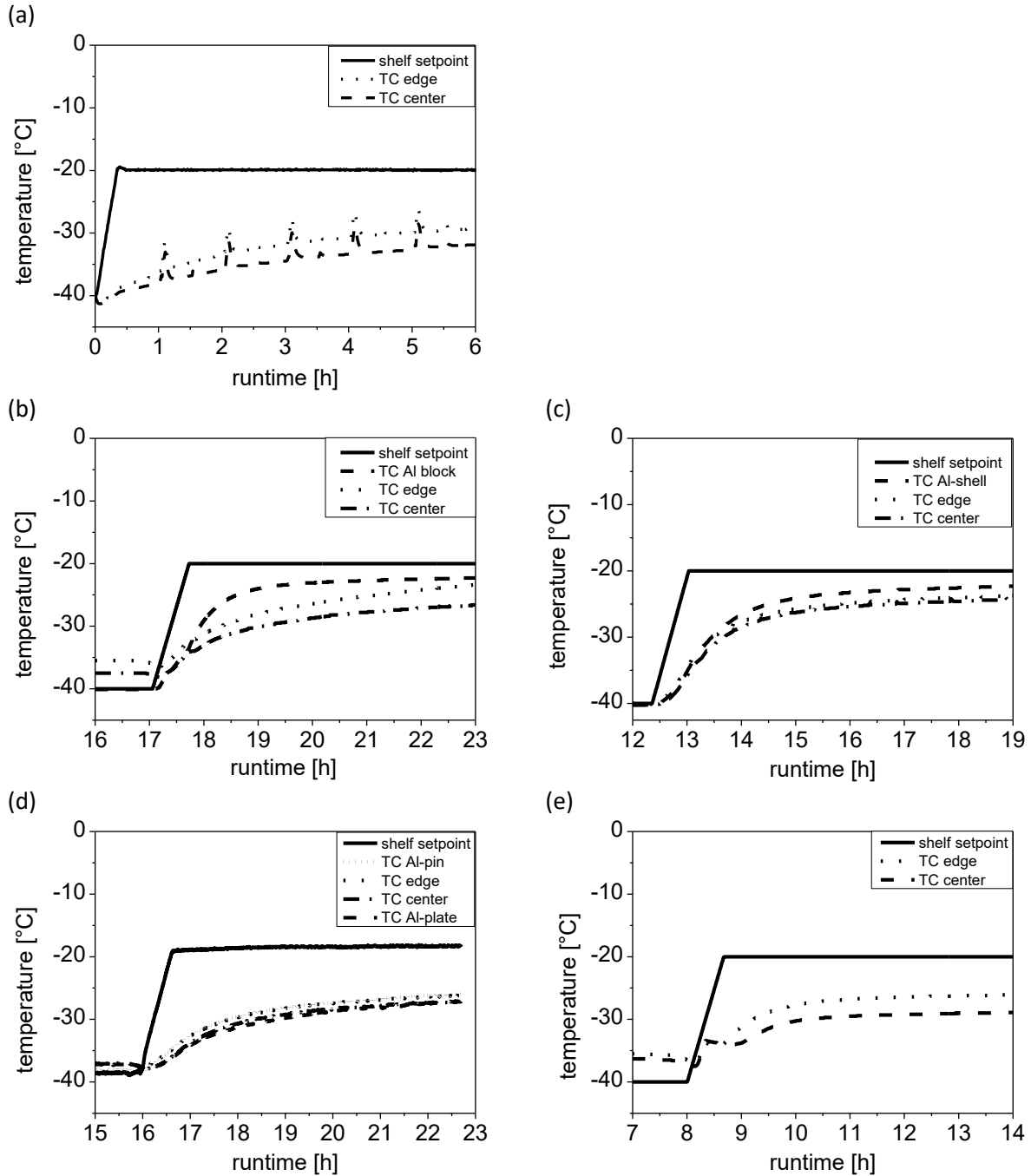


**Figure 5-4 Typical temperature profiles during the drying step of a 5% mannitol solution filled into vials (a) and DCCs standing in the block holder (b), shell holder (c), flexible holder (d) and the guardrail holder (e). The steep temperature increase in Figure 5-4 (a) every hour primary drying originated from the pressure rise test.**

The shell holder successfully diminished the influence of atypical radiation: Temperature differences between edge and center DCCs could be reduced to 0.5°C during primary drying which lies within the range of error of the thermocouples. The aluminum shell temperature quickly adapted to the increasing shelf temperature in the ramping phase as well. The temperature difference between shelf and holder was around 4.2°C after 3 hours and hence not quite as good as for the block. Presumably, this was due to the smaller contact area between both surfaces as compared to the block holder.

The flexible holder could reduce the influence of atypical radiation as well ( $\Delta T$  center-edge of 1°C). However, there was a large temperature difference between the shelf and the aluminum plate of around 11°C after 3 hours of primary drying, implying a suboptimal heat transfer between both parts. This was the result of the small contact area between the shelf and the pins of the holder system and will be outlined in the following section.

Atypical radiation seemed to have the same impact on the guardrail holder (Figure 5-4 (e)) as on the block device. The temperature difference between edge and center DCCs was around 3°C. But it has to be kept in mind that there is a substantial variance in sublimation rates in this holder device (chapter 5.4.1), independent of the DCCs' positions which may overwrite the difference between center and edge DCCs.

Overall, the same trend in the holder's potential for process design in the drying phase resulted as for the freezing phase (chapter 5.4.2). The shell was the superior holder device since it provided the best radiation shielding which is very important for scale-up. The flexible holder provided a good radiation shielding too, but the due to a third barrier against energy transfer resulted in a higher temperature difference between shelf and product. Block and guardrail holder were again the least efficient systems. With temperature differences between center and edge DCCs, that were 6 times higher than in for the shell, a thorough process design is problematic.

#### 5.4.4 Comparison of heat transfer coefficients

For a good lyophilization process development, it is key to have sufficient information about the energy transfer of the container- and holder device and its pressure dependence. By plotting the different heat transfer coefficients against chamber pressure, one can gain valuable information for example at which pressure setpoint energy transfer is most efficient and how the energy transfer is affected by the different modes of heat transfer.<sup>5</sup>

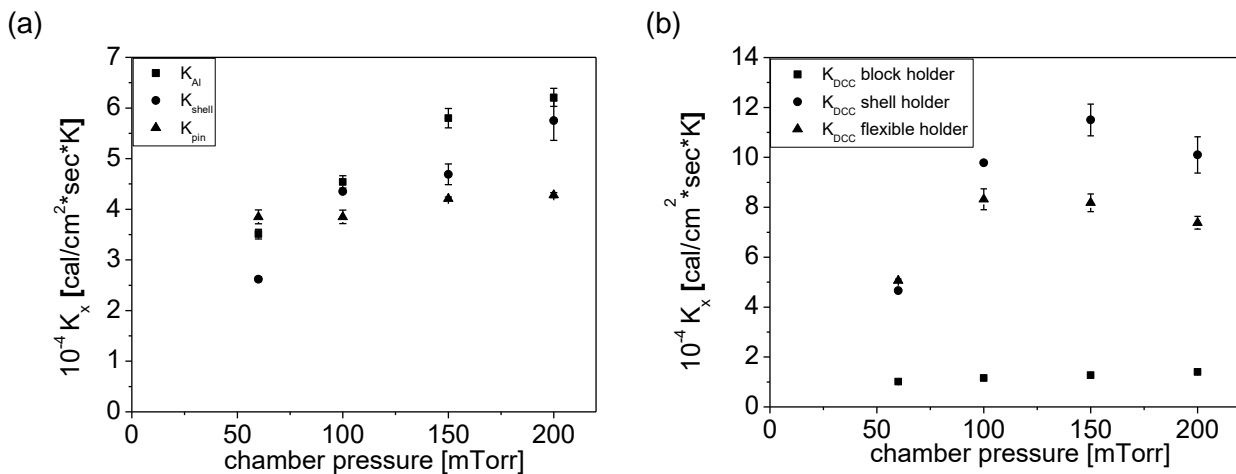


**Figure 5-5 Heat transfer coefficients between the shelf and the first part of the holder device (a) ( $K_{Ai}$  for the block holder;  $K_{shell}$  for the shell holder and  $K_{pin}$  for the flexible holder) and the holder device and the product (b) plotted against chamber pressure.**

Figure 5-5 (a) depicts the effect of chamber pressure on the energy transfer between the shelf and the first part of the particular holder system.  $K_{Ai}$ , for the block holder showed a clear nonlinear pressure dependence with values ranging from  $3.51E-04 \pm 9.65E-06$  cal/(s\*cm<sup>2</sup>\*K) at 60 mTorr to  $6.21E-04 \pm 1.79E-05$  cal/(s\*cm<sup>2</sup>\*K) at 200 mTorr.<sup>5</sup> This corresponds to an increase of around 43%.  $K_{shell}$  followed the same trend and increased from  $2.62E-4 \pm 4.64E-6$  cal/(s\*cm<sup>2</sup>\*K) to  $5.75E-4 \pm 3.89E-5$  cal/(s\*cm<sup>2</sup>\*K) in the same pressure range. This pressure dependence of both coefficients was a clear indicator that gas conduction played a major role during energy transfer.<sup>13</sup> In contrast,  $K_{pin}$  stayed almost constant over the whole pressure range between  $3.85E-4 \pm 1.38E-5$  cal/(s\*cm<sup>2</sup>\*K) at 60 mTorr and  $4.28E-4 \pm 4.75E-6$  cal/(s\*cm<sup>2</sup>\*K) at 200 mTorr. The trend for the pressure dependence of  $K_{Ai} \approx K_{shell} > K_{pin}$  was, however, surprising since gas conduction mainly depends on the contact area between two surfaces as long as the holder materials are the same. This was the case in this setup with the stainless steel shelf

and the untreated aluminum for the holders. The contact area between the shelf and the first part of the holder devices were as follows: 2.56 cm<sup>2</sup>/DCC for the block holder, 2.96 cm<sup>2</sup>/DCC for the shell holder and 0.9 cm<sup>2</sup>/DCC for the flexible holder. Hence, it was expected that  $K_{\text{shell}}$  would depend more on pressure than  $K_{\text{Al}}$ . The higher extend of pressure dependence of  $K_{\text{Al}}$  was most probably caused by the aluminum holder's geometry in combination with the unevenness of the shelf: Since the block was made of one piece of aluminum (193 × 96 mm<sup>2</sup>) it was more likely that gas was entrapped between the shelf and the block than for the individual shells. This entrapped gas is the root cause of pressure dependent energy transfer.<sup>13</sup>

Figure 5-5 (b) illustrates the pressure dependence of  $K_{\text{DCC}}$  for the different holder devices. This heat exchange between holder system and product within the DCC is very important for the actual product temperature during primary drying. The aluminum block, having no direct contact area with the DCC product region, was the least efficient system and  $K_{\text{DCC}}$  slightly increased from 1.01E-4 ± 4.88E-7 cal/(s\*cm<sup>2</sup>\*K) at 60 mTorr to 1.4E-4 ± 3.78E-6 cal/(s\*cm<sup>2</sup>\*K) at 200 mTorr. The linear increase was unexpected as gas conduction follows a nonlinear trend.<sup>19</sup> Possibly, the gas layer formed between aluminum block and DCC only heated up the glass of the DCC and thus minimized the overall influence of chamber pressure on  $K_{\text{DCC}}$ .<sup>5</sup> Overall,  $K_{\text{DCC}}$  can be regarded as low. The consequence is a rather warm holder device, due to the good energy transfer between shelf and holder, in combination with a cold product temperature during freeze-drying in DCCs standing in the aluminum block. This leads to long lyophilization cycles and holding times during freezing which is not desirable.

By embedding the DCCs into a shell holder and thereby completely surrounding them with aluminum, it was possible to increase this important energy transfer by factors of around 4 to 7, depending on the chamber pressure.  $K_{\text{DCC}}$  in the shell holder increased from 4.66E-4 ± 6.8E-6 cal/(s\*cm<sup>2</sup>\*K) at 60 mTorr to 1.01E-3 ± 7.29E-5 cal/(s\*cm<sup>2</sup>\*K) at 200 mTorr chamber pressure. In the flexible holder, only the part of the DCC filled with product solution was completely surrounded by aluminum.<sup>6</sup> This contact area was limited by the height of the plate (15 mm) which was the basis of the holder and the only part having contact to the DCCs. In order to achieve a good comparability of the results, each DCC in every holder system was filled with 0.75 ml of product solution. This corresponded to an

initial thickness of the frozen layer ( $L_{ice}$ ) of 14.4 mm. As  $K_{DCC}$  is time depended and therefore more complex to define.<sup>5,6</sup> The decrease of  $L_{ice}$  during primary drying due to the ongoing sublimation, was calculated according to Equation (5-3).  $L_{ice}$  was then used to calculate the actual contact area between holder system and product in the DCC ( $A_{DCC}$ ) at the time point  $t$  with Equation (5-4), where  $m(0)$  is the initial amount of product solution [g] and  $m(t)$  the amount of ice removed during the time interval  $t$ . Further, the density of ice ( $\rho_I = 0.92 \text{ g/cm}^3$ ), the geometric dimension of the DCC ( $A_p$  and  $r$ ) and the porosity of the 5% mannitol solution ( $\epsilon = 0.97$ ) were taken into account.<sup>6</sup>

$$L_{ice} = \frac{m(0) - m(t)}{\rho_I * A_p * \epsilon} \quad (5-3)$$

$$A_{DCC} = 2 * r * \pi * L_{ice} \quad (5-4)$$

Values of  $K_{DCC}$  for the flexible holder ranged from  $5.06E-4 \pm 6.53E-6 \text{ cal}/(\text{s} * \text{cm}^2 * \text{K})$  at 60 mTorr to  $7.38E-4 \pm 2.52E-5 \text{ cal}/(\text{s} * \text{cm}^2 * \text{K})$  at 200 mTorr. The  $K_{DCC}$  values with the flexible holder showed a nonlinear pressure dependence similar to the shell device, but to a different extend. In the 60 to 100 mTorr chamber pressure range  $K_{DCC}$  values differed at most by 15% between shell and flexible holder. At higher pressure setpoints this difference in heat transfer effectiveness was increased to up to 27% at 200 mTorr. This pressure-dependent, increasing deviation was most probably due to the fact that the overall contact area between the whole DCC-glass-barrel and the holder with an overall contact area of  $212 \text{ mm}^2$  was larger in the case of the shell system: Therefore the shell holder could continuously heat up almost the complete glass barrel of the DCC, leading to a similar effect as observed for the aluminum block holder where it resulted in a linear increase of  $K_{DCC}$ . One has to keep in mind that energy transfer only takes place at the contact area between the frozen product in the DCC and the holder<sup>6</sup> (Equation (5-4)) – which was at least in the beginning the same for all holder devices analyzed ( $A_{DCC\_initial} = 485 \text{ mm}^2$ ). Nevertheless, it seemed that a large contact area between holder system and the wall of the container system could additionally increase the heat transfer effectiveness.

An efficient, virtual heat transfer coefficient ( $K_{tot}$ ) can be defined, taking into account all individual barriers against energy transfer.<sup>6</sup> This coefficient can be used to compare different holder system with each other. Equation (5-5) was used to calculate  $K_{tot}$  for the block- and shell holder. For the flexible holder,  $K_{tot}$  was calculated according to Equation (5-6).

$$K_{tot} = \frac{1}{\left( \frac{1}{K_{Al/shell} * A_{Al/shell}} + \frac{1}{K_{DCC} * A_{DCC}} \right) * A_{tot}} \quad (5-5)$$

$$K_{tot} = \frac{1}{\left( \frac{1}{K_{pin} * A_{pin}} + \frac{1}{K_{plate} * A_{plate}} + \frac{1}{K_{DCC} * A_{DCC}} \right) * A_{tot}} \quad (5-6)$$

In both cases,  $A_{tot}$  represents the mean of the all areas of energy transfer. The major drawback of this virtual coefficient is that it only provides relevant data if systems with the same number of barriers against energy transfer are compared. This means, that the flexible holder that consist of 3 pieces cannot be directly compared with the shell- and aluminum holder. To compare all holder devices, it is important to combine information about  $K_{tot}$  with the previously shown results for sublimation rates and temperatures profiles.

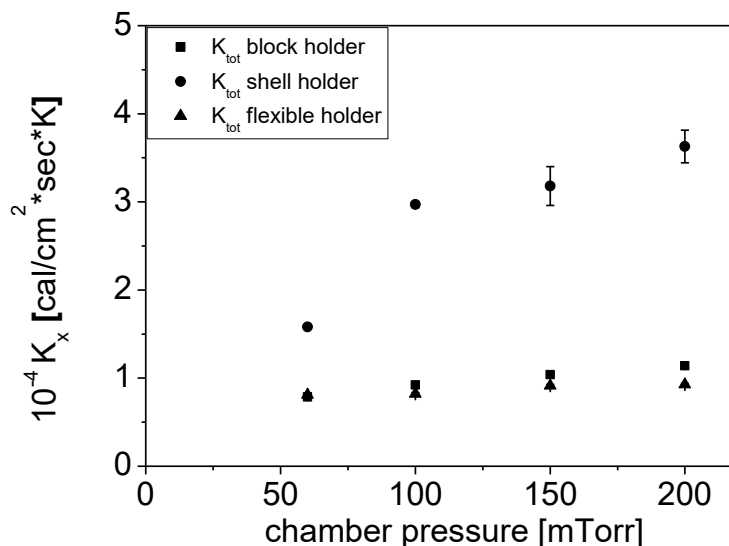


**Figure 5-6 Efficient virtual coefficients of all holder systems plotted against chamber pressure.**

Figure 5-6 demonstrates that the shell holder device was the best holder device in terms of heat transfer effectiveness. Still, with values ranging from  $1.58\text{E-}4 \pm 2.06\text{E-}6 \text{ cal}/(\text{s}\cdot\text{cm}^2\cdot\text{K})$  at 60 mTorr to  $3.63\text{E-}4 \pm 1.85\text{E-}5 \text{ cal}/(\text{s}\cdot\text{cm}^2\cdot\text{K})$  at 200 mTorr, the overall energy transfer was around 3 times less effective than for freeze-drying in the traditional vial container system ( $3\text{E-}4$  to  $6\text{E-}4 \text{ cal}/(\text{s}\cdot\text{cm}^2\cdot\text{K})$ ) for the investigated pressure range.<sup>19</sup> However, for vials only one barrier against energy transfer needs to be taken into account.  $K_{\text{tot}}$  values for aluminum- and flexible holder did barely exceed the level of  $1\text{E-}4 \text{ cal}/(\text{s}\cdot\text{cm}^2\cdot\text{K})$  showing a significant optimization potential for both devices.

## 5.5 Summary and Conclusion

The aim of this study was to compare four different holder systems commonly used for freeze-drying in DCCs. The main criteria were drying homogeneity, ability of the device to minimize the influence of atypical radiation on product temperatures and heat transfer effectiveness (Table 5-5).

**Table 5-5 Overall evaluation of the different holder devices concerning 1.) drying homogeneity, 2.) shielding from atypical radiation and 3.) effectiveness of heat transfer.**

Holder type	Homogeneity	Shielding	Heat transfer
Guardrail	- -	-	
Block	-	- -	-
Shell	++	++	++
Flexible	+	+	+

Drying homogeneity was characterized via sublimation experiments, where the position depended sublimation rate of each DCC was assessed. These shelf mapping experiments showed that the holder devices, in which the DCCs were embedded in the holder (shell holder) or at least the product containing part of the DCC was surrounded by aluminum (flexible holder), provide a much better drying homogeneity: Flexible- and shell holder could reduce the influence of atypical radiation by almost 60% compared to the block system. With a standard deviation of only 7% and min./max. values of 112.9 mg/h and 191.4 mg/h respectively for the whole batch, the use of the shell holder yielded the most homogenous sublimation rates during the shelf mapping experiments. The use of the guardrail holder resulted in a sublimation rate standard deviation of around 45% with min./max. values of 9.1 mg/h and 284.3 mg/h respectively. This clearly demonstrated that this device is not recommended as a holder for freeze-drying in DCCs.

The temperature profile analysis during the freezing step Figure 5-4 revealed that the traditional vial container is still superior to the DCCs standing in a holder device in terms of reaction times to shelf temperature changes. However, the shell holder system comes very close to the vial concerning reaction times and even provided a faster freezing than the vial (Figure 5-3 (c)). The product temperature followed the shelf temperature very closely and a “lag time” of only 10 min between both temperatures could be observed. The temperature difference between shelf and product at the end of ramp (15°C) was in a very good range as well for the shell system. In contrast, lag times and temperature differences at the end of the ramp for the block and flexible holder were increased by factors of around 4 and 3 respectively, compared to the shell device. Therefore holding times need to be significantly prolonged if a block- or flexible holder should be used.

Product temperature profiles recorded during primary drying revealed that the block holder did not sufficiently shield the DCC standing in the edge positions of the array from atypical radiation. Compared to vials the temperature difference between edge and center DCCs was increased by 1°C up to 3°C as a result of the DCCs being elevated above the holder. In the case of the flexible- and shell holder the product solution was completely surrounded by the holder material. This helped to reduce the influence of atypical radiation significantly which could be seen in lower temperature differences of around 1°C for the flexible- and only 0.5°C for the shell holder. Hence, the shell holder provided the best radiation shielding, enhanced the transferability of the results to a larger scale and improved the homogeneity between DCCs of whole the array. Heat transfer coefficient analysis showed that the holders'  $K_x$  values depended on pressure to different extends.  $K_{Al}$  and  $K_{shell}$  showed pronounced, nonlinear pressure dependence, indicating that gas conduction played a major role in this particular heat transfer. In contrast,  $K_{pin}$  of the flexible holder stayed almost constant over the pressure range from 60 to 200 mTorr. The heat transfer coefficient  $K_{DCC}$  describes the energy transfer between holder system and product within the DCC. The block holder was the least efficient holder device with values ranging from  $1.01E-4 \pm 4.88E-7 \text{ cal}/(\text{s}\cdot\text{cm}^2\cdot\text{K})$  at 60 mTorr to  $1.4E-4 \pm 4.88E-7 \text{ cal}/(\text{s}\cdot\text{cm}^2\cdot\text{K})$  at 200 mTorr.<sup>5</sup> This was again due to the missing direct contact surface between block holder and product region of the DCCs. By creating an area of direct contact between both surfaces it was possible to increase this important energy transfer by factors of up to 5 in the case of the flexible holder and 10 in the case of the shell device:

With values for  $K_{DCC}$  from  $4.66E-4 \pm 6.8E-6 \text{ cal}/(\text{s}\cdot\text{cm}^2\cdot\text{K})$  at 60 mTorr to  $1.01E-3 \pm 7.29E-5 \text{ cal}/(\text{s}\cdot\text{cm}^2\cdot\text{K})$  at 200 mTorr chamber pressure, the shell holder had the most efficient energy transfer. For the overall energy transfer efficiency an “efficient virtual coefficient,  $K_{tot}$ ” was defined and confirmed that the shell holder is the best holder device in terms of overall heat transfer effectiveness. Still, with values ranging from  $1.58E-4 \pm 2.06E-6 \text{ cal}/(\text{s}\cdot\text{cm}^2\cdot\text{K})$  at 60 mTorr to  $3.63E-4 \pm 1.85E-5 \text{ cal}/(\text{s}\cdot\text{cm}^2\cdot\text{K})$  at 200 mTorr, the overall energy transfer is around 3 times less efficient than for freeze-drying in the traditional vial container system ( $3E-4$  to  $6E-4 \text{ cal}/(\text{s}\cdot\text{cm}^2\cdot\text{K})$ ) for the investigated pressure range.<sup>19</sup>

The differences in heat transfer effectiveness between the traditional vial container and even the most efficient holder system for freeze-drying in DCCs make it clear that a thorough process transfer is necessary and that one cannot simply transfer an existing vial based lyophilization cycle to a DCC without further scale-up experiments. Furthermore, the decision on which holder to use should carefully take the energy transfer properties into account.

## 5.6 References

1. Carpenter J, Pikal M, Chang B, Randolph T 1997. Rational Design of Stable Lyophilized Protein Formulations: Some Practical Advice. *Pharm Res* 14(8):969-975.
2. Hibler S, Gieseler H 2012. Heat transfer characteristics of current primary packaging systems for pharmaceutical freeze-drying. *Journal of Pharmaceutical Sciences* 101(11):4025-4031.
3. Patel SM, Pikal MJ 2011. Emerging freeze-drying process development and scale-up issues. *AAPS PharmSciTech* 12(1):372-378.
4. Polin JB 2003. The ins and outs of prefilled syringes. *Pharm Med Packag News* 11(5):40-43.
5. Korpus C, Haase T, Sönnichsen C, Friess W 2015. Energy Transfer During Freeze-Drying in Dual-Chamber Cartridges. *Journal of Pharmaceutical Sciences* 104(5):1750-1758.
6. Korpus C, Pikal M, Friess W 2016. Heat Transfer Analysis of an Optimized, Flexible Holder System for Freeze-Drying in Dual Chamber Cartridges Using Different State-of-the-Art PAT Tools. *Journal of Pharmaceutical Sciences* 105(11):3304-3313.
7. Franks F 1998. Freeze-drying of bioproducts: putting principles into practice. *European Journal of Pharmaceutics and Biopharmaceutics* 45(3):221-229.
8. Tang X, Nail S, Pikal M 2006. Evaluation of manometric temperature measurement (MTM), a process analytical technology tool in freeze drying, part III: Heat and mass transfer measurement. *AAPS PharmSciTech* 7(4):E105-E111.
9. Tang X, Nail SL, Pikal MJ. 2006. Evaluation of manometric temperature measurement, a process analytical technology tool for freeze-drying: Part I, product temperature measurement. *AAPS PharmSciTech* 7(4): E95-E103.
10. Wang W 2000. Lyophilization and development of solid protein pharmaceuticals. *International Journal of Pharmaceutics* 203(1–2):1-60.
11. Rambhatla S, Pikal M 2003. Heat and mass transfer scale-up issues during freeze-drying, I: Atypical radiation and the edge vial effect. *AAPS PharmSciTech* 4(2):22-31.
12. Geidobler R, Mannschedel S, Winter G 2012. A new approach to achieve controlled ice nucleation of supercooled solutions during the freezing step in freeze-drying. *Journal of Pharmaceutical Sciences* 101(12):4409-4413.
13. Pikal MJ, Roy ML, Shah S 1984. Mass and heat transfer in vial freeze-drying of pharmaceuticals: Role of the vial. *Journal of Pharmaceutical Sciences* 73(9):1224-1237.

14. Teagarden DL, Speaker SM, Martin SWH, Österberg T. 2010. Practical Considerations for Freeze-Drying in Dual Chamber Package Systems. *Freeze Drying/Lyophilization of Pharmaceutical and Biological Products*, ed. p 494-526.
15. Pisano R, Fissore D, Barresi AA, Rastelli M 2013. Quality by Design: Scale-Up of Freeze-Drying Cycles in Pharmaceutical Industry. *AAPS PharmSciTech* 14(3):1137-1149.
16. Tang XC, Nail SL, Pikal MJ 2005. Freeze-drying process design by manometric temperature measurement: design of a smart freeze-dryer. *Pharm Res* 22(4):685-700.
17. Patel SM, Jameel F, Pikal MJ 2010. The effect of dryer load on freeze drying process design. *Journal of Pharmaceutical Sciences* 99(10):4363-4379.
18. Pikal MJ 1985. Use of laboratory data in freeze drying process design: heat and mass transfer coefficients and the computer simulation of freeze drying. *Journal of parenteral science and technology : a publication of the Parenteral Drug Association* 39(3):115-139.
19. Patel SM, Pikal MJ 2010. Freeze-drying in novel container system: Characterization of heat and mass transfer in glass syringes. *Journal of Pharmaceutical Sciences* 99(7):3188-3204.

6 *LYOPHILIZATION-CYCLE DESIGN FOR DUAL  
CHAMBER CARTRIDGES AND A METHOD FOR  
ONLINE PROCESS CONTROL:  
THE DCC-LYOMATE PROCEDURE*

Parts of the following chapter are intended for publication.

## 6.1 Abstract

Freeze-Drying process design is a challenging task that necessitates a profound understanding of the complex interrelation between critical process parameters (e.g. shelf temperature and chamber pressure), heat transfer characteristics of the involved materials (e.g. product container and holder devices) and critical quality attributes of the drug product (e.g. collapse temperatures and residual moisture). The Dual Chamber Cartridge “(DCC) LyoMate” (from **lyophilization** and **automated**), is a manometric temperature measurement (MTM) -based process control strategy that was developed within this study to streamline this complicated task. It was successfully applied, using 5% sucrose formulations with 0.5 and 1 ml fill volumes. 150 DCCs, corresponding to a sublimation front area of 87.7 cm<sup>2</sup>, were identified to be the minimum number to assure reliable MTM calculations. The system was further challenged using 2, 20 and 100 mg/ml formulations of a monoclonal antibody (mAb). The DCC LyoMate method did not only produce pharmaceutically acceptable cakes but was also able to maintain the desired product temperature irrespective of formulation and protein content. Controlled nucleation could significantly improve the correlation between calculated and measured product temperatures, but enhanced fogging for the 2 mg/ml antibody formulation. For the highly concentrated 100 mg/ml mAb formulation, calculated and measured temperatures differed up to 8°C, already with the first MTM and here the use of thermocouple data for LyoMate-based shelf temperature calculations is mandatory. Despite these challenges, the DCC LyoMate procedure enabled a successful process design even at these high concentrations and yielded pharmaceutical elegant cakes that were lyophilized within the desired target product range. That is why the DCC LyoMate is a powerful tool that can help to design and online control the optimum lyophilization process for DCCs within the very first development run and thus helps to reduce development costs and to build up in-depth process knowledge. Plus, the DCC-LyoMate can be easily installed on every freeze-dryer capable of performing a MTM, without the need for any kind of hardware modification.

## 6.2 Introduction

Protein drugs, are often not sufficiently stable in liquid formulation.<sup>1</sup> In this case, lyophilization is typically applied to assure product quality.<sup>2</sup> In general, the vial is the most common container system for lyophilisates.<sup>3</sup> Reconstitution in vials implies several steps with a substantial risk of incorrect handling. Hence, there is a market need for an advanced container system, like the dual chamber cartridge (DCC, Figure 6-1) that is easy to use and improves patient compliance.<sup>4-6</sup>



**Figure 6-1 The shell holder system and a DCC with lyophilized product standing next to it.**

Lyophilization process design is a challenging task and various research articles address this in the context of freeze-drying in vials, with their comparably straightforward heat transfer characteristics.<sup>7,8</sup> For DCCs, lyophilization process design is disparately more complex than for vials due to different heat transfer features. Therefore, additional factors need to be taken into account for a successful process design.<sup>6</sup> Both, the use of an appropriate holder system for the DCCs as well as an in-depth knowledge of the mass and heat transfer processes is mandatory. There are basically four major differences between vials and DCCs: 1.) the energy transfer efficiency is decreased for DCCs due to the large distance

between shelf and product, 2.) the contact area decrease for energy transfer between the holder system and the product in the DCCs is more pronounced for DCCs due to a larger height to diameter ratio, 3.) the DCC holder systems acts as an energy reservoir which either absorbs or releases energy to the product during the process and 4.) the holder system presents an additional barrier against energy transfer from shelf to product. Previous studies addressed these challenges, and we gave advice how they can be overcome and showed how steady-state equations need to be adapted for a successful process design for lyophilization in DCCs.<sup>6,9,10</sup> Hereby, the shell holder system (Figure 6-1) was identified as the best device to assure an efficient and homogenous freeze-drying process.<sup>9</sup> Consequently the shell holder was the system of choice for the experiments performed in the present study.<sup>9</sup>

The purpose of the present study was to develop a MTM-based process control strategy, the DCC LyoMate (from **lyophilization** and **automated**) (Figure 6-2), that can be employed to purposefully plan and optimize lyophilization processes for DCCs. The research previously performed by Tang, Nail and Pikal<sup>11-14</sup> focusing on freeze-drying in vials formed the base of this study, in combination with our recently performed energy transfer and holder system studies for lyophilization in DCCs (Chapter 5).<sup>6,9,10</sup> The DCC LyoMate can be used right at the beginning of the process development phase and helps to save development times and costs. Today, lyophilization cycle process design for DCCs is commonly performed by repeating several development runs that are designed on a trial and error principle. This leads to suboptimal and conservative lyophilization cycles.<sup>6</sup> Due to its complexity, lyophilization process design for DCCs should only be done by highly trained personnel to avoid product damage. In contrast, the DCC LyoMate yields the optimum process already during the very first development run and can be executed also by less trained personnel due to its easy handling and clear recommendations for actions. It can be easily installed on every freeze-drying unit that is capable of performing manometric temperature measurement without the need for equipment modification.<sup>12</sup>

## 6.3 Materials and Methods

### 6.3.1 Materials

The DCCs (outer diameter 10.75 mm, inner diameter 8.65 mm, 1 ml max. fill volume) were purchased from Nuova Ompi (Piombino Dese, Italy), with plungers made of bromobutyl rubber (FM457-0; Helvoet Pharma, Lommel, Belgium).

A 5% sucrose [m/V] (Sigma-Aldrich, Seelze, Germany) solution as well as mAb formulations with concentrations of 2, 20 and 100 mg/ml, formulated with 5% sucrose in a 25 mM histidine buffer (pH 6.2) were filtered through a 0.2  $\mu\text{m}$  membrane filter (VWR, Radnor, USA) prior to filling into the DCCs. Concentrations were analyzed with a NanoDrop 2000 photometer ( $\epsilon_{280\text{nm}}$  of  $1.49 \text{ ml g}^{-1} \text{ cm}^{-1}$ ). (Thermo Scientific, Wilmington, Delaware, USA).

### 6.3.2 Freeze-drying microscopy

Collapse temperatures ( $T_c$ ) were assessed using a Linksys 32 freeze-dry microscope (FDM) (Linkam Scientific Instruments, Tadworth, UK) that was connected to a Linkam FDSD 196 stage. The according freeze-drying protocol is shown in Table 6-1. 2  $\mu\text{l}$  of the corresponding formulation were analyzed at a pressure of 75 mTorr during the drying phase.

**Table 6-1 Freeze-drying protocol for the FDM analysis performed at 75 mTorr.**

Step	Start temp. [ $^{\circ}\text{C}$ ]	End temp. [ $^{\circ}\text{C}$ ]	Step duration [min]
Freezing	$\approx 20$	-50	$\approx 70$
	-50	-50	10
Drying	-50	-40	2
	-40	-40	10
	-40	0	40
	0	20	20

### 6.3.3 Lyophilization unit

A Lyostar III freeze-dryer (SP Scientific, Stone Ridge, USA) with a chamber volume of 104 L, equipped with a self-made pressure rise test (PRT) system was used. The specifications and the implementation of the PRT system were described and discussed in detail in a previous study (Chapter 4).<sup>10</sup> Surface temperatures were measured using adhesive type-T thermocouples. Product temperatures were measured with 36-gauge type-T thermocouples (TCs) (both Omega Engineering, CT, USA). Thermocouples (TCs) were inserted into the product solution through the plunger. A capacitive manometer (MKS Baratron) and a pirani gauge sensor (Mini-Convector™ vacuum gauge, Helix Technology Corp., Mansfield, USA) were used to monitor the pressure in the freeze-dryer chamber. A data logger MSR-145 (MSR Electronics GmbH, Seuzach, CH) was connected to the capacitance manometer, recording the voltage data with a frequency of 10 Hz to enable the DCC LyoMate procedure (see section 6.3.6).

### 6.3.4 DCC holder system

A shell holder system (Figure 6-1) with a height of 65 mm, an outer diameter of 21 mm and a weight of 39 g was used.<sup>9</sup> In order to optimize the center of gravity and to improve the machinability of the shell, the outer diameter was narrowed down to 19 mm starting at a height of 31 mm up to the top. A major drilling with a diameter of 10.9 mm and a smaller drilling, with a diameter of 4 mm for the bypass, guaranteed that each DCC was fixed in the holder system. The major drilling stopped at a depth of 63 mm, making sure that the bottom of the DCC rested on a 2 mm thick base. For the sake of weight reduction and heat sterilizability, a second hole with a diameter of 8 mm was drilled through the bottom of the shell holder.<sup>9</sup>

### 6.3.5 Sample preparation and freezing protocols

0.5 ml or 1 ml of the filtered solutions were filled into each DCC. Four arrays of DCCs from 75 to 444 DCCs, corresponding to a sublimation interface of 0.42 cm<sup>2</sup>/L to 2.5 cm<sup>2</sup>/L, respectively were used. For the mAb formulation experiments 150 DCCs, each filled with 0.5 ml product solution, was used per run. Controlled nucleation was performed with the previously described ice fog method ( $T_s$ : -6°C, holding time: 45 min)<sup>10,15</sup> (Chapter 4), followed by a ramping phase to -50°C at 1°C/min. Regular, shelf-ramped freezing was performed with a ramp rate of 1°C/min and holding times

of 60 min at 5°C and - 5°C. After an overnight hold phase at - 50°C, prior to pulling the vacuum, the shelf temperature was elevated at 0.5°C/min to the desired setpoint that was determined via the first step of the LyoMate procedure (see section 6.3.6) and held for 60 min.

### 6.3.6 The DCC LyoMate procedure

The DCC LyoMate procedure (Figure 6-2) is a strategy that recommends actions to find and adjust the shelf temperature to achieve the desired target product temperature during primary drying. In order to enhance the transferability of the low scale experiments performed in this study to a larger scale, the processes were designed for DCCs standing in the middle of the array (center DCCs). Hereby, the first two rows of DCCs acted as thermal shields to protect the center DCCs from additional radiation coming from the freeze-dryer walls and door. This should mimic the setup of a large scale freeze-dryer with wall-cooling.<sup>6,16,17</sup> Therefore, product temperatures mentioned in this study always refer to center DCCs. This system is based on a self-made manometric temperature (MTM) system<sup>10</sup> in combination with steady-state equations for freeze-drying<sup>11,18</sup>, adapted for in DCCs.

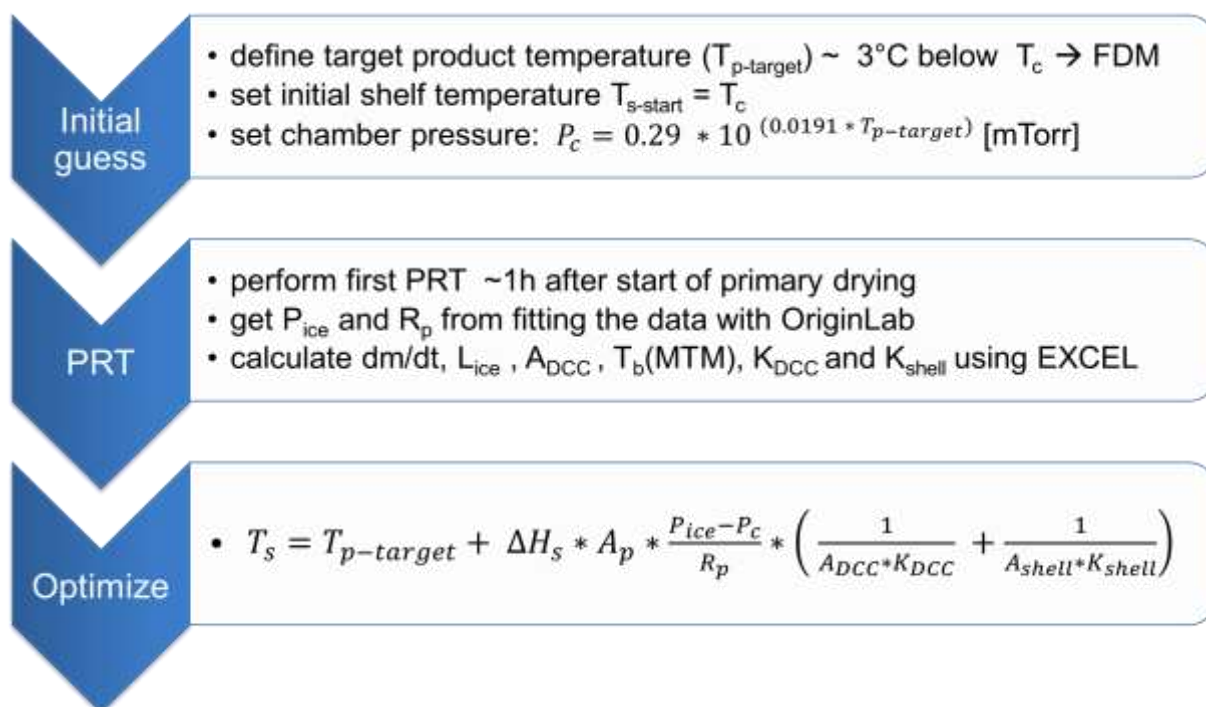


**Figure 6-2 Scheme of the DCC-LyoMate procedure**

The first step in the DCC LyoMate procedure, the “initial guess” of starting shelf temperature ( $T_{s-start}$ ) and the optimum chamber pressure ( $P_c$ ) (Figure 6-2), is the

same as for vials. The target  $T_p$  is set equal to the collapse temperature ( $T_c$ ) of the formulation determined by Freeze-Drying-Microscopy with a 3°C safety margin.  $T_{s-start}$  however equals  $T_c$ , thus higher than for vials because of the less efficient energy transfer from shelf to product. The chamber pressure is set according to the Tang et al. by:<sup>11</sup>

$$P_c = 0.29 * 10^{(0.0191 * T_{p-target})} \quad (6-1)$$

Next, during “PRT”, the first PRT<sup>10</sup> is performed after one hour of primary drying. Subsequently, the vapor pressure of ice at the sublimation interface ( $P_{ice}$ ) [Torr] and the area-normalized mass transfer resistance rate of the dried layer ( $R_p$ ) [ $\text{cm}^2 * \text{h} * \text{Torr} * \text{g}^{-1}$ ] are calculated<sup>10,19</sup> to the raw data using OriginLab software (OriginLab Corporation, Northampton, USA).<sup>10,19</sup>

Values for  $P_{ice}$  and  $R_p$  are used to calculate the sublimation rate ( $dm/dt$ ) [g/s] using Equation (6-2), where  $A_p$  [ $\text{cm}^2$ ] is the inner surface area of the DCC and  $P_c$  [Torr] is the chamber pressure by EXCEL.

$$\frac{dm}{dt} = A_p * \frac{P_{ice} - P_c}{R_p} \quad (6-2)$$

The remaining ice layer thickness ( $L_{ice}$ ) and the decreasing contact area for energy transfer between holder device and DCC ( $A_{DCC}$ ) are calculated by Equations (6-3) and (6-4), where  $m(0)$  is the initial amount of product solution [g] and  $m(t)$  the amount of ice removed during the time interval  $t$ . The density of ice ( $\rho_I = 0.92 \text{ g/cm}^3$ ),  $A_p$  and the radius of one DCC ( $r$ ) as well as the porosity of the product solution ( $\varepsilon = 0.97$ ) were taken into account.<sup>10,11</sup>

$$L_{ice} = \frac{m(0) - m(t)}{\rho_I * A_p * \varepsilon} \quad (6-3)$$

$$A_{DCC} = 2 * r * \pi * L_{ice} \quad (6-4)$$

The product temperature at the bottom of the product chamber in the DCC  $T_b(\text{MTM})$  [K] can be calculated using the following relationship.

$$T_b(MTM) = \frac{-6144.96}{(\ln P_{ice} - 24.01849)} + \frac{24.7 * L_{ice} * \frac{(P_{ice} - P_0)}{R_p} - 0.0102 * L_{ice} * (T_s - T_i)}{(1 - 0.0102 * L_{ice})} \quad (6-5)$$

In Equation (6-5), the first term represents the product temperature at the sublimation interface ( $T_i$ ) [K] and the second term is the temperature difference,  $\Delta T$  [K], from the sublimation interface to the bottom of the DCC across the frozen layer.  $T_b(MTM)$  was used as a surrogate parameter for the accuracy of the whole MTM method and compared to product temperatures measured via thermocouples readouts  $T_b(TC)$ .

Energy transfer coefficients for the transfer between shelf and shell holder ( $K_{shell}$ ) and between the shell and the DCC ( $K_{DCC}$ ) were calculated using Equations (6-6) and (6-7).

$$K_{shell} = \frac{\Delta H_s * A_p * \frac{P_{ice} - P_c}{R_p}}{A_{shell} * (T_{shelf} - T_{shell})} \quad (6-6)$$

$$K_{DCC} = \frac{\Delta H_s * A_p * \frac{P_{ice} - P_c}{R_p}}{A_{DCC} * (T_{shell} - T_b)} \quad (6-7)$$

In both Equations,  $\Delta H_s$  represents the heat of sublimation of ice (660 cal/g).<sup>18</sup>  $T_{shell}$  [K] is the temperature of the shell holder device and was measured using adhesive thermocouples. In contrast to freeze-drying in vials, this is necessary since the MTM method cannot calculate the temperature of the holder system.  $T_b$  [K] is the product temperature and can be assed either noninvasively via MTM or direct and invasively with thermocouple readouts.

In the third step of the DCC LyoMate procedure, “Optimize”, the previously gained data is used to calculate the optimum shelf temperature setpoint by Equation (6-8) and manually adjusted for the lyophilizer control software, as soon as the difference between current and newly calculated shelf temperature setpoint is  $\geq 0.5^{\circ}\text{C}$ . Also automated adjustment is possible.

$$T_s = T_{p\text{-target}} + \Delta H_s * A_p * \frac{P_{ice} - P_c}{R_p} * \left( \frac{1}{A_{DCC} * K_{DCC}} + \frac{1}{A_{shell} * K_{shell}} \right) \quad (6-8)$$

Step two and three of the DCC LyoMate procedure were repeated approximately every 30 or 60 min during the first 5 hours of primary drying. The end of primary drying was determined via comparative pressure measurement between the pirani gauge pressure sensor in the freeze-drying chamber and the capacitance manometer. As soon as the pressure difference between both sensors fell below 2 mTorr, secondary drying started. Hereby, the primary drying chamber pressure was maintained and the shelf temperature was elevated with a ramp rate of  $0.1^{\circ}\text{C}$  to  $10^{\circ}\text{C}$  and kept there for 15 min. Afterwards, the shelf temperature was further increased to  $20^{\circ}\text{C}$  with  $0.1^{\circ}\text{C}/\text{min}$  and a final holding step of 60 min was applied.

## 6.4 Results and Discussion

### 6.4.1 DCC LyoMate proof of concept study

The DCC LyoMate was developed to streamline the lyophilization cycle development for state-of-the-art container systems like DCCs that pose an increased complexity compared to vials due to a decreased heat transfer from shelf to product and longer reaction times to shelf temperature changes.<sup>6</sup> This novel tool should enable a thoughtful process -design and -online control, based on a sound process understanding instead of several, inefficient and time-consuming trial and error development runs which are still very common today and lead to suboptimal cycles.<sup>6,10</sup> In order to check if the DCC LyoMate procedure worked and if the previously delineated calculations were correct and a proof of concept study was performed using a 5% sucrose formulation with a fill volume of 0.5 ml and a total number of 324 DCCs which corresponds to a fully loaded lyophilizer tray. The ice-fog method was used for controlled nucleation. Sucrose was chosen as a model formulation due to its very low glass transition temperature of - 35°C and its sensitive reaction to thermal stresses that can easily lead to macroscopic issues e.g. shrinkage or meltback.<sup>20</sup> According to the FDA Guide to inspections of lyophilization of parenterals, meltback is a severe problem that can lead to product instability and degradation.<sup>21</sup> Macroscopic appearance was defined as the main critical quality attribute for the proof of concept. The difference between the LyoMate-based, calculated  $T_b(\text{MTM})$  and measured product temperature  $T_b(\text{TC})$ ,  $\Delta T_b (\text{MTM-TC})$ , was the process- related success criteria.

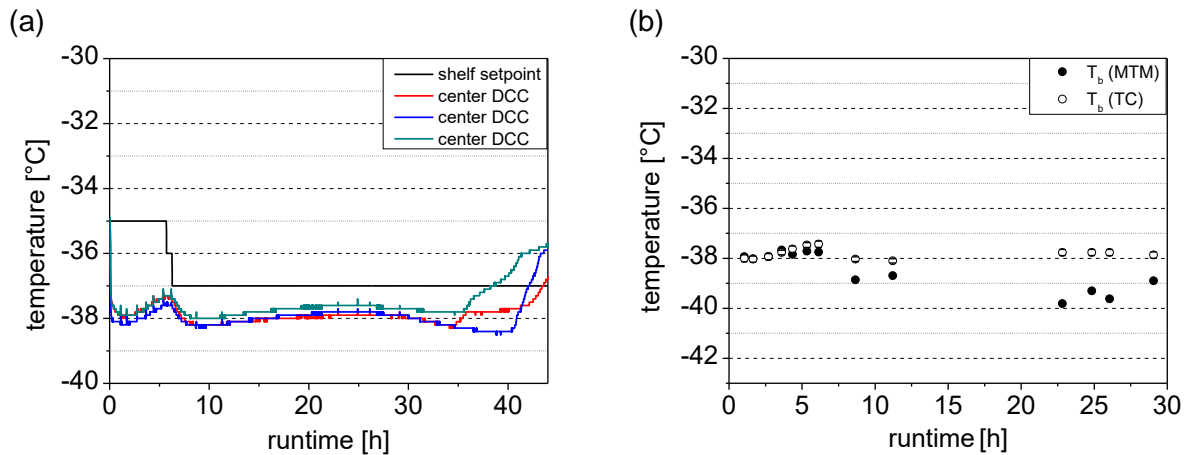


**Figure 6-3 (a)  $T_p$  and  $T_c$  profile during primary drying of 324 DCCs filled with 5% sucrose, freeze-dried with the DCC LyoMate procedure at  $T_{p\text{-target}} = -38^\circ\text{C}$ . (b) Correlation between the LyoMate-based, calculated product temperature,  $T_b(\text{MTM})$ , and the product temperature measured with thermocouples,  $T_b(\text{TC})$ .**

For this experiment we used  $T_{p\text{-target}} = -38^\circ\text{C}$ ,  $T_{s\text{-start}} = -35^\circ\text{C}$  and a chamber pressure of 60 mTorr. Figure 6-3 (a) illustrates the  $T_s$  and  $T_p$  profile during primary drying. After equilibrating the DCCs at  $-35^\circ\text{C}$  for 60 min, the vacuum was pulled which resulted in an initial cooling of the product to  $-38^\circ\text{C}$ . Afterwards,  $T_p$  slowly increased up to  $-37.5^\circ\text{C}$  at a runtime of 5.3 h. At that point, the DCC LyoMate calculation yielded a new shelf temperature setpoint of  $-35.5^\circ\text{C}$  (Table 6-2) and  $T_s$  was manually adjusted to  $-36^\circ\text{C}$ .

**Table 6-2 Various process parameters gained with the DCC LyoMate during the primary drying phase of a 0.5 ml 5% sucrose formulation.**

runtime [h]	LyoMate $T_s$ [°C]	new $T_s$ setpoint [°C]	$10^{-4} K_{shell}$ [cal/(s*cm <sup>2</sup> *K)]	$10^{-4} K_{DCC}$ [cal/(s*cm <sup>2</sup> *K)]
1.0	-35.0	-35	8.9	11.1
1.7	-35.0	-35	7.1	11.6
2.7	-35.1	-35	7.3	12.7
3.6	-35.2	-35	6.4	10.8
4.4	-35.4	-35	7.8	13.2
5.3	-35.5	-36	7.7	12.5
6.1	-36.6	-37	22.3	15.4
8.7	-37.0	-37	17.9	23.9
11.2	-36.9	-37	17.9	19.7
22.8	-37.2	-37	44.4	14.8
24.8	-37.2	-37	35.8	12.7
26.1	-37.2	-37	66.3	11.3
29.1	-37.1	-37	62.6	10.2

At a runtime of 6.1 h, the average  $T_b(TC)$  was - 37.4°C and the LyoMate calculations yielded a new shelf setpoint of - 37°C, which was adjusted immediately. These two shelf temperature adjustments led to a noticeable decrease in  $T_b(TC)$  and no more changes were needed to maintain  $T_{p-target}$  in a range of - 38°C ± 1°C over the whole primary drying phase. The end of primary drying was indicated by a steep increase in  $T_b(TC)$  after 35 to 41 h. Comparative pressure measurement indicated the end of primary drying at 44 h.

Until a runtime of 6 h,  $T_b(MTM)$  and  $T_b(TC)$  correlated very well with a difference of less than 0.3°C which is within the range of error for the thermocouples. Between 6 and 9 h of primary drying,  $\Delta T_b$  (MTM-TC) increased up to 0.9°C and between 11 h and 29 h up to 2.1°C. This large difference indicates that the MTM-based temperature determination only yielded accurate values in the early phase of primary drying as described in literature.<sup>14,19</sup> This was due to the decreasing sublimation area since the DCCs standing at the edges of the array finished primary drying earlier as a

result of the additional amount of radiation.<sup>6,16</sup> As a consequence of this inaccuracy,  $T_p$  needed to calculate  $K_{shell}$  and  $K_{DCC}$  (Equations (6-6) and (6-7)) was always assessed using the thermocouple readouts. This way, we could assure that the new shelf temperature setpoint, calculated with the LyoMate procedure, was accurate until the end of primary drying. In this experiment the last PRT was performed after 29.1 hours of primary drying and still yielded the correct shelf temperature setpoint, until primary drying was finished after around 44 hours. However, the increase of  $K_{shell}$  and  $K_{DCC}$  by factors of up to 3 after a runtime of 6.1 hours (Table 6-2) within one hour of primary drying is not plausible and therefore must be an error in calculation most probably due to the inaccuracy of the MTM at these time points. The final product is illustrated in Figure 6-4 and showed no signs of shrinkage or microcollapse. Hence, the DCC LyoMate procedure was successfully applied to plan and online-control a lyophilization cycle for freeze-drying in DCCs and yielded a pharmaceutically acceptable and elegant cake structure.



**Figure 6-4 Macroscopic appearance of a 5% sucrose formulation with a fill volume of 0.5 ml freeze-dried with the DCC LyoMate procedure.**

#### 6.4.2 Determination of the minimum number of DCC needed for valid MTM measurements using a 5% sucrose formulation.

Subsequently, it was necessary to find the minimum number of DCCs needed to perform accurate MTM measurements, and hence accurate LyoMate procedures, firstly, to know the limitations of the procedure with regards to the sublimation front area to chamber volume ratio<sup>19</sup> and secondly to enable mAb formulation experiments with low protein consumption.

Four different arrays with 75, 150, 324 and 444 DCCs filled with 0.5 ml 5% sucrose solution were freeze-dried at a  $P_c = 60$  mTorr, and  $T_{p\text{-target}} = -38^\circ\text{C}$ . Figure 6-5 (a) displays the  $T_b(\text{MTM})$  and  $T_b(\text{TC})$  for an array of 75 DCCs corresponding to a total sublimation surface area of  $0.42 \text{ cm}^2/\text{L}$  chamber volume. The temperature difference between  $T_b(\text{MTM})$  and  $T_b(\text{TC})$ , left the acceptable range of  $0.5^\circ\text{C}$  already after one hour of primary drying and further increased to  $1^\circ\text{C}$  and  $2^\circ\text{C}$  after 2 and 3 h runtime respectively. Since the previous experiment showed that at least 5 hours of primary drying were necessary to find the optimum shelf temperature (Table 6-2), a total number of 75 DCCs was not sufficient to guarantee a successful LyoMate procedure. For 150 DCCs, corresponding to  $0.84 \text{ cm}^2/\text{L}$  (Figure 6-5 (b)), the situation was different. Here,  $\Delta T_b (\text{MTM-TC})$  stayed in the acceptable corridor of  $0.5^\circ\text{C}$  until a primary drying runtime of around 6 hours.

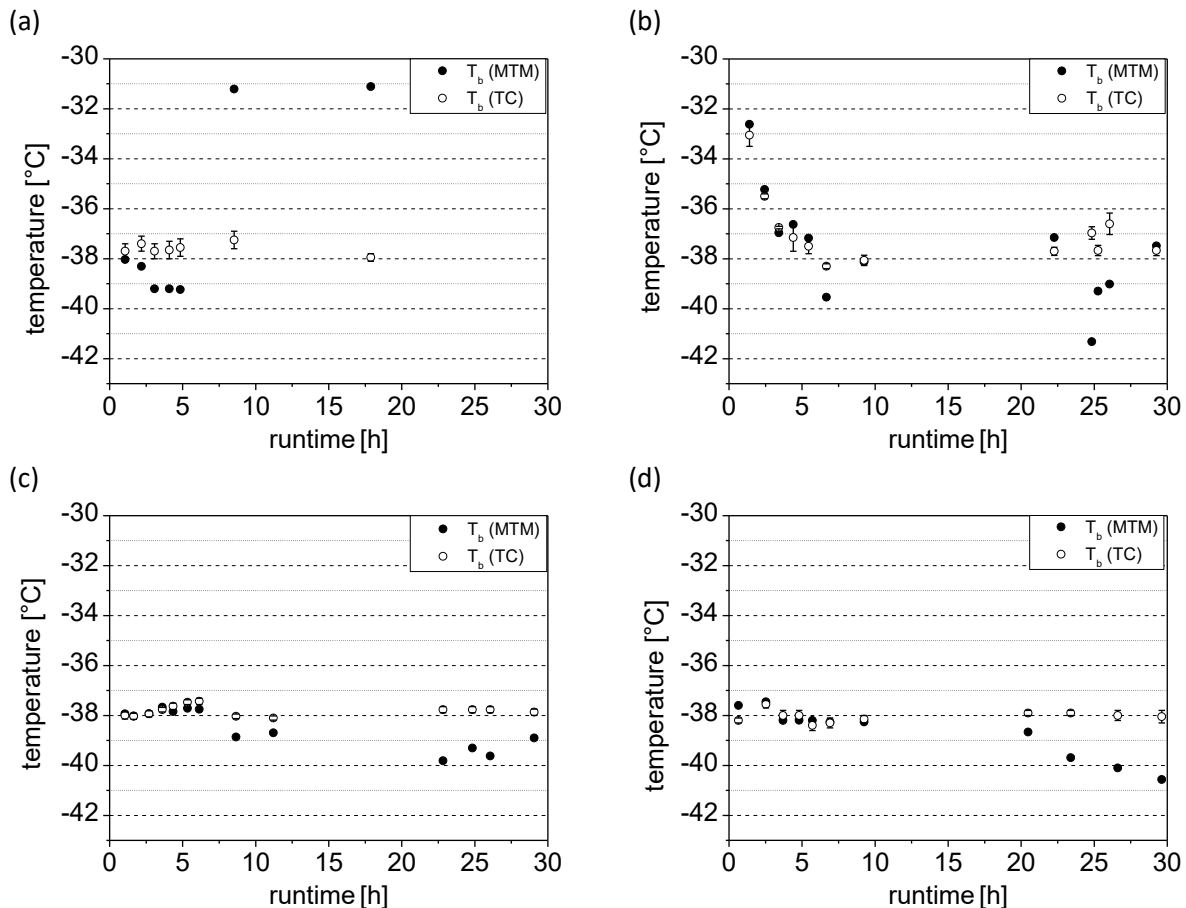


**Figure 6-5**  $T_b(\text{MTM})$  and  $T_b(\text{TC})$  values for a 5% sucrose formulation freeze dried with a  $V_{\text{fill}} = 0.5$  ml in (a) 75 DCCs, (b) 150 DCCs, (c) 324 DCCs and (d) 444 DCCs.

This period of accurate  $T_b(\text{MTM})$  could be further increased to around 10 hours in the case of 324 DCCs, equal to  $1.82 \text{ cm}^2/\text{L}$  and to around 20 hours for 444 DCCs ( $2.50 \text{ cm}^2/\text{L}$ ) (Figure 6-5 (c)-(d)). The MTM sensitivity is in good accordance with literature data, where Tang et al. suggested a sublimation area of approx.  $300 \text{ cm}^2$  for a 104 L chamber volume ( $2.88 \text{ cm}^2/\text{L}$ ) to get reliable MTM data until at least  $2/3^{\text{rd}}$  of primary drying.<sup>12</sup> As mentioned above, for the DCC LyoMate method it is sufficient to get reliable MTM data during the first 5 hours of primary drying in order to find the optimum shelf temperature setpoint (Figure 6-3 (a)). Therefore, 150 DCCs per run were selected for the mAb formulation experiments as a compromise between a reliable MTM measurement and a cost-saving process development.

### 6.4.3 High fill volume case study and the influence of the nucleation method on the DCC LyoMate's accuracy

In a next step, the applicability of the DCC LyoMate method for high fill volumes as well as the influence of the nucleation method on the LyoMate's accuracy were tested. Two sets of experiments were conducted using 1 ml of a 5% sucrose solution in 150 DCCs. At first, controlled nucleation performed using the ice-fog technique was compared a shelf-ramped freezing protocol Figure 6-6 indicates, that the  $T_b(\text{MTM})$  values after controlled nucleation were in better accordance with TC readouts than for the shelf-ramped freezing procedure.

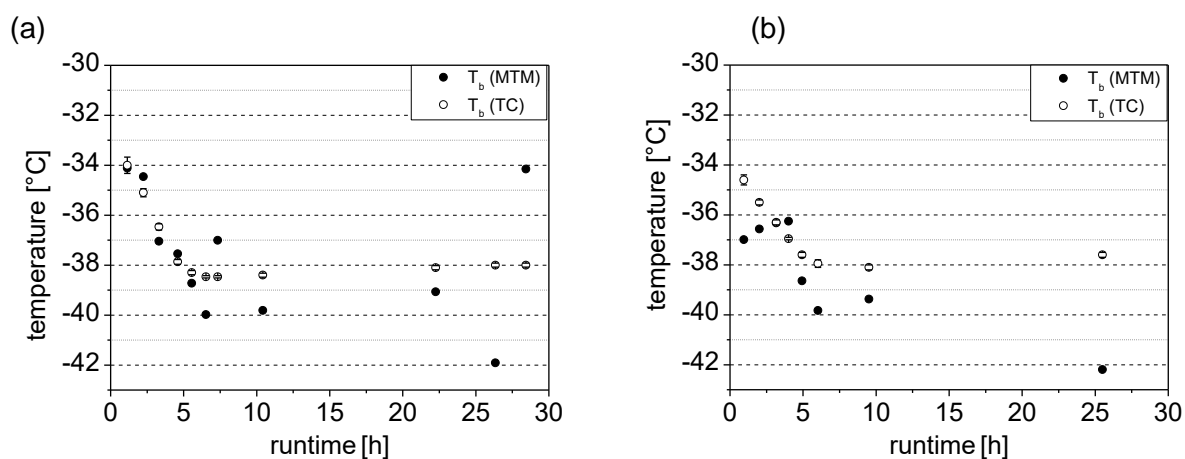


**Figure 6-6  $T_b(\text{MTM})$  and  $T_b(\text{TC})$  values for a 5% sucrose formulation freeze dried with a fill volume of 1 ml in 150 DCCs where (a) controlled nucleation (ice-fog technique) and (b) regular shelf-ramped freezing was used.**

For the controlled nucleation experiment  $\Delta T_b$  (MTM-TC) was below  $0.5^\circ\text{C}$  for at least 5.5 hours of primary drying. Whereas, using the shelf-ramped freezing protocol,  $\Delta T_b$  (MTM-TC) was  $2.3^\circ\text{C}$  for the first and  $0.9^\circ\text{C}$  for the second PRT. Only the 3<sup>rd</sup> LyoMate temperature measurement yielded an acceptable value of less than  $0.5^\circ\text{C}$ . By controlling the nucleation temperature, ice crystal structure and ultimately the pore size of the lyophilized cake, the ice fog method increases the drying homogeneity.<sup>10,22</sup> Accordingly, controlled nucleation increased the accuracy of the LyoMate procedure and was therefore used for subsequent mAb formulation experiments. For freeze-drying in vials, controlled nucleation often comes with an increased sublimation rate due to the larger pore size within the dried layer and hence faster primary drying.<sup>23</sup> This effect could not be observed for the current setup with sublimation rates for the controlled nucleation of  $20.5 \pm 7.4 \text{ mg/h}$  and

21.03 ± 5.6 mg/h and primary drying runtimes of 108.2h and 111.4 h for the shelf-ramped freezing method respectively. The DCC LyoMate method yielded elegant cakes without signs of shrinkage or collapse for both nucleation methods (Figure 6-7). Lyophilisates produced with the ice-fog technique showed a more porous and less compact appearance without a marked cone structure at the top as the one produced with shelf-ramped freezing. The cone is a result of the radial freezing behavior, towards the center promoted by the excellent energy transfer capability of the shell holder device. Upon nucleation by the ice-fog freezing took place from top to bottom which prevented a concentration of solid material forming a cone in the middle.<sup>15,24,25</sup>

In both cases, the DCC LyoMate method did not only yield pharmaceutically acceptable cakes but was also able to maintain the desired target product temperature of  $-38^{\circ}\text{C} \pm 1^{\circ}\text{C}$ . Hence, the DCC LyoMate procedure can be used to freeze-dry large fill volumes of up to 1 ml even though  $\Delta T_b$  (MTM-TC) values might be higher than  $0.5^{\circ}\text{C}$  if the regular shelf-ramped freezing is used.

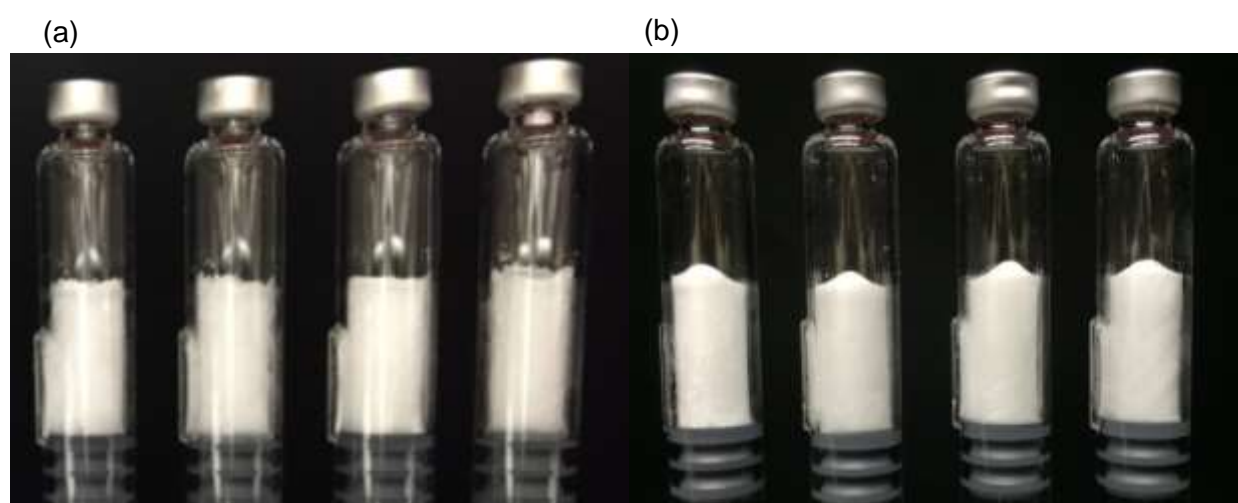


**Figure 6-7 Macroscopic appearance of 5% sucrose formulation with a fill volume of 1 ml, freeze-dried with the DCC LyoMate procedure where (a) controlled nucleation (ice-fog technique) and (b) regular shelf-ramped freezing was used.**

#### 6.4.4 Collapse temperature determination of different mAb formulations and definition of target product temperatures

After the verification of the DCC LyoMate procedure and the determination of the minimum amount of DCCs, the LyoMate method was tested for mAb formulations. The first step was the definition of the target product temperature, using freeze-drying microscopy. For the formulation containing 2 mg/ml mAb, the onset of collapse at  $-33.6^{\circ}\text{C}$  is displayed in Figure 6-8 (a), resulting in a target product temperature ( $T_{p\text{-target}}$ ) of  $-37^{\circ}\text{C}$  (safety margin of  $3^{\circ}\text{C}$ ). For the 20 mg/ml and 100 mg/ml mAb formulation a  $T_{c\text{-onset}}$  of  $-31.1^{\circ}\text{C}$  and  $-30.2^{\circ}\text{C}$  respectively was determined leading to a  $T_{p\text{-target}}$  of  $-34^{\circ}\text{C}$  and  $-33^{\circ}\text{C}$  respectively. A higher collapse temperature with an increasing protein concentration is in accordance with literature data.<sup>26,27</sup>

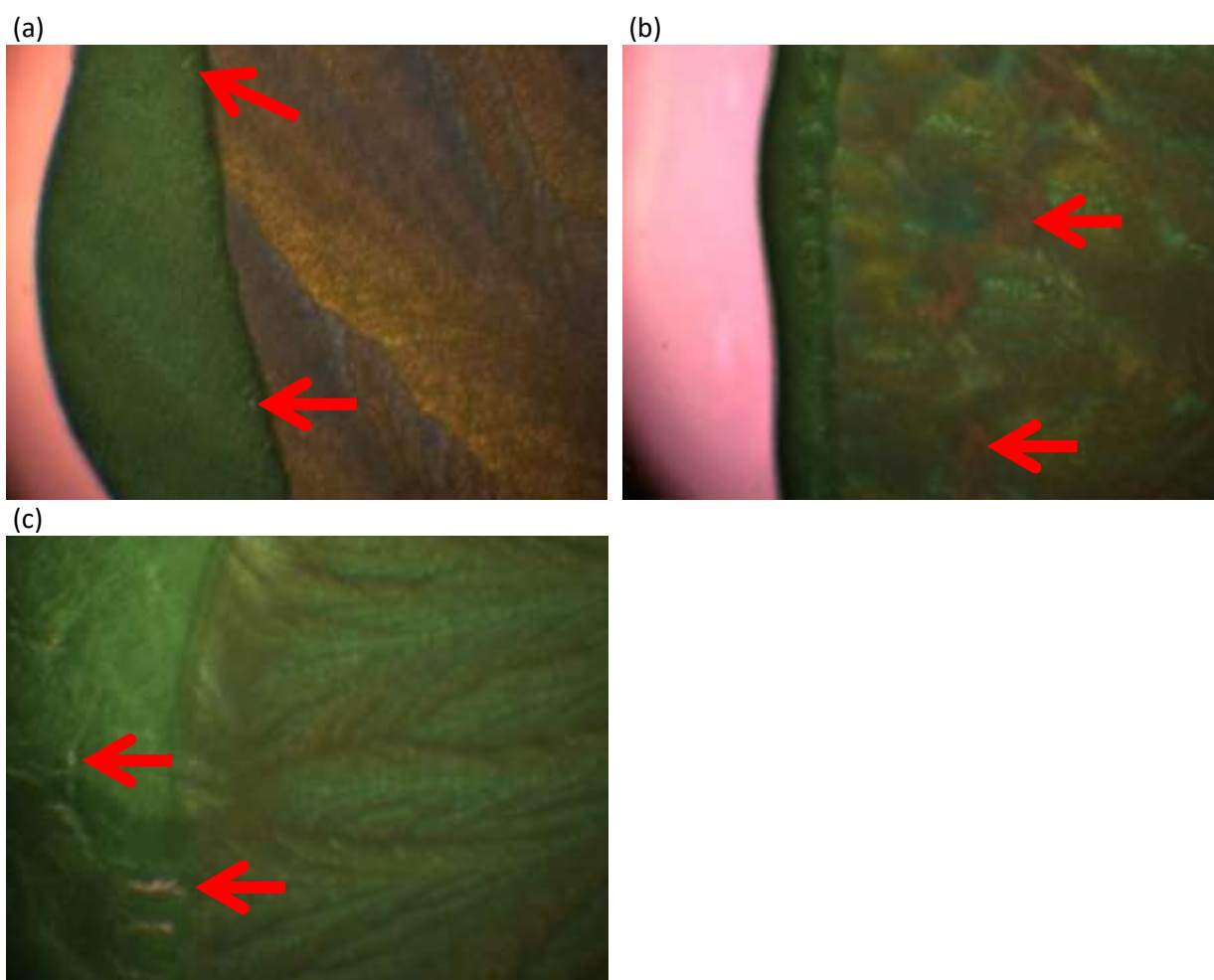


**Figure 6-8** Freeze-Drying microscopy images for a  $I_gG1$  monoclonal antibody formulation showing the onset of collapse, indicated via red arrows, for a concentration of 2 mg/ml mAb with a  $T_{c\text{-onset}} = -33.6^{\circ}\text{C}$  (a), 20 mg/ml with a  $T_{c\text{-onset}} = -31.1^{\circ}\text{C}$  (b) and 100 mg/ml with a  $T_{c\text{-onset}} = -30.2^{\circ}\text{C}$  (c).

### 6.4.5 DCC LyoMate results for the 2 mg/ml mAb formulation and the influence of controlled nucleation on product appearance

For the 2 mg/ml mAb formulation experiment the chamber pressure was set to 65 mTorr and the initial shelf temperature to  $-34^{\circ}\text{C}$  according to the first step in the DCC LyoMate procedure (Figure 6-2). After the initial holding period of 60 min at  $-34^{\circ}\text{C}$ , the vacuum was pulled and the self-cooling effect of sublimation led to a product temperature drop to  $-38^{\circ}\text{C}$  (Figure 6-9 (a)).

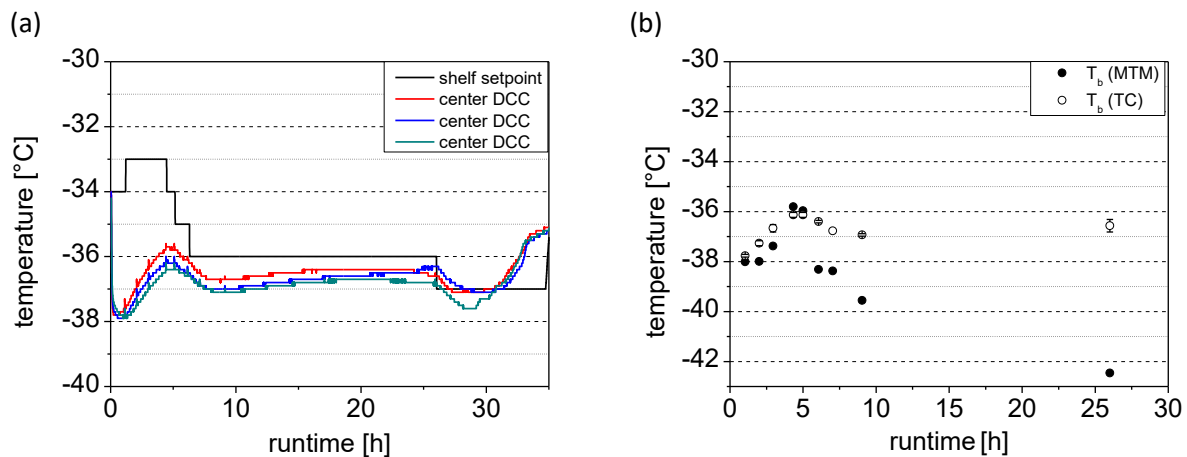


**Figure 6-9 Impact of controlled nucleation: (a) Product- and shelf-temperature profile during primary drying of 150 DCCs filled with a 2 mg/ml mAb formulation ( $V_{\text{fill}} = 0.5$  ml), freeze-dried with the DCC LyoMate at  $T_{\text{p-target}} = -37^{\circ}\text{C}$ . (b) Corresponding  $T_b$  (MTM) and  $T_b$  (TC) values.**

The DCC LyoMate calculations gave a new shelf temperature setpoint of  $-33^{\circ}\text{C}$  after the first hour of primary drying.  $T_s$  was adapted accordingly and maintained for almost 3 h. After 5h of primary drying,  $T_p$  reached  $-31.2^{\circ}\text{C}$  and at this time, the LyoMate calculations yielded a new shelf setpoint of  $-34^{\circ}\text{C}$ . Additional  $T_s$  adjustments based on the LyoMate procedure were performed after 6 h ( $-35^{\circ}\text{C}$ ) and 26 h ( $-37^{\circ}\text{C}$ ) of primary drying. During the first 5 h of primary drying,  $\Delta T_b$  (MTM-TC) did not exceed  $0.5^{\circ}\text{C}$  and at the 6 h time point  $\Delta T_b$  (MTM-TC) was increased to  $0.9^{\circ}\text{C}$ . However, after 26 h of primary drying the PRT results were not reliable any more with  $\Delta T_b$  (MTM-TC) of  $8^{\circ}\text{C}$  and a doubling in  $K_{\text{shell}}$  between 5 h and 26 h runtime. Overall, the DCC LyoMate gave reliable shelf temperature setpoints during the whole processing time with product temperatures within the desired corridor of  $-37^{\circ}\text{C} \pm 1^{\circ}\text{C}$ .

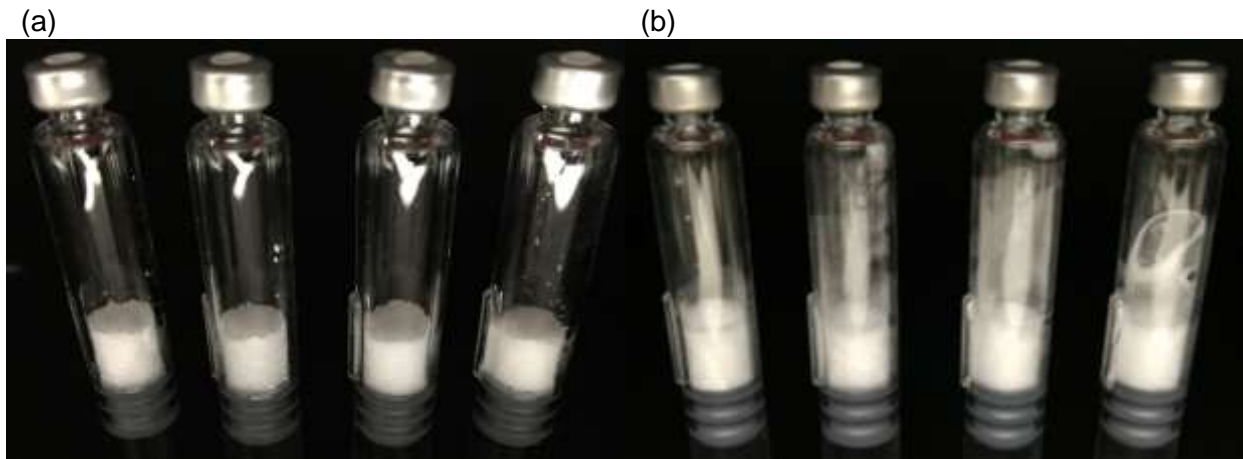


**Figure 6-10 Macroscopic appearance of 2 mg/ml mAb formulation ( $V_{\text{fill}} = 0.5$  ml), freeze-dried with the DCC LyoMate procedure showing no signs of fogging (a) and showing fogging as well as signs of vacuum induced freezing (b).**

The macroscopic appearance of 95% of the whole batch of DCCs was impeccable without any signs of structural loss in form of meltback or shrinkage (Figure 6-10 (a)). Interestingly, 5% of the finished product showed fogging (Figure 6-10 (b)). Reasons for fogging are manifold and can relate to formulation composition, DCC washing or filling procedure.<sup>28</sup> Since these factors were kept the same for all experiments in this study and this was the first time that fogging occurred, it was concluded that the root cause could be process related. This assumption was fostered by boiled looking lyophilized cakes in 2 of the 150 DCCs which could be a sign of vacuum induced freezing (Figure 6-10 (b)). The ice-fog technique used to perform controlled nucleation implied a chamber pressure reduction to 3 Torr<sup>10</sup> prior to venting the system via the condenser which could result in boiling of the product solution. Thus, the method of nucleation was assumed as a possible root cause for both cosmetic damages.

### 6.4.6 DCC LyoMate results for the 2 mg/ml mAb formulation and the influence of shelf-ramped freezing on product appearance

After shelf-ramped freezing, the DCC LyoMate procedure yielded that the initial chamber pressure of 65 mTorr and shelf temperature of  $-34^{\circ}\text{C}$  was maintained for almost 5.2 h of primary drying. At that point, the average product temperature reached  $-36.3^{\circ}\text{C}$  and the shelf temperature was adjusted to  $-35^{\circ}\text{C}$  and held for 1 h, followed by two more adjustments of  $T_s$  to  $-36^{\circ}\text{C}$  and  $-37^{\circ}\text{C}$ .

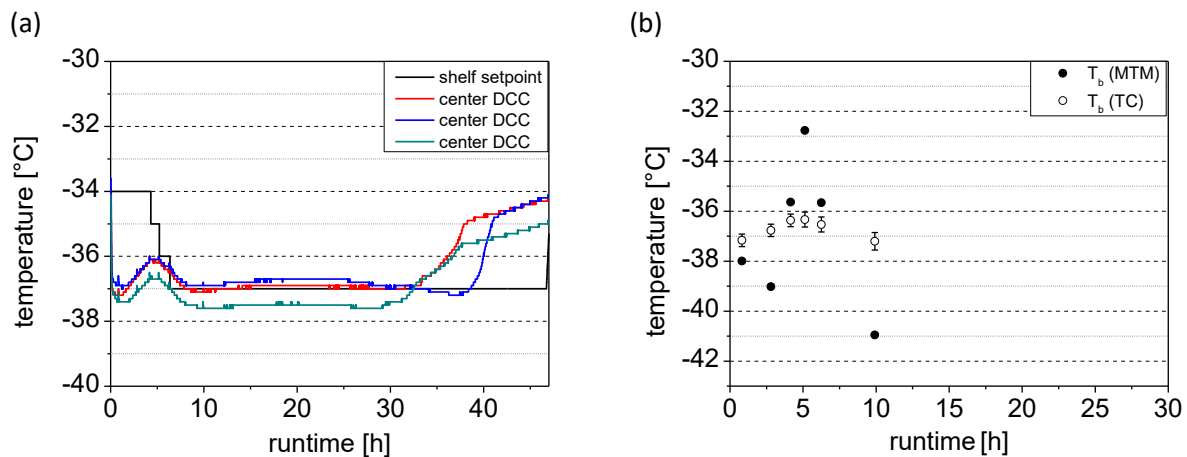


**Figure 6-11 Impact of shelf-ramped freezing (a) Product- and shelf-temperature profile during primary drying of 150 DCCs filled with a 2 mg/ml mAb formulation ( $V_{\text{fill}} = 0.5$  ml), freeze-dried with the DCC LyoMate procedure at  $T_{p\text{-target}} = -37^{\circ}\text{C}$ . (b) Corresponding  $T_b$  (MTM) and  $T_b$  (TC) values.**

$T_b$ (MTM) deviated more substantially from  $T_b$ (TC) (Figure 6-11 (b)) (up to  $2.5^{\circ}\text{C}$  during the first 5 h) than for the previously experiment using controlled nucleation. This was in line with the results obtained earlier using a 5% sucrose solution.



**Figure 6-12 Macroscopic appearance of 2 mg/ml mAb formulation ( $V_{fill} = 0.5$  ml), freeze-dried with the DCC LyoMate procedure and shelf-ramped freezing.**

None of the DCCs containing the final product (Figure 6-12) showed signs of fogging or boiling. Since the freezing procedure was the only variable between the process shown in chapter 6.4.5 and the present experiment it was concluded that the ice fog method was the root cause of these cosmetic defects.

### 6.4.7 Applicability of the DCC LyoMate procedure for highly concentrated mAb formulations

The last part of this study focuses on the applicability of the DCC LyoMate procedure for highly concentrated mAb formulations. DCCs are of special interest for highly concentrated protein formulations for subcutaneous self-administration. For the 20 mg/ml and 100 mg/ml mAb formulation, the target product temperature was defined as  $-34^{\circ}\text{C}$  and  $-33^{\circ}\text{C}$  and the chamber pressure setpoints were 65 mTorr and 70 mTorr respectively. The DCC LyoMate method was able to keep the product temperature in the desired corridor with a maximal tolerance of  $\pm 1^{\circ}\text{C}$  for both formulations (Figure 6-13 (a),(c)).

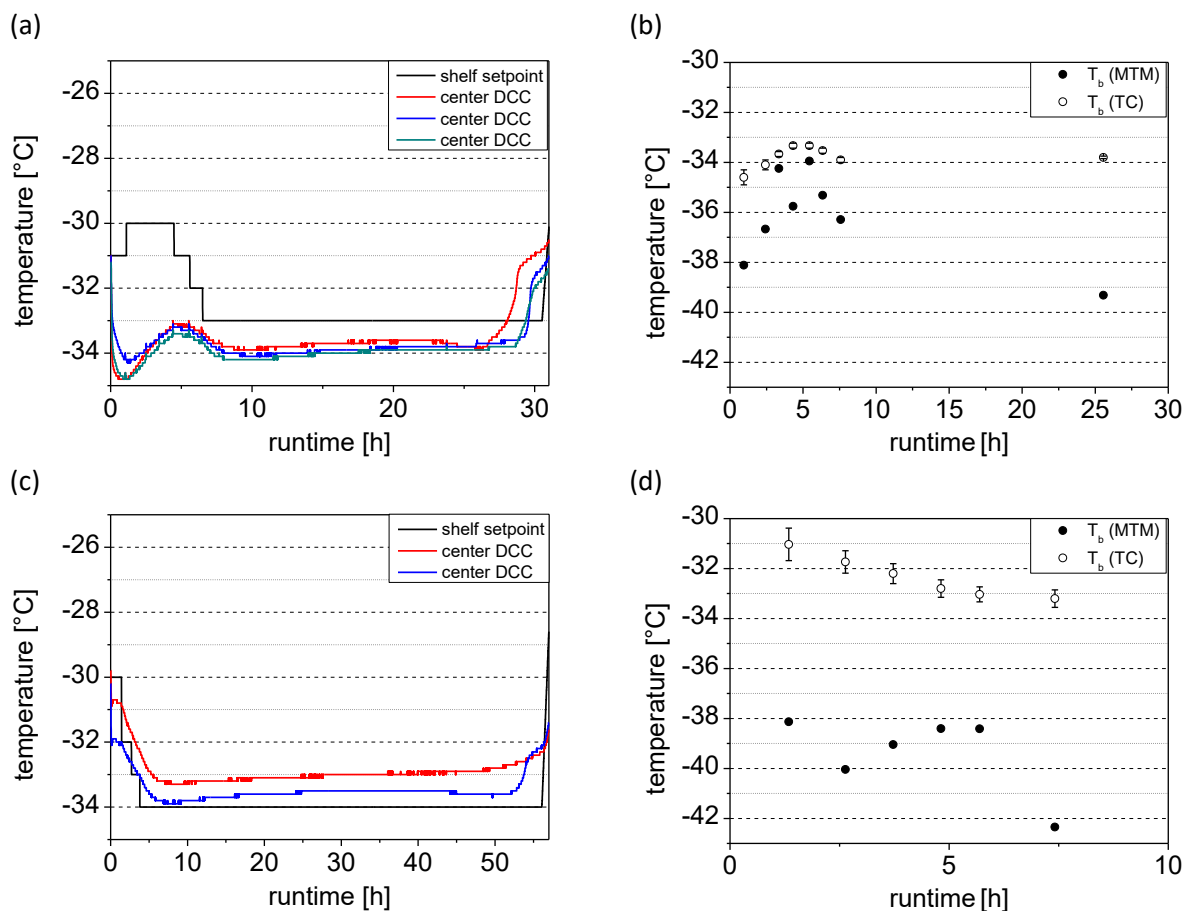


**Figure 6-13 Product- and shelf-temperature profile during primary drying of 150 DCCs filled with 0.5 ml of a (a) 20 mg/ml mAb formulation ( $T_{p\text{-target}} = -34^{\circ}\text{C}$ ) and (c) a 100 mg/ml mAb formulation ( $T_{p\text{-target}} = -33^{\circ}\text{C}$ ). (b) Corresponding  $T_b$  (MTM) and  $T_b$  (TC) values for the 20 mg/ml mAb formulation and (d) for the 100 mg/ml mAb formulation.**

Four shelf temperature adjustments during the first 7.6 hours of primary drying were sufficient for the 20 mg/ml formulation experiment and only three changes during the first 4.8 hours were necessary for the 100 mg/ml formulation. Interestingly, Figure 6-13 (c) shows that the product temperatures of the 100 mg/ml formulation exceeded the shelf temperature by about 1°C. This was probably due to the high solid content in form of protein.

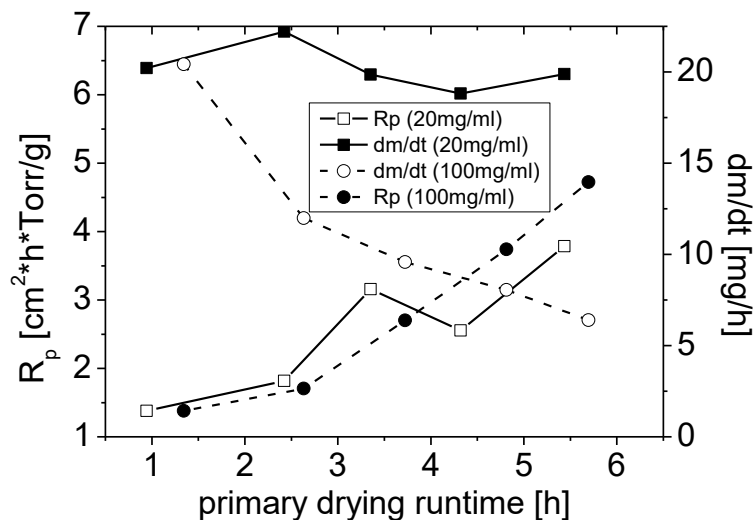


**Figure 6-14 Area-normalized mass transfer resistance rate ( $R_p$ ) and sublimation rate ( $dm/dt$ ) over the runtime of primary drying.**

A higher protein content led to a steeper increase in the mass transfer resistance and hence to a much more pronounced decrease in the sublimation rate as primary drying progresses (Figure 6-14). This resulted in less self-cooling and ultimately in a higher product temperature for the 100 mg/ml formulation because of a denser dried layer hindering the vapor flow and readsorption of the water vapor trespassing this dried layer. Both effects are assumed to be more pronounced at higher protein concentrations.<sup>13</sup> Another effect of these phenomena was that  $\Delta T_b$  (MTM-TC) for both formulations exceeded the tolerance level of 0.5°C directly at the beginning of primary drying with about 4°C and 8°C for the 20 mg/ml and 100 mg/ml formulation respectively. Since these values are not sufficiently accurate for a thorough shelf temperature calculation,  $T_b$ (TC) data is required at high protein concentration for the DCC LyoMate procedure. Figure 6-15 displays the pressure rise of the first MTM measurement, after 1 h of primary drying.

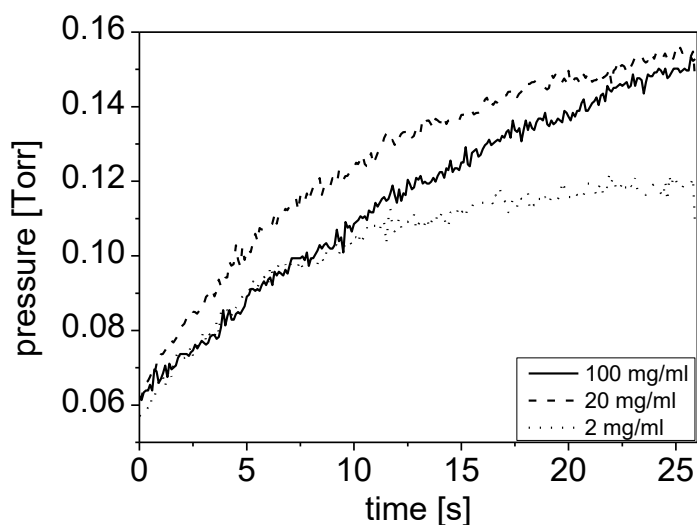


**Figure 6-15 Chamber pressure data for mAb formulations with 2, 20, and 100 mg/ml mAb concentrations during the first MTM measurement. Final pressure differences are due to different  $T_s$  and  $P_c$  setpoints.**

Whereas at 2 mg/ml the important plateau phase was reached after around 15 s, the 20 mg/ml formulation only showed a slight levelling off starting after 10 s.<sup>12,19</sup> At 100 mg/ml mAb, a plateau did not form but pressure increased almost linearly, which explains the high  $\Delta T_b$  (MTM-TC) value.

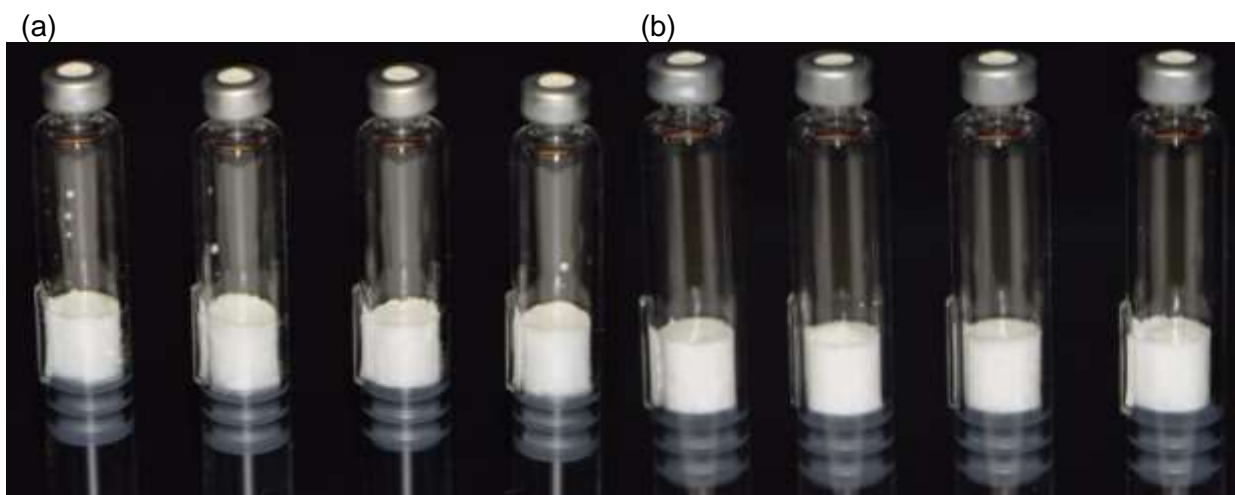


**Figure 6-16 Macroscopic appearance of mAb formulations ( $V_{\text{fill}} = 0.5$  ml) freeze-dried with DCC LyoMate procedure at a concentration of (a) 20 mg/ml (b) 100 mg/ml.**

Despite these challenges, the most important benchmark for a successful lyophilization process development is the final product quality, which is assured for both the 20 and the 100 mg/ml formulation (Figure 6-16). The cakes looked elegant without signs of macroscopic damage.

## 6.5 Summary and Conclusion

The purpose of this study was to develop a “MTM –based” process control strategy, the DCC LyoMate (from lyophilization and automated), that can be used to purposefully plan and optimize lyophilization processes for DCCs. The ultimate goal of the DCC LyoMate procedure was to create the optimum, most efficient lyophilization cycle during the very first development run while assuring product quality. Hereby, the macroscopic integrity was assessed as the critical quality attribute and the ability to maintain  $T_{p\text{-target}}$  and the correlation between  $T_b(\text{MTM})$  and  $T_b(\text{TC})$  were the process related success criteria.

At first, a proof of concept study using a fully loaded tray of 324 DCCs, each filled with 0.5 ml of a 5% sucrose formulation was performed. The DCC LyoMate was able to keep  $T_{p\text{-target}}$  in a range of  $-38^\circ\text{C} \pm 1^\circ\text{C}$  over the whole primary drying phase using only two shelf temperature adjustments (Figure 6-3 (a)). The  $\Delta T_b$  (MTM-TC) stayed in the acceptable range below  $0.5^\circ\text{C}$  during the first 6 h of primary drying. It increased to  $0.9^\circ\text{C}$  at the end of the process, indicating that the MTM-based temperature determination only yielded accurate values in the early phase of primary drying. However, the initial 5-6 hours were enough to determine the optimum shelf temperature (Figure 6-3 (a)). To assure accurate DCC LyoMate calculations beyond these 5 - 6 hours,  $T_b(\text{TC})$  was used for all calculations. This enabled an accurate shelf temperature calculation until at least  $2/3^{\text{rd}}$  of primary drying. The final product (Figure 6-4) showed no signs of shrinkage or microcollapse. Hence all success criteria were accomplished. In a next step, the minimum number of DCCs needed to perform accurate MTM measurements, and therefore accurate LyoMate procedures was assessed. A number of 150 DCC, corresponding to a sublimation front area of  $0.84 \text{ cm}^2/\text{L}$  chamber volume, was found to be sufficient to keep  $\Delta T_b$  (MTM-TC) values in the acceptable corridor until approximately 6 hours of primary drying (Figure 6-5 (b)). As mentioned above, this time period appeared to be sufficient to find the optimum process conditions

Subsequently, the applicability of the DCC LyoMate method for higher fill volumes and the influence of the method of nucleation on the LyoMate's accuracy were tested.

The use of controlled nucleation could significantly improve  $\Delta T_b$  (MTM-TC) with values of  $\leq 0.5^\circ\text{C}$  during the first 5.5 hours of primary drying compared to values of up to  $2.3^\circ\text{C}$  for the shelf-ramped freezing protocol during the same period of time. This was presumably the result of an increased pore size homogeneity in the dried layer for the DCCs that were nucleated with the ice-fog method. Nevertheless, the DCC LyoMate method did not only produce pharmaceutically acceptable cakes but was also able to maintain the desired target product temperature of  $-38^\circ\text{C} \pm 1^\circ\text{C}$  for the high fill volume formulations, irrespective of the freezing protocol (Figure 6-7). During the first protein containing lyophilization experiment using a 2 mg/ml mAb formulation ( $V_{\text{fill}} = 0.5$  ml), the target product temperature stayed within the desired corridor of  $-37^\circ\text{C} \pm 1^\circ\text{C}$  during the whole process and primary drying was finished after a total runtime of 34.6 hours. The macroscopic appearance of 95% of the DCCs was impeccable but 5% of the DCCs showed fogging (Figure 6-10). In contrast, shelf-ramped freezing yielded elegant cakes without container fogging but higher  $\Delta T_b$  (MTM-TC) values of  $2.5^\circ\text{C}$ . Furthermore the suitability of the DCC LyoMate procedure for highly concentrated mAb formulations of 20 and 100 mg/ml was assessed. Interestingly,  $\Delta T_b$  (MTM-TC) values exceeded the  $0.5^\circ\text{C}$  limit already after the first MTM measurement ( $4^\circ\text{C}$  for 20 and  $8^\circ\text{C}$  for 100 mg/ml mAb formulation) and  $T_b(\text{TC})$  of the 100 mg/ml mAb formulation exceeded the shelf temperature setpoint. Both facts resulted from the higher mass transfer resistances with higher mAb concentrations. Despite these challenges, the DCC LyoMate yielded elegant cakes at both concentrations and was able to maintain the product temperature within the designated target product temperature range.

Overall, the DCC LyoMate procedure enables the creation of efficient lyophilization cycles for DCCs, independent of the amount of protein, as long as some simple rules are followed: 1.) adherence to the LyoMate scheme displayed in Figure 6-2 and 2.) use of  $T_b(\text{TC})$  for shelf temperature calculations, facultative for low mAb concentrations but compulsory if highly concentrated mAb formulations should be processed. Thereby the DCC LyoMate procedure is applicable during the very first development run and thus enables a cost-saving process development instead of many trial and error approaches that lead to very conservative, inefficient cycles with low shelf temperature setpoints and high development costs.

## 6.6 References

1. Wang W 1999. Instability, stabilization, and formulation of liquid protein pharmaceuticals. *International journal of pharmaceutics* 185(2):129-188.
2. Franks F 1998. Freeze-drying of bioproducts: putting principles into practice. *European Journal of Pharmaceutics and Biopharmaceutics* 45(3):221-229.
3. Hibler S, Gieseler H 2012. Heat transfer characteristics of current primary packaging systems for pharmaceutical freeze-drying. *Journal of Pharmaceutical Sciences* 101(11):4025-4031.
4. Reynolds G 2006. The market need for reconstitution systems. *BioProcess Int* 4(10).
5. Polin JB 2003. The ins and outs of prefilled syringes. *Pharm Med Packag News* 11(5):40-43.
6. Korpus C, Haase T, Sönnichsen C, Friess W 2015. Energy Transfer During Freeze-Drying in Dual-Chamber Cartridges. *Journal of Pharmaceutical Sciences* 104(5):1750-1758.
7. Tang X, Pikal M 2004. Design of Freeze-Drying Processes for Pharmaceuticals: Practical Advice. *Pharm Res* 21(2):191-200.
8. Gieseler H, Kramer T, Pikal MJ 2007. Use of manometric temperature measurement (MTM) and SMART™ freeze dryer technology for development of an optimized freeze-drying cycle. *Journal of Pharmaceutical Sciences* 96(12):3402-3418.
9. Korpus C, Friess W 2017. Evaluation of different holder devices for freeze-drying in dual chamber cartridges with a focus on energy transfer. *Journal of Pharmaceutical Sciences* 106(4):1092-1101.
10. Korpus C, Pikal M, Friess W 2016. Heat Transfer Analysis of an Optimized, Flexible Holder System for Freeze-Drying in Dual Chamber Cartridges Using Different State-of-the-Art PAT Tools. *Journal of Pharmaceutical Sciences* 105(11):3304-3313.
11. Tang XC, Nail SL, Pikal MJ 2005. Freeze-drying process design by manometric temperature measurement: design of a smart freeze-dryer. *Pharm Res* 22(4):685-700.
12. Tang X, Nail SL, Pikal MJ. 2006. Evaluation of manometric temperature measurement, a process analytical technology tool for freeze-drying: Part I, product temperature measurement. *AAPS PharmSciTech* 7(4): E95-E103.
13. Tang XC, Nail SL, Pikal MJ. 2006. Evaluation of manometric temperature measurement, a process analytical technology tool for freeze-drying: Part II measurement of dry-layer resistance. *AAPS PharmSciTech* 7(4): E77-E84.

14. Tang X, Nail S, Pikal M 2006. Evaluation of manometric temperature measurement (MTM), a process analytical technology tool in freeze drying, part III: Heat and mass transfer measurement. *AAPS PharmSciTech* 7(4): E105-E111.
15. Geidobler R, Mannschedel S, Winter G 2012. A new approach to achieve controlled ice nucleation of supercooled solutions during the freezing step in freeze-drying. *Journal of Pharmaceutical Sciences* 101(12):4409-4413.
16. Rambhatla S, Pikal M 2003. Heat and mass transfer scale-up issues during freeze-drying, I: Atypical radiation and the edge vial effect. *AAPS PharmSciTech* 4(2):22-31.
17. Patel SM, Pikal MJ 2011. Emerging freeze-drying process development and scale-up issues. *AAPS PharmSciTech* 12(1):372-378.
18. Pikal MJ, Roy ML, Shah S 1984. Mass and heat transfer in vial freeze-drying of pharmaceuticals: Role of the vial. *Journal of Pharmaceutical Sciences* 73(9):1224-1237.
19. Milton N, Pikal MJ, Roy ML, Nail SL 1997. Evaluation of manometric temperature measurement as a method of monitoring product temperature during lyophilization. *PDA journal of pharmaceutical science and technology / PDA* 51(1):7-16.
20. Johnson RE, Kirchhoff CF, Gaud HT 2002. Mannitol–sucrose mixtures—versatile formulations for protein lyophilization. *Journal of Pharmaceutical Sciences* 91(4):914-922.
21. Association USFaD. U.S. Food and Drug Administration. Guide to inspections of lyophilization of parenterals (7/93)
22. Awotwe-Otoo D, Agarabi C, Khan MA 2014. An Integrated Process Analytical Technology (PAT) Approach to Monitoring the Effect of Supercooling on Lyophilization Product and Process Parameters of Model Monoclonal Antibody Formulations. *Journal of Pharmaceutical Sciences* 103(7):2042-2052.
23. Geidobler R, Konrad I, Winter G 2013. Can Controlled Ice Nucleation Improve Freeze-Drying of Highly-Concentrated Protein Formulations? *Journal of Pharmaceutical Sciences*: 102(11):3915-3919.
24. Geidobler R, Winter G 2013. Controlled ice nucleation in the field of freeze-drying: Fundamentals and technology review. *European Journal of Pharmaceutics and Biopharmaceutics* 85(2):214-222.
25. Patel SM, Bhugra C, Pikal MJ 2009. Reduced pressure ice fog technique for controlled ice nucleation during freeze-drying. *AAPS PharmSciTech* 10(4):1406-1411.
26. Carpenter J, Pikal M, Chang B, Randolph T 1997. Rational Design of Stable Lyophilized Protein Formulations: Some Practical Advice. *Pharm Res* 14(8):969-975.

27. Wang W 2000. Lyophilization and development of solid protein pharmaceuticals. *International Journal of Pharmaceutics* 203(1–2):1-60.
28. Abdul-Fattah AM, Oeschger R, Roehl H, Bauer Dauphin I, Worgull M, Kallmeyer G, Mahler HC 2013. Investigating factors leading to fogging of glass vials in lyophilized drug products. *European journal of pharmaceutics and biopharmaceutics* 85(2):314-326.



## 7 FINAL SUMMARY

Recent advances in the development of new biological entities (NBEs) enabled novel treatments for various diseases with an increasing demand for self-administration devices. This obligates long-term stable formulations of the drug product and user-friendly application devices that can be operated by the patient at home. Freeze-dried products in Dual Chamber Cartridges (DCCs) suffice both criteria. Freeze-drying is a moderate way to generate stable NBE formulations and, DCCs after coupling with a pen injector, significantly improve the usability and safety for the patient compared to a traditional vial.

Due to their large height to stand ratio and with the product being elevated above the shelf, DCCs need to be supported by special holder devices to assure accurate positioning within the lyophilizer and an efficient drying behavior. Consequently, freeze-drying in DCCs demands expertise about the energy transfer attributes of the DCC itself and the supporting holder system to ensure product quality.

Fundamental knowledge about the basics of energy transfer during lyophilization in DCCs was generated in **Chapter 3**. Customized aluminum blocks ( $19.3 \times 9.6 \times 3.0 \text{ cm}^3$ ) with a loading capacity of 72 DCCs per block were used as a basic model system. Heat transfer coefficients that describe how effective energy is transferred from one surface to another were assessed gravimetrically by performing sublimation experiments using pure water at a shelf temperature ( $T_s$ ) setpoint of  $0^\circ\text{C}$ , and chamber pressure ( $P_c$ ) setpoints of 60, 100, 150, and 200 mTorr. Two heat transfer coefficients were characterized: i)  $K_{AI}$  ( $3.5 - 6.2\text{E-}04 \text{ cal}/(\text{s} \cdot \text{cm}^2 \cdot \text{K})$ ) defining the energy transfer between shelf and holder, and ii)  $K_{DCC}$  ( $1.0 - 1.4\text{E-}04 \text{ cal}/(\text{s} \cdot \text{cm}^2 \cdot \text{K})$ ) between holder and DCC. To gain a better mechanistic understanding of the energy transfer process, the different contributions were identified and subsequently quantified. We could show that  $K_{AI}$  depended on all three forms of energy transfer, contact conduction, gas conduction as well as radiation, with gas conduction being the major form of energy transfer, contributing 48 - 71% to  $K_{AI}$  within the pressure range of 60 - 200 mTorr. In contrast,  $K_{DCC}$  was mainly affected by radiation with a portion of 91% at 60 mTorr and 69% at 200 mTorr, leading to significant drying heterogeneity for DCCs standing in the outer rows of the setup.

In general, an increased contribution of gas conduction to energy transfer enhances process control since it can be directly influenced via the chamber pressure setpoint of the freeze-dryer. The overall heat transfer coefficient,  $K_{\text{tot}}$ , with very low values ranging from 0.85 - 1.27E-04 cal/(s\*cm<sup>2</sup>\*K) between 60 and 200 mTorr made it obvious that the aluminum holder bears a significant potential for optimization concerning its energy transfer properties.

**Chapter 4** deals with the complete characterization of an optimized three-piece holder system, the “flexible holder”, that was constructed and analyzed based on the previously gained knowledge about energy transfer. In general, the usage of a holder device significantly complicates the analysis of heat transfer parameters due to a continuous energy uptake leading to nonsteady-state conditions. Therefore, this chapter also focused on the implementation of state-of-the-art process analytical tools (PAT) like Tunable Diode Laser Absorption Spectroscopy (TDLAS) and Pressure Rise Test (PRT). Guidance for the installation of a self-made Manometric Temperature Measurement (MTM) system is given. This MTM system can be easily installed on every freeze-dryer capable of performing a PRT without the need of any kind of equipment modification. In contrast to the gravimetric method, where each DCC is weighed before and after a certain time of primary drying to get individual sublimation rates, TDLAS and MTM are batch methods that yield an averaged sublimation rate and hence necessitate comparable mass transfer resistances ( $R_p$ ) of all DCCs within the batch. For this reason, two controlled nucleation methods were tested for their suitability in combination with DCCs. It was demonstrated, that the ControlLy<sup>®</sup> depressurization technique was not able to nucleate the product solution whereas an ice fog method, comprising an equilibration step at  $T_s - 8^\circ\text{C}$  and subsequent depressurization of the product chamber of the lyophilizer to 3 Torr, resulted in complete nucleation of 100% of the DCCs. Next, a reproducible method for the determination of heat transfer coefficients via TDLAS and MTM was established involving a preheating of the holder system for 60 min at  $T_s - 5^\circ\text{C}$ . This enabled subsequent online sublimation rate analysis during steady-state conditions. The new approach was compared to the traditional gravimetric technique and advice was given how to adapt the traditional technique to obtain accurate results if these novel PAT tools are not available.  $K_{\text{DCC}}$ -values for the flexible holder ranged from 3.81E-04 cal/(s\*cm<sup>2</sup>\*K) at 40 mTorr to 7.38E-04 cal/(s\*cm<sup>2</sup>\*K) at 200 mTorr. This 3 to 6-fold increase in energy transfer efficiency compared to the aluminum block holder

was due to the embedding of the product containing part of the DCC within a massive aluminum plate (210\*115\*15 mm<sup>3</sup>, 104 DCCs/plate). Overall, combining advanced PAT tools with the optimized flexible holder substantially improves process control and helps to sustain product quality throughout the lyophilization process.

The substantial influence of the holder system on the drying behavior of the product in the DCCs and the large differences between aluminum block and flexible holder revealed the need for an elaborate analysis of all currently available holder devices for freeze-drying in DCCs. In **Chapter 5** one type out of each group of typically utilized holder devices, block-, flexible-, shell- and guardrail holder, were analyzed and benchmarked. Reference points were i) drying homogeneity, ii) capability to minimize additional radiation effects (“atypical radiation”) and iii) energy transfer. The individual sublimation rate for each DCC within the particular holder was determined with the gravimetric method. For the block device an average sublimation rate of  $121.9 \pm 32.1$  mg/h ( $T_s$ : 0°C,  $P_c$ : 100 mTorr) was determined. As delineated in **Chapter 3**, the large portion of radiative heat transfer led to marked drying heterogeneity which in this case increased the sublimation rates for DCCs standing in the outer rows by up to 50%. This large disparity in sublimation rate is unfavorable because it can impair product quality and reduces the accuracy of applied PAT tools. For the guardrail holder this edge effect could not be observed. However the sublimation rate was overall highly variable ranging from 9.1 mg/h to 284.3 mg/h for individual DCCs. This, in combination with the lowest average sublimation rate of 84.7 mg/h, revealed that the guardrail holder was the least efficient system tested and is in general not recommended for a lyophilization cycle development for DCCs. The shell holder provided the highest overall sublimation rate ( $133.2 \pm 9.4$  mg/h), which allows adequately short processing times, and the lowest sublimation rate standard deviation of only 7% of all holder devices tested. The trend shell- superior to flexible- superior to block holder was validated for all applied reference points. It became apparent that these devices in which the product is embedded within the holder (flexible- and shell holder) provided better drying performance, both with regards to drying homogeneity and shielding from atypical radiation. Product temperature ( $T_p$ ) analysis during primary drying confirmed this trend and showed distinct differences between the devices to protect the product from atypical radiation. With the direct contact area between holder device and product,  $K_{DCC}$  values

increased by factors of up to 5 and 10 for flexible- and shell holder respectively compared to block holder.

The shell system provided the most efficient energy transfer with  $K_{DCC}$  values of  $4.66E-4 \pm 6.8E-6$  cal/(s\*cm<sup>2</sup>\*K) at 60 mTorr to  $1.01E-3 \pm 7.29E-5$  cal/(s\*cm<sup>2</sup>\*K) at 200 mTorr, improved the drying homogeneity and is thus the most favorable system for lyophilization cycle design for DCCs tested within this study.

For this reason, the shell holder was used in **Chapter 6** to develop an automated MTM-based process control strategy, the “DCC LyoMate” (from lyophilization and automated). The aim of this chapter was to create a methodology that comprises the combined knowledge about energy transfer, differences between holder systems and applicability of novel PAT tools, to consciously plan and optimize freeze-drying cycles for DCCs. The LyoMate was designed to simplify process development for DCCs by giving clear recommendations for actions that enable a science-based process design and control instead of a trial and error approach that is still very common today due to insufficient process knowledge. The macroscopic integrity of the lyophilisates was assessed as the critical quality attribute and coherence between the  $T_p$  determined via MTM  $T_b$ (MTM) and with thermocouples  $T_b$ (TC) was the process related success criterion. With the DCC LyoMate elegant lyophilization cakes for 0.5 and 1 ml fill volume of 5% sucrose solutions were obtained. The target product temperature ( $T_{p-target}$ ) was kept in the aspired range of  $-38^\circ\text{C} \pm 1^\circ\text{C}$  using only two shelf temperature adjustments.  $T_b$ (MTM) and  $T_b$ (TC) were within  $0.5^\circ\text{C}$  difference during the first 6 hours of primary drying. A sublimation front area to chamber volume ratio of  $0.84$  cm<sup>2</sup>/L was identified to be the minimum to assure accurate MTM calculations. In a next step, the system was tested using 2, 20 and 100 mg/ml mAb formulations. For all mAb concentrations, the LyoMate kept  $T_p$  at  $T_{p-target} \pm 1^\circ\text{C}$  and produced impeccable lyophilisates. However, at higher mAb concentration the difference between  $T_b$ (MTM) and  $T_b$ (TC) was substantial already after the first hour of primary drying with values of  $5^\circ\text{C}$  and  $8^\circ\text{C}$  for the 20 and the 100 mg/ml mAb formulation respectively. Therefore, the use of thermocouples is highly recommended for LyoMate-based shelf temperature calculations in the case of highly concentrated mAb formulations.

Overall, the DCC LyoMate is a powerful methodology that can be easily installed on every freeze-dryer able to perform a PRT. It enables a science-based lyophilization cycle development for DCCs already during the first development run and abrogates the need for costly, empirically developed freeze-drying cycles.

In conclusion, this work contributed to a sound process understanding for freeze-drying in DCCs and created fundamental knowledge in the field with a focus on energy transfer during the primary drying stage of the freeze-drying process. Furthermore this thesis highlights the importance of the holder device for a successful product development for DCCs as well as the rational application of new process analytical tools and science-based process control strategies.

## 8 *APPENDIX*

### 8.1 Publications included in this thesis

#### 8.1.1 Research articles

**Korpus C**, Haase T, Sönnichsen C, Friess W 2015. Energy Transfer during Freeze-Drying in Dual Chamber Cartridges. *Journal of Pharmaceutical Sciences* 104(5):1750-1758.

**Korpus C**, Pikal M, Friess W 2016. Heat Transfer Analysis of an Optimized, Flexible Holder System for Freeze-Drying in Dual Chamber Cartridges Using Different State-of-the-Art PAT Tools. *Journal of Pharmaceutical Sciences* 105(11):3304-3313.

**Korpus C**, Friess W 2017 Evaluation of Different Holder Devices for Freeze-Drying in Dual Chamber Cartridges with a Focus on Energy Transfer, *Journal of Pharmaceutical Sciences* 106(4): 1092-1101.

**Korpus C**, Friess W, Lyophilization-cycle design for Dual Chamber Cartridges and a method for online process control: The “DCC-LyoMate” procedure. *Journal of Pharmaceutical Sciences*, submitted manuscript.

#### 8.1.2 Book Chapters

**Korpus C**, Pikal M, Friess W, Lyophilization in Dual Chamber Cartridges In: *Lyophilization of Pharmaceuticals ,Vaccines and Medical Diagnostics*, Eds.: Ward K, Matejtschuk P, Springer, in preparation

### 8.1.3 Oral Presentations

Friess W, **Korpus C**; Freeze drying in Dual Chamber Cartridges, CPPR Freeze-Drying of Pharmaceuticals and Biologicals, Breckenridge, Colorado, USA, July 12-15, 2016

**Korpus C**, Friess W; Lyophilization-Cycle Development for Dual Chamber Cartridges - Focus on Energy Transfer and Holder Devices, 7<sup>th</sup> International Conference: International Society of Lyophilization – Freeze Drying (ISL-FD), Barcelona, July 6-10, 2015

**Korpus C**, Friess W; Energy Transfer during Freeze-Drying in Dual Chamber Cartridges, Freeze Drying of Pharmaceuticals & Biologicals, Short Course and Conference, Garmisch-Partenkirchen, September 23–26, 2014

**Korpus C**, Friess W; Energy transfer during Lyophilization of Dual Chamber Cartridges, Biopharmaceutical Interest Group (BIG) meeting, Copenhagen, Denmark, September 23-24, 2013

#### 8.1.4 Poster Presentations

**Korpus C**, Pikal M, Friess W; Heat Transfer Analysis of an optimized Holder System for Freeze-Drying in Dual Chamber Cartridges, PBP Worldmeeting, Glasgow, United Kingdom, April 4-7, 2016

**Korpus C**, Pikal M, Friess W; Heat Transfer Analysis of an optimized Holder System for Freeze-Drying in Dual Chamber Cartridges, "The Universe of Pre-filled Syringes and Injection Devices" Conference, Vienna, Austria, November 3-4 , 2015

**Korpus C**, Haase T, Friess W; Energy Transfer during Lyophilization in Dual Chamber Cartridges, 9<sup>th</sup> World Meeting on Pharmaceutics, Biopharmaceutics and Pharmaceutical Technology, Lisbon, Portugal, March 31 - April 3, 2014

**Korpus C**, Haase T, Friess W; Challenges in Energy Transfer during Freeze-Drying in Dual Chamber Cartridges, 2013 Munich Protein Formulation and Stability Conference, Munich, Germany, October 17, 2013

## 8.2 Curriculum vitae

### Christoph Korpus

**Date of Birth** 29<sup>th</sup> April 1987,  
**Place of Birth** Idar-Oberstein (Germany)  
**Citizenship** German

### Work Experience

08/2016 - present Laboratory Head, Liquid Formulation Stability, Merck KGaA, Darmstadt  
05/2014 - 08/2014 Visiting Scientist, University of Connecticut, School of Pharmacy, Storrs,  
Supervisor: Prof. Dr. Michael Pikal  
12/2012 - 05/2016 PhD Student, LMU Munich, Department for Pharmacy, Pharmaceutical  
Technology and Biopharmaceutics  
Supervisor: Prof. Dr. Wolfgang Frieß  
08/2012 - 11/2012 Pharmacist, Hirsch-Apotheke, Mannheim  
05/2011 - 10/2011 Pharmacist Trainee, Novartis Pharma Stein AG, Stein (PU Solids)

### Education

07/2012 Licensure as a pharmacist (Approbation)  
04/2007 - 04/2011 Study of Pharmacy, University Frankfurt am Main  
- Graduated with 2<sup>nd</sup> state examination  
08/1997 - 03/2006 Gymnasium an der Heizenwies, Idar-Oberstein  
- General qualification for university entrance